EINSTEIN
Albert Einstein College of Medicine

Montefiore

Arnold and Madaleine Penner

13th Annual Musculoskeletal Repair and Regeneration Symposium

Wednesday, November 13, 2024

Presented by: Musculoskeletal and Orthopaedic Research Laboratories and Department of Orthopaedic Surgery at Montefiore Einstein
Program Director: **Mia M. Thi, PhD**
University Chairman: **Neil J. Cobelli, MD**

Price Center/Block Research Pavilion
Albert Einstein College of Medicine
1301 Morris Park Avenue
Bronx, NY 10461

Dear colleagues and friends,

We extend a warm welcome to the **13th Annual Arnold and Madaleine Penner Musculoskeletal Repair and Regeneration Symposium**. We express our sincere gratitude to the faculty and attendees who have contributed to the success of this event over the years.

We anticipate that this symposium will foster new collaborations and innovative research initiatives. Through the exchange of ideas and the discussion of cutting-edge research, we aim to advance the field of musculoskeletal repair and regeneration.

We would like to acknowledge the invaluable contributions of the Steering Committee Chairs, who have curated an exceptional program of translational research sessions. We also thank the Chairs of the Poster Session and Young Investigator Award Committee for their diligent review of abstracts. We extend our appreciation to all poster presenters and their co-authors for their participation.

The dedication and hard work of the Department of Orthopaedic Surgery staff at Einstein and Montefiore have been instrumental in organizing this event. We also thank the Program Overseers and faculty members for their insightful feedback, which has consistently enhanced the quality of the symposium.

We are deeply grateful to our sponsors, particularly Mr. and Ms. Arnold and Madaleine Penner, for their generous support and unwavering commitment to this annual symposium. Finally, we thank all attendees for your contributions to the intellectual richness and future impact of our research community. We hope you enjoy a productive and stimulating day.

With our very best wishes,

Mia M. Thi, Ph.D.
Program Director of the Symposium

Neil J. Cobelli, M.D.
Professor and University Chairman
Department of Orthopaedic Surgery

Acknowledgements

We express our sincere gratitude to our benevolent patrons, the late Mr. Arnold Penner and Mrs. Madaleine Penner, for their unwavering support and generous contribution, which made the symposium possible over the years.

Arnold and Madaleine Penner

Arnold and Madaleine Penner

13th Annual Musculoskeletal Repair and Regeneration Symposium

Wednesday, November 13, 2024

SYMPOSIUM MISSION

The Albert Einstein College of Medicine and Montefiore Medical Center's Musculoskeletal Repair and Regeneration Symposium is an annual event that aims to advance knowledge, foster innovation, and promote collaboration among researchers in the field. This year's symposium will highlight recent breakthroughs in translational research, focusing on the following areas:

- **New technologies in clinical and translational orthopaedic science**
- **Tissue crosstalk in musculoskeletal diseases**
- **Musculoskeletal pain and inflammation**

GOALS AND FEATURES

This symposium delves into cutting-edge research in musculoskeletal repair, regeneration, and disease treatment. Presentations and discussions will highlight recent scientific discoveries and their potential clinical implications. Key features of this symposium include:

- 6 outstanding speakers from the region and nationwide
- Poster sessions and Young Investigator Award session

REGISTRATION

Deadline: **November 6, 2024**

Please register online at: **https://einsteinmed.edu/departments/orthopaedic-surgery/symposium**

Registration is free. Early registration is highly recommended.

CALL FOR ABSTRACTS FOR POSTER SESSION AND YOUNG INVESTIGATOR AND CLINICAL YOUNG INVESTIGATOR AWARDS

We invite investigators to submit abstracts for the poster session, which is an important component of this conference.

Abstracts from graduate and medical students, residents and postdoctoral fellows will be considered for basic science and clinical **Young Investigator Awards**. Four winners, three from Young Investigator and one from Clinical Young Investigator categories will be announced and each will be presented with a prize and a plaque. To qualify, you must register and submit an abstract to Dr. Zeynep

Seref-Ferlengez, the chair of the Poster Session and Young Investigator Award committee, by **October 25, 2024** via email to: **msk.einstein.symposium@gmail.com**.

The abstract is limited to 1 page. Include in your abstract the study's objective, a brief statement of methods, a summary of the results obtained, conclusions, and significance. **Please see abstract template on the website.** If you have multiple posters, please assign one of your co-authors for presentation. As the Symposium aims to promote communication within our region, we encourage you to submit your recent work (within 2024) to this Symposium, including work that may have been submitted to other meetings.

AGENDA

7:15 – 8:00 am	**Check-in and Continental Breakfast**
8:00 – 8:10 am	**Introduction and acknowledgements** Mia M. Thi, PhD **Opening remarks** Neil J. Cobelli, MD

8:10 – 8:15 am	**Introduction** Eric Fornari, MD Albert Einstein College of Medicine and Montefiore Medical Center
8:15 – 8:45 am	**Leveraging Big Data and AI to Improve Orthopedic Care and Research** Ata Kiapour, PhD Boston Children's Hospital, Harvard Medical School
8:45 – 9:15 am	**Delivering on Disruption in Orthopedic Surgery** Martha M. Murray, MD Boston Children's Hospital, Harvard Medical School
9:15 – 9:30 am	**Discussion / Conclusions**

9:30 – 9:40 am BREAK

9:40 – 9:45 am	**Introduction** Alice Huang, PhD Columbia University
9:45 – 10:15 am	**Uncovering the fundamental role of systemic factors secreted by fat in the pathogenesis of osteoarthritis** Kelsey Collins, PhD UCSF School of Medicine
10:15 – 10:45 am	**Development and regeneration of the tendon enthesis** Steve Thomopoulos, PhD Columbia University
10:45 – 11:00 am	**Discussion / Conclusions**

11:00 – 11:10 am BREAK

Session 3 – Beyond musculoskeletal pain and inflammation
Steering chair: Miguel Otero, PhD

11:10 – 11:15 am	**Introduction** Miguel Otero, PhD Hospital for Special Surgery
11:15 – 11:45 am	**Synovial Fibroblasts and Joint Pain** Dana Orange, PhD Rockefeller University
11:45 – 12:15 pm	**Unlocking the Role of Toll-like Receptors in OA** Carla Scanzello, PhD University of Pennsylvania
12:15 – 12:30 pm	**Discussion / Conclusions**

12:30 – 1:30 pm LUNCH BREAK

3:00 – 3:30 pm	**Young Investigator Awards** Hosted by: *Young Investigator Award Committee*

Closing Remarks

3:30 pm	**Closing remarks** Neil J. Cobelli, MD

Arnold and Madaleine Penner
13th Annual Musculoskeletal Repair and Regeneration Symposium
Wednesday, November 13, 2024

Chairs, Co-Chairs, and Speakers

Leila Alvandi, PhD
Clinical Research Associate of Orthopaedic Surgery
Albert Einstein College of Medicine and Montefiore Medical Center
Bronx, NY

Ugur Ayturk, PhD
Assistant Scientist of Musculoskeletal Integrity Program Hospital for Special Surgery
New York, NY

Alessandra Carriero, PhD
Associate Professor of Biomedical Engineering
The City College of New York
New York, NY

Neil J. Cobelli, MD
Professor and University Chairman of Orthopaedic Surgery
Albert Einstein College of Medicine and Montefiore Medical Center
Bronx, NY

Kelsey Collins, PhD
Assistant Professor of Orthopedic Surgery
University of California San Francisco
San Francisco, CA

David T. Corr, PhD
Professor of Biomedical Engineering
Rensselaer Polytechnic Institute
Troy, NY

Ananth S. Eleswarapu, MD
Assistant Professor of Orthopaedic Surgery
Albert Einstein College of Medicine and Montefiore Medical Center
Bronx, NY

Eric Fornari, MD
Associate Professor of Orthopaedic Surgery and Pediatrics
Albert Einstein College of Medicine and Montefiore Medical Center
Bronx, NY

Woojin Han, PhD
Assistant Professor of Leni & Peter W. May Department of Orthopaedics and Black Family Stem Cell Institute
Icahn School of Medicine at Mount Sinai
New York, NY

David M. Hirsh, MD
Professor of Orthopaedic Surgery
Albert Einstein College of Medicine and Montefiore Medical Center
Bronx, NY

Alice Huang, PhD
Associate Professor of Bioengineering (in Orthopedic Surgery)
Columbia University
New York, NY

Ata Kiapour, PhD, MMSc
Director of Musculoskeletal Informatics Group (MIG)
Department of Orthopaedic Surgery and Sports Medicine, Boston Children's Hospital
Assistant Professor of Orthopedic Surgery,
Harvard Medical School
Boston, MA

Robert J. Majeska, PhD
Professor of Biomedical Engineering
The City College of New York
New York, NY

Martha M. Murray, MD
Orthopedic Surgeon-in-Chief
Catharina Ormandy Professor of Orthopedic Surgery
Boston Children's Hospital
Harvard Medical School
Boston, MA

Dana Orange, MD, MSc
Chapman-Perelman Associate Professor of Clinical Investigation
The Rockefeller University
New York, NY

Miguel Otero, PhD
Associate Scientist of the Orthopedic Soft Tissue Research Program
Co-Director, Derfner Foundation Precision Medicine Laboratory
Hospital for Special Surgery
Assistant Professor of Cell and Developmental Biology in Orthopaedic Surgery
Weill Cornell Medical College
New York, NY

Carla Scanzello, MD, PhD
Associate Professor of Medicine (Rheumatology)
The Hospital of the University of Pennsylvania
Perelman School of Medicine
University of Pennsylvania
Philadelphia, PA

Zeynep Seref-Ferlengez, PhD
Research Assistant Professor of Orthopaedic Surgery
Albert Einstein College of Medicine and Montefiore Medical Center
Bronx, NY

Sylvia O. Suadicani, PhD
Professor of Urology and Molecular Pharmacology
Albert Einstein College of Medicine and Montefiore Medical Center
Bronx, NY

Mia M. Thi, PhD
Associate Professor of Orthopaedic Surgery and Molecular Pharmacology
Albert Einstein College of Medicine and Montefiore Medical Center
Bronx, NY

Stavros Thomopoulous, PhD
Director of Carroll Laboratories for Orthopedic Surgery
Vice Chair of Basic Research in Orthopedic Surgery
Robert E. Carroll and Jane Chace Carroll Professor
Orthopedic Surgery
Columbia University
New York, NY

CONTACT INFORMATION

Mia M. Thi, PhD
Program Director
Email: mia.thi@einsteinmed.edu
P: 718-430-3460

Zeynep Seref-Ferlengez, PhD
Chair, Poster Session and Young Investigator Award Committee
Email: sereffer@montefiore.org
P: 929-246-6352

LaTarsha Arthur
Symposium Coordinator
Email: latarsha.arthur@einsteinmed.edu
P: 718-430-2911

SYMPOSIUM LOCATION

Albert Einstein College of Medicine
Michael F. Price Center and Harold and Muriel Block Research Pavilion
1301 Morris Park Avenue
Bronx, NY 10461
Directions:
http://www.einsteinmed.edu/visitors/

HOTEL INFORMATION

Residence Inn by Marriott New York The Bronx at Metro Center Atrium
1776 Eastchester Road
Bronx, NY 10461
The hotel is a 10-minute walk from the Symposium.
www.marriot.com/nycbx
P: 718-239-3939

PARKING INFORMATION

The Quik Park Parking Lot
1975 Eastchester Road
Bronx, NY 10461

Campus Map

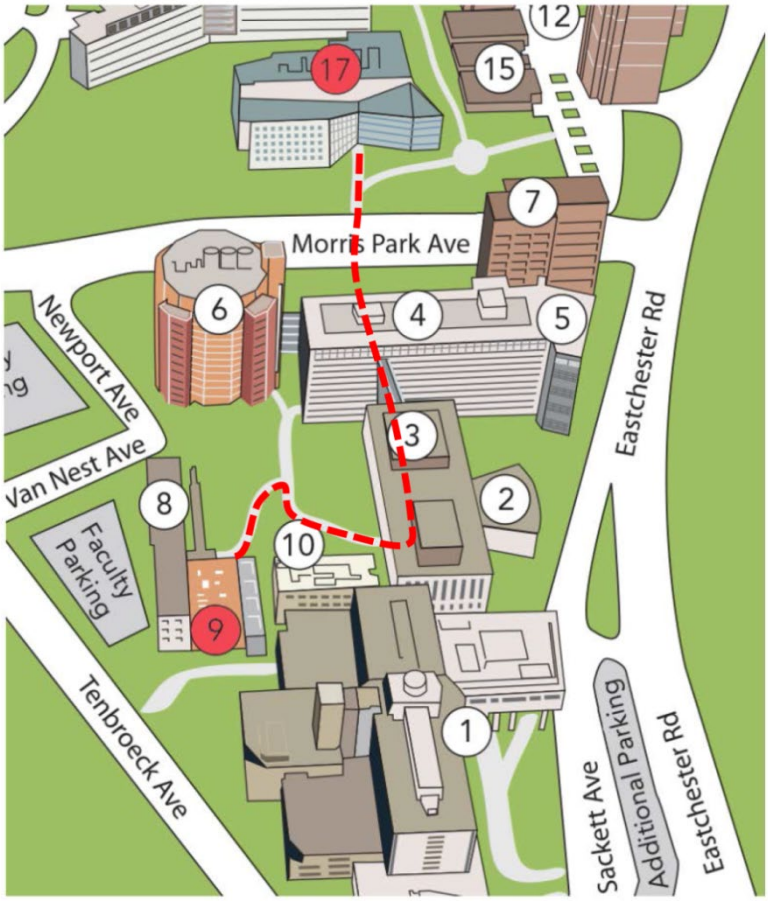

- **17** - Price Center
- **9** - Lubin Hall
- **Red line** - Path from Price Center to Lubin Hall

Abstracts

Abstract#	Title	Presenter	Affiliation
A001	Functional Expression of Mechanosensitive ion channels in regenerating axolotl Limbs	Vineel Kondiboyina	Northeastern University
A002	3D mechanical confinement directs muscle stem cell fate and function	GaYoung Park	Icahn School of Medicine at Mount Sinai
A003	Comprehensive single cell transcriptomics analysis of murine osteosarcoma uncovers SKP2 function in metastasis, genomic instability and immune	Ranxin Zhang	Montefiore-Einstein
A004	EXPERIMENTAL INVESTIGATION FOR DETERMINATION OF DEJ CHANGE IN DGI MICE	Sobhan Katebifar	UConn Health Center
A005	Trans-Signaling by Soluble CD14 Sensitizes Chondrocytes to Lipopolysaccharide Stimuli, Increasing Chondrocyte Inflammatory Responses	Anna E. Rapp	Division of Rheumatology, University of Pennsylvania
A006	Enhancing Drug Delivery to Bone Tumors via Convection: A Multiphasic Model	Eda Biricik	The City College of New York
A007	A Novel Platform to Interrogate Osteocyte Endocytosis with Intravital Imaging	Melia Matthews	Cornell University
A008	Changes in shape but not curvature: Distal femoral response to an introduction of bipedal walking in rats	Christopher O'Connor-Coates	Stony Brook University
A009	Characterizing Human Enthesis Development	Angel Moonilall	Icahn School of Medicine at Mount Sinai
A010	Determining the Role of Mechanosensitive PIEZO1 Ion Channel in Directing Skeletal Muscle Fibro-Adipogenic Progenitor Function	Kasoorelope (Soore) Oguntuyo	Icahn School of Medicine at Mount Sinai
A011	Treatment with Parathyroid Hormone Following a Single Bout of Loading Does Not Attenuate Post-Traumatic Osteoarthritis Progression	Ana Witkowski	Cornell University
A012	Evaluating the Role of Klotho Deficiency in Intervertebral Disc Health: No Evidence of Accelerated Degeneration in Mice	Veeraj Shah	Hospital of Special Surgery
A013	Effect of bisphosphonates on the middle ear ossicles in brittle bone disease	Maialen Ugarteburu	The City College of New York
A014	3D Bone Composition and Fiber Alignment at fracture sites to explain crack path	Aimar Silvan Ortubay	The City College of New York
A015	Intraoperative Second Harmonic Generation Imaging Diagnoses Acute Median Nerve Injury Linked to Long-term Dysfunction and Neuroma-	Christoph A. Schroen	Icahn School of Medicine at Mount Sinai
A016	Activation of Hedgehog Signaling in Fibroadipogenic Progenitors Causes Pseudoarthrosis	Ezgi Aydin	Hospital for Special Surgery
A017	Preliminary characterization of an *in vivo* model for investigating the role of mechanical tension on muscle stem cell behavior in regeneration	Josh Grey	Icahn School of Medicine at Mount Sinai
A018	Biomechanical Comparison of Glenohumeral Stability Before and After Superior Labrum Anterior-Posterior Tear and Repair versus Biceps Tenodesis	Aaron Teng-Hei Hui	Montefiore-Einstein
A019	Defining the epigenetic signature of fate reprogramming in ligamentocytes after joint injury in zebrafish	Safiyah Ali	Columbia University Irving Medical Center
A020	Dynamic Changes in Bone Cellular and Sub-Cellular Porosity Across Reproductive Phases in C57BL/6 Mice	Asier Muñoz	The City College of New York
A021	Differential Effects of Continuous Salt-Inducible Kinase Inhibition on Cortical and Cancellous Bone Responses to Mechanical Loading	Muyin (Mia) Huang	Cornell University
A022	Inhibition of Fibroblast Activation Protein Restores the Homeostatic Phenotype of Mechano-activated Synovial Fibroblasts	Elizabeth (Ellie) Bernstein	University of Pennsylvania
A023	A mouse model for study of mechanisms and alleviation of osteoarthritis (OA) pain	Giulia DiRaimo	Montefiore-Einstein
A024	Potential Role of Irisin in the Association of Diabetic Neuropathy with Bone Loss	Hassan Ainani	Montefiore-Einstein
A025	A New Mouse Model to Understand Pathogenesis of Heterotopic Ossification in Tendon	Julia Robbins	Icahn School of Medicine at Mount Sinai

Abstract#	Title	Presenter	Affiliation
A026	Microenvironment-specific transcriptomic changes in OS metastasis	Shimara Gunawardana-Zeigler	Montefiore-Einstein
A027	Investigating the role of mechanical stimulation in guiding stem cell activation and differentiation during scar-free ligament regeneration post-	Maryam Kamel	Columbia University Vagelos College of Physicians and
A028	Novel Analgesic ART26.12 as a Fatty Acid Binding Protein 5 Inhibitor for Osteoarthritic Pain	Kai Logan Bou	Stony Brook University
A029	A Multi-functional Small Molecule to Enhance Healing of Avascular Meniscus Tears	Meng Feng	Columbia University
A030	Elastin peptide-functionalized hydrogels support collagen production by bovine annulus fibrosus (AF) cells but are not conducive to cell proliferation	Sabrina Delva	The City College of New York/Icahn School of
A031	Characterization of ethanol post-treatment on collagen type I scaffolds for pathological tendon modelling	Katherine Arnold	UConn Health
A032	Gli1 Function in Intervertebral Disc Development	Andrew Parker Hallmark	Hospital for Special Surgery
A033	*WNT7A* mRNA-LNPs reduce skeletal muscle fibro-adipogenic progenitor adipogenesis	Larion Martin Santiago	Icahn School of Medicine at Mount Sinai
A034	*FiberO* for an Automated Quantification of Fibers Orientation and Organization in Biological Tissues	Julen Fernandez	The City College of New York
A035	Short-Term Immobilization Using Semi-Rigid Casting Improves Early Tendon-to-Bone Healing in a Murine Model of Anterior Cruciate Ligament	Yuki Suzuki	Hospital for Special Surgery
A036	Biomechanical Impact of Simulated Microgravity on Osteoblasts and Osteoclasts	Isaiah Taylor	Stony Brook University
A037	Elastin Collagen Nanovesicles – A Novel Platform for Targeted and Controlled Drug Delivery	Ann Thomas	University of Delaware
A038	Bone toughens during skeletal growth. A study on healthy and osteogenesis imperfecta mouse bone	Anxhela Docaj	The City College of New York
A039	Disparities in Education and Socioeconomic Status Are Associated with Increased Severity of Presentation of Early-Onset Blount Disease	Eduardo Valero-Moreno	Montefiore-Einstein
A040	Assessing The Relationship Between Spanish Language and Postoperative Outcomes	Jessica Chao	Montefiore-Einstein
A041	Presentation and Outcomes of Pediatric Patients with Osteochondral Defects of the Knee	Edmund Corcoran	Montefiore-Einstein
A042	AI Patient Resources for Lumbosacral Radiculopathy: An Objective Analysis of Available Materials	Michael Birnhak	Touro College of Osteopathic Medicine
A043	AI Patient Resources for Ankle Instability: An Objective Analysis of Available Materials	Rajwinder Singh	Stony Brook university
A044	The Sclerotic Hip Index in Patients with Sickle Cell Disease (SHIPS)	Hannah Kareff	Montefiore-Einstein
A045	Influence of CD4 Count on Three-Month and One-Year Surgical Outcomes of Total Joint Arthroplasty in HIV Patients	Vishal Shankar	Montefiore-Einstein
A046	Short-term outcomes and complications in patients treated with a knee implantable shock absorber (ISA) system.	Janet Hsu	Montefiore-Einstein
A047	Assessing Child Opportunity Index 2.0 as a Risk Factor for Patellar Dislocatio	Eliana Weinstein	Montefiore-Einstein
A048	Higher Distressed Community Index and Initial Fracture Treatment Outside of the United States Associated with Failure to Achieve Bone Union Within 12	Morgan Roche	Montefiore-Einstein
A049	Disparities in Education and Socioeconomic Status Are Associated with Increased Severity of Presentation of Early-Onset Blount Disease	Eduardo Valero-Moreno	Montefiore-Einstein
A050	Predictors of Quality of Life After Pediatric Anterior Cruciate Ligament Reconstruction: A Longitudinal Analysis of Knee Injury and Osteoarthritis	Zachariah Samuel	Montefiore-Einstein

Abstract#	Title	Presenter	Affiliation
A051	Unicompartmental Knee Arthroplasty or Total Knee Arthroplasty? An Analysis of Randomized Controlled Trials Utilizing Dichotomous and	Adriano Cuadros	Icahn School of Medicine at Mount Sinai
A052	Socioeconomic Disadvantage Predicts Decreased In-Hospital Ambulation After Hip Fracture Surgery	Brandon Wang	Montefiore-Einstein
A053	Union rate of pathologic fractures sustained in patients with metastatic bone disease: a retrospective study	Dylan Horan	Montefiore-Einstein
A054	Impact of Patient Matched Constitutional Alignment on the Early Clinical Outcomes of Robotic-Assisted Total Knee Arthroplasty	Carlos Salazar	Montefiore-Einstein
A055	Analysis of Comorbidities and Short-Term Complication Risk in Diabetic Patients Undergoing Peripheral Nerve Neuroplasty	Lekha Yaramada	Stony Brook Renaissance School of Medicine
A056	Orthopedic Injuries Among Adults Associated with Electric Skateboard Use	Rachel Katz	Montefiore-Einstein
A057	Impact of Surgical Timing on Complications in Pediatric Ankle ORIF: A Retrospective Analysis of Socioeconomic Factors and Outcomes	Andrea Muñoz	Montefiore-Einstein
A058	A Classification System of Trochlear Dysplasia Severity Utilizing the Sulcus Angle	Jason Brenner	Montefiore-Einstein
A059	Molecular heterogeneity within an untreated osteosarcoma following upfront surgery	Sung-Suk Chae	Montefiore-Einstein
A060	Using percutaneous microfracture induced bone healing in the treatment of unicameral bone cyst in pediatric patients	Sara Orr	Montefiore-Einstein
A061	Post-Pandemic Disparities in Access to Care Among Ankle Fracture Patients	Mohammed Bashier	Montefiore-Einstein
A062	Proinflammatory Cytokines Are Expressed In Bone After Rotator Cuff Tears	Dylan Horan	Montefiore-Einstein

Functional Expression of Mechanosensitive ion channels in regenerating axolotl Limbs

Vineel Kondiboyina (1), Melissa Miller (2), James R. Monaghan (2), Sandra J. Shefelbine (1,3)

(1) Dept. of Bioengineering, Northeastern University, Boston, MA, USA
(2) Dept. of Biology, Northeastern University, Boston, MA, USA
(3) Dept of Mechanical and Industrial Engineering, Northeastern University, Boston, MA, USA

Abstract:

Background: Axolotls possess unparalleled regenerative abilities, distinct from most mammals, enabling full limb regeneration that parallels mammalian limb development. In mammalian limb development, mechano-sensitive channels like TRPV4, PIEZO1, and PIEZO2 play crucial roles in guiding cell fate through mechanical cues. The roles of mechanosensitive ion channels in axolotl limb regeneration remain unexplored. This study investigates the expression of mechanosensitive ion channels, specifically TRPV4, PIEZO1, and PIEZO2, during axolotl limb regeneration.

Methods: Single-cell RNA sequencing, Chain Reaction Fluorescence In-Situ Hybridization, and Immunofluorescence, were employed to assess the mRNA and protein expression of TRPV4 and PIEZO1/2 ion channels in regenerating axolotl tissues at three different timepoints representing early and late blastema stages, as well as fully grown limb tissues serving as positive controls.

Results: As expected, TRPV4 and PIEZO2 exhibited mRNA and protein expression in mature cartilage, while PIEZO1 showed low to undiscernible expression, in contrast to observations in mammalian cartilage. TRPV4 and PIEZO2 were highly expressed in blastemal cells both at transcriptional and protein levels during both early and late regeneration stages, with increased expression noted in the condensing mesenchyme during the late blastema stage. Conversely, PIEZO1 mRNA was not consistently detectable in the blastema.

Conclusions: This study establishes the presence of mechanosensitive ion channels TRPV4, PIEZO1, and PIEZO2 in regenerating axolotl limb blastemas, with differential expression observed across distinct regeneration timepoints.

Significance: These findings emphasize the potential role of mechanical cues in the regeneration process. Future studies will explore the functional roles of these channels in mechanotransduction and calcium signaling, providing insights into how mechanical forces may influence limb regeneration and guiding potential advancements in regenerative medicine.

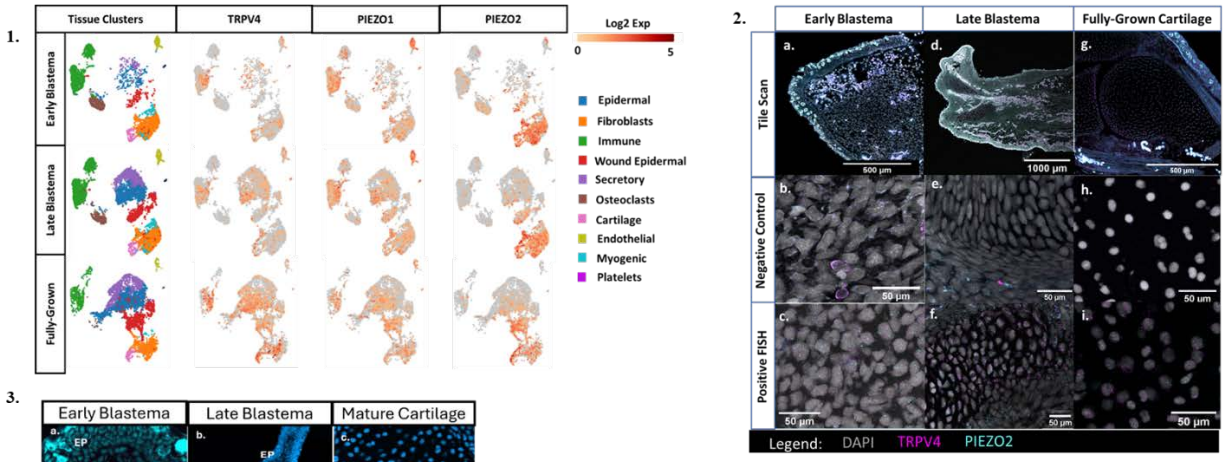

Figure 1: Single Cell RNA data organized by regeneration timepoint, and trpv4, piezo1 and piezo2 expression.

Figure2: Chain Reaction Fluorescence In-Situ Hybridization mRNA expression of trpv4 and piezo2 during limb regeneration at early (a-c) and late stage (d-f) blastema, and fully-grown cartilage (g-i)

Figure 3: Immunofluorescence Protein expression of TRPV4 AND PIEZO2 (a-c). Negative controls (d-f) TRPV4 expression (g-i) PIEZO2 expression in early and late blastema, and mature axolotl cartilage. Cyan stains for the nucleus and magenta stains for the presence of TRPV4/ PIEZO2 ion channels. EP: Epithelium, BL : De-differentiated Blastemal cells, CM: Condensed Mesenchyme

3D mechanical confinement directs muscle stem cell fate and function

GaYoung Park[1], Josh A. Grey[1], Foteini Mourkioti[2], Woojin M. Han[1]

1. Department of Orthopaedics, Icahn School of Medicine at Mount Sinai
2. Department of Orthopaedic Surgery, Perelman School of Medicine, University of Pennsylvania

Introduction: Muscle stem cells (MuSCs) are essential for skeletal muscle regeneration, responding dynamically to their niche's physical and mechanical properties. During the regeneration process, the MuSC niche undergoes dimensional changes, shifting between two-dimensional (2D) and three-dimensional (3D) environments that impose varying degrees of mechanical confinement. While previous studies have focused on the role of stiffness in 2D systems (1,2,3), the impact of 3D confinement on MuSC function remains unknown. This study explores how 3D confinement and stiffness regulate MuSC behavior, particularly their effects on stemness, activation, proliferation, and differentiation.

Brief Statement of Methods: We engineered a 3D asymmetric hydrogel bilayer platform with tunable confinement and stiffness to replicate the dynamic MuSC niche during muscle regeneration. To fabricate the hydrogel, multi-arm PEG-norbornene conjugated with cell-adhesive RGD peptide was photopolymerized. By varying the concentration of the thiol-flanked crosslinker, hydrogels with diverse mechanical properties, specifically stiffness, were produced (**Fig. 1 A, B**). MuSCs were isolated from *Pax7*EGFP reporter mice (4), where EGFP is directly driven by *Pax7* expression, and cultured in either confined 3D or unconfined 2D environments. To mimic the biophysical conditions of MuSCs, these cells were positioned at the interface of the 3D bilayer hydrogel (2D mimics the ghost fiber environment; 5/12 kPa represents a soft regenerating asymmetric niche; 12/12 kPa represents a homeostatic asymmetric niche; 35/12 kPa represents a stiff regenerating niche) (**Fig. 1 C, D**). We tracked MuSC behavior over time, assessing *Pax7* expression, MyoD and Myogenin levels, nuclear size, and H4K16ac—a marker of chromatin accessibility. Comparisons were made between soft, intermediate, and stiff 3D environments to investigate the role of varying mechanical cues on MuSC function.

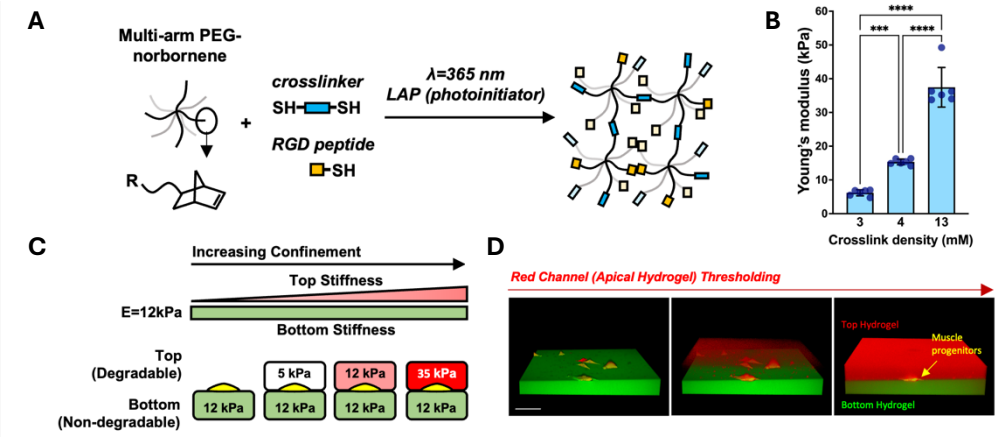

Figure 1. Facile assembly of 3D bilayer hydrogel system. (A) Schematic of multi-arm PEG-norbornene hydrogel. (B) Young's modulus of hydrogel as a function of crosslink density. n=6 hydrogels. *** p<0.001, **** p<0.0001 via 1-way ANOVA with Tukey's post-hoc tests. (C) Schematic of bilayer hydrogel conditions. (D) 3D-reconstructed confocal micrograph demonstrating sandwiched muscle progenitors between two hydrogel layers. Scale bar: 100 µm.

Results: The proliferation of muscle stem cells (MuSCs) in 3D confinement was reduced compared to cells cultured in 2D environments. 3D confinement promoted MuSC *Pax7*EGFP expression over 5 days. 3D confinement significantly delayed activation, as indicated by MyoD staining, and differentiation, as indicated by Myogenin staining, assessed on days 3 and 5. MuSCs in confined conditions displayed smaller nuclei and lower levels of H4K16ac, suggesting reduced chromatin accessibility. In contrast, MuSCs in unconfined environments exhibited larger nuclei, higher proliferation rates, and more rapid differentiation, alongside increased H4K16ac expression on days 3 and 5. These findings indicate that mechanical confinement may slow MuSC commitment and maintain stemness, likely by modulating their epigenetic state and influencing gene expression and differentiation pathways.

Conclusions: Our findings demonstrate that 3D confinement delays MuSC activation, proliferation, and differentiation, promoting the maintenance of stemness. The suppression of chromatin accessibility through reduced H4K16ac levels in confined environments suggests a mechano-epigenetic mechanism by which physical constraints regulate MuSC function. These insights highlight the importance of 3D mechanical cues in directing MuSC fate decisions and provide a new understanding of the role of confinement in muscle regeneration.

Significance: This study reveals how 3D mechanical confinement in the MuSC niche during regeneration regulates stem cell function by acting as a brake on activation and differentiation. By modulating nuclear size and chromatin accessibility, confinement maintains MuSC stemness and limits proliferation, offering new insights into the mechano-epigenetic control of muscle regeneration. These findings have broad implications for understanding stem cell behavior in tissue regeneration and could inform the development of therapeutic strategies targeting the mechanical environment of stem cells in disease and aging.

Reference: [1] Gilbert et al. Science, 2010. [2] Silver et al. Science Advances, 2021. [3] Madl et al. Biomaterials, 2021. [4] Tichy et al. Skeletal Muscle, 2018.

**This work has been posted to BioRxiv: Park et al. "3D mechanical confinement directs muscle stem cell fate and function," BioRxiv, 2024.*

Comprehensive single cell transcriptomics analysis of murine osteosarcoma uncovers SKP2 function in metastasis, genomic instability and immune activation

Ranxin Zhang[1], Alexander Ferrena[2], Jichuan Wang[1], Sung-Suk Chae[1], Hasibagan Borjihan[1], Rui Yang[1], David Geller[1], Deyou Zheng[2], Bang Hoang[1]

1 Department of Orthopedic Surgery, Montefiore Medical Center, Albert Einstein College of Medicine, Bronx, New York, United States
2 Institute for Clinical and Translational Research, Albert Einstein College of Medicine, Bronx, New York, United States

Objective

Osteosarcoma (OS) is the most common primary pediatric bone malignancy. One promising new therapeutic target is SKP2, encoding a substrate recognition factor of the SCF E3 ubiquitin ligase responsible for ubiquitination and proteasome degradation of substrate p27, thus driving cellular proliferation. We have shown previously that knockout of Skp2 in an immunocompetent transgenic mouse model of OS improved survival, drove apoptosis, and induced tumor inflammation. However, tumor formation is not totally blocked after Skp2 disruption. We wish to study the underlying mechanism of this survival benefit and Skp2 function loss escape.

Methods

We applied single-cell RNA-sequencing (scRNA-seq) to study primary OS tumors derived from Osx-Cre driven conditional knockout of Rb1 and Trp53 (DKO). We further compared this model with OS models with functional disruption of Skp2: one with Skp2 knockout(TKO) and the other with the Skp2-p27 interaction disrupted (DKOAA, resulting in p27 overexpression).

Results

We showed that murine OS models recapitulate the tumor heterogeneity and microenvironment complexity observed in patient tumors. We found reduction of T cell exhaustion and upregulation of interferon activation, along with evidence of replicative and endoplasmic reticulum-related stress in the Skp2 disruption models, and showed that interferon induction was correlated with improved survival in OS patients. Additionally, our scRNA-seq analysis uncovered decreased activities of metastasis-related gene signatures in the Skp2-disrupted OS, which we validated by observation of a strong reduction in lung metastasis in the Skp2 knockout mice. Finally, we report several potential mechanisms of escape from targeting Skp2 in OS, including upregulation of Myc targets, DNA copy number amplification and overexpression of alternative E3 ligase genes, and potential alternative lineage activation.

Conclusion

These mechanistic insights into OS tumor biology and Skp2 function suggest novel targets for new, synergistic therapies, while the data and our comprehensive analysis may serve as a public resource for further big data-driven OS research.

ABSTRACT #04

EXPERIMENTAL INVESTIGATION FOR DETERMINATION OF DEJ CHANGE IN DGI MICE

Sobhan Katebifar (1), Kai Clark (1), Bradley S. Rosenberg (2), Michael Truhlar (2), Alix C. Deymier (1)
(1) Biomedical Engineering, UConn Health, Farmington, CT (2) School of Dental Medicine, UConn Health, Farmington, CT

INTRODUCTION: Dentinogenesis Imperfecta (DGI) is an inherited disorder affecting dentin and enamel [1]. DGI type I, associated with COL1A1 or COL1A2 mutations, causes translucent or discolored teeth, rapid enamel loss, and increased tooth wear [2]. Understanding of the structural and mechanical causes of tooth attrition in DGI, particularly at the Dentin-Enamel Junction (DEJ), is limited. The DEJ, the interface that connects dissimilar dentin and enamel, has a graded structural design that minimizes stress concentrations in healthy teeth, making it fracture-resistant [3]. Enamel loss in DGI is suggested to originate from or near the compromised DEJ [4]. This study aims to elucidate the murine DEJ's structure and composition in relation to DGI type I, utilizing Micro-Computed Tomography (µCT), high-resolution Raman Spectroscopy mapping, and Scanning Electron Microscopy (SEM) for analysis.
METHODS: Tooth Acquisition & Sample Preparation: The Col1a2oim mouse (OIM) was used as a model for DGI. Age-matched wild-type (WT) littermates served as controls. At 12 weeks of age, 20 OIM and 20 WT mice were sacrificed for analysis of their upper and lower molars. The lower right molars (n=5 per group) underwent µCT scanning without additional preparation. The left lower molars (n=5 per group) were embedded and polished for Raman spectroscopy. A subset of embedded samples (n=3 per group) underwent acid etching before SEM imaging. **µCT:** The thawed tooth samples were examined with Scanco 50 µCT system. Attenuation coefficients (AC) across the DEJ of all teeth were determined and gradients in the AC, which is correlated to tissue density, were fit with a logistic function. The full-width half max (FWHM) of the derivative of the logistic function was used to determine the gradient width. **Raman spectroscopy:** Raman spectra were acquired over a 15x15 µm area across the DEJ using a Witec Alpha 300 Raman Spectrometer. The 960 cm^{-1} PO_4^{3-} peak FWHM and intensity were determined using Lorentzian fitting and plotted as a function of position. Gradients in peak FWHM, which inversely correlates to crystallinity, and peak intensity, which correlates to mineral content, were fit with logistic functions. Gradient widths and locations were determined from the FWHM and peak center of the logistic function derivative. **SEM imaging:** After gold sputtering, SEM imaging was conducted on acid etched (n=3) and unetched samples (n=3) using a TENEO LVSEM device. Using ImageJ software, DEJ structural widths were measured for unetched samples, while acid-etched samples were used for mantle dentin width. SEM images were filtered and thresholded for tubule analysis using ImageJ, and porosity was calculated based on tubule count and diameter.
RESULTS: **DEJ gradient widths:** The average density gradient width across the DEJ was not statistically different between DGI (44.26±2.2 µm) and WT (40.32±1.3 µm) samples. Raman spectroscopy revealed a larger mineral content gradient in OIM males (16.1±4.5 µm) compared to WT males (10.2±3.4 µm), irrespective of DGI status. The mineral crystallinity gradient (inverse FWHM of PO_4^{3-} v_1 peak) averaged 17.6±3.9 µm, with no significant differences based on sex or DGI status. **Structural properties:** Etching revealed a unique zone between enamel and dentin termed the structural DEJ. DGI mice showed a broader structural DEJ compared to WT (Fig. 1). In DGI females there was a significant increase in the number of tubules per area in DGI molars compared to WT. Conversely, the greatest mean diameter belongs to the WT males while the smallest value is for WT males. Although the number of dentinal tubules is greater in DGI mice than in WT, the diameter of the tubules is smaller; as a result, the total porosity remains unchanged as a function of both DGI status and sex. The average value of mantle dentin width is significantly greater in DGI versus WT molars (Fig. 2).

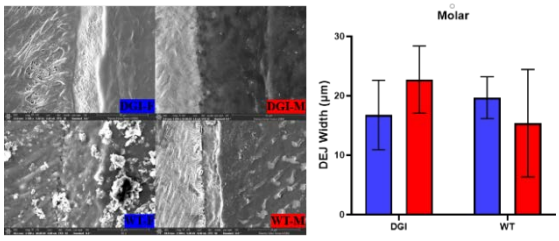

Figure 1: DEJ width as measured by SEM (SE). Male=red, female=blue.

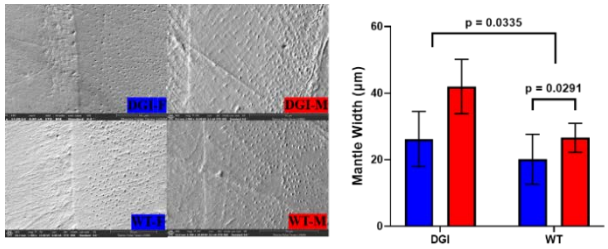

Figure 2: Mantle dentin measured by SEM (BSE). Male=red, female=blue.

DISCUSSION: This study shows that the DEJ structure and composition is affected both by DGI and sexual dimorphism. Density gradient widths were unaffected by either factor but agreed with other studies [5]. However, Raman and SEM indicated that the gradients in crystallinity, mineral content, and structural features were significantly smaller in compare to other studies, suggesting that the DEJ exhibits multiple overlapping graded structures. The DEJ width as measured by SEM or mineral content was significantly lower in the male mice than the females. This could possibly contribute to the higher diagnosis of DGI in men. Although DGI had minimal effects on DEJ width, it had significant effects on the dentin. We found significantly more dentinal tubules in DGI teeth compared to wild types; however, the size of the tubules was reduced in the DGI mice. Finally, the mantle dentin, a thin layer found between the DEJ and the dentin, was significantly thinner in DGI mice compared to WT. This drastic change may be responsible for the higher mechanical failure of DGI teeth; however, little is known about the mechanical role of mantle dentin [6]. This provides an entirely new insight into the compositional and structural features that may be critical to controlling tooth mechanics in conditions such as DGI.
REFERENCES: [1] Barron, M.J., et al., 2008. [2] Andersson, K., et al. 2017. [3] Imbeni, V., et al., 2005. [4] Verdelis, K., et al., 2016. [5] Fong, H et al., 1999. [6] Goldberg, M. et al., 2011.

Trans-Signaling by Soluble CD14 Sensitizes Chondrocytes to Lipopolysaccharide Stimuli, Increasing Chondrocyte Inflammatory Responses

Anna E. Rapp[1,2], Baofeng Hu[1,2], Carla R. Scanzello[1,2]

[1] *Division of Rheumatology, Perelman School of Medicine, University of Pennsylvania;*

[2] *Translational Musculoskeletal Research Center, Philadelphia Veterans Affairs Medical Center; Philadelphia, PA, USA.*

The understanding of osteoarthritis (OA) has evolved significantly over the past decade. Recently attention is being drawn to the role of pattern-recognition receptor (PRR) signaling in chondrocytes. In OA, chondrocytes face a pro-inflammatory environment, influenced by various soluble factors within the synovial fluid, which includes both known and potential PRR ligands. Studies have identified elevated concentrations of lipopolysaccharide (LPS) and its soluble co-receptor CD14 (sCD14) within the synovial fluid of OA patients, correlating with disease severity. The interaction of (s)CD14 with LPS facilitates binding of LPS to its receptor TLR4, thereby sensitizing certain cell types and allowing them to respond to lower ligand concentrations. However, if sCD14 has a similar trans-activating effect on chondrocytes has never been tested. In this study, we aimed to investigate the responsiveness of chondrocytes to TLR4 stimulation by LPS, and test whether sCD14 amplifies their response, as previously observed in fibroblasts.

We exposed human chondrocyte-like cells (cell line C28/I2, Merck Millipore) to varying concentrations of LPS (1 ng to 1 µg/ml; Ultrapure LPS, InvivoGen), both with and without the addition of recombinant soluble hCD14 (2 µg/ml; R&D Systems). A control group with no LPS was included. We evaluated the activation of the NFκB signaling pathway through western blot analysis after 30 and 60 min of incubation and assessed the expression of pro-inflammatory and catabolic genes via RT-qPCR after 24 hours. Statistical analysis was performed using 2-way ANOVA followed by Dunnet's post-hoc test.

We observed both a concentration and time-dependent effect of LPS ± CD14 stimulation on chondrocytes. When stimulated with LPS, we observed a significant up-regulation of NFκB activation only after 60 min when cells were exposed to 100 and 1,000 ng/ml. However, when we added CD14, NFκB was significantly induced after 30 min in presence of 1,000 ng/ml LPS (Fig. 1A) and activation was significantly enhanced by sCD14 addition after 60 min incubation (Fig. 1B). Gene expression analysis revealed a significant up-regulation of IL-8 starting from 10 ng/ml LPS, with further significant elevation upon addition of sCD14 (Fig. 2A). Similar effects were observed for MMP13 expression in the presence of both 10 and 100 ng/ml LPS combined with CD14 (Fig. 2C). IP-10 expression was significantly enhanced by sCD14 when cells were stimulated with 100 ng/ml LPS (Fig. 2B).

In conclusion, our findings demonstrate a robust pro-inflammatory response of chondrocytes to LPS stimulation, which is potentiated by the addition of sCD14. sCD14 had a sensitizing effect, resulting in augmented and earlier activation of chondrocytes to LPS, as evidenced by NFκB activation and increased expression IL-8, IP-10 and MMP13. Notably, IP-10 expression suggests the activation of TRIF-dependent TLR-signaling in chondrocytes, a novel finding in this context that will be explored in future studies. Overall, our study sheds light on the previously unexplored role of CD14 trans-signaling in OA pathology, with direct implications for chondrocyte function in the inflammatory milieu of the osteoarthritic joint.

Enhancing Drug Delivery to Bone Tumors via Convection: A Multiphasic Model

Eda Biricik[1], Michelle J. Gelbs[1], Gene R. DiResta[2], Pat B. Zanzonico[3], John H. Healey[3], Susannah P. Fritton[1]
[1]*Department of Biomedical Engineering, The City College of New York, New York, NY*
[2]*Microflow Associates, Pleasantville, NY*
[3]*Memorial Sloan Kettering Cancer Center, New York, NY*

Introduction

Bone is a preferable site for metastasis, especially for breast, prostate, and lung cancers [**1**], and skeletal-related events (e.g., pain and fracture) can greatly reduce the quality of life for patients with bone metastases. Within the tumor microenvironment, there is increased interstitial fluid pressure that hinders fluid flow and consequently drug delivery to the tumor [**2**]. Our lab has shown that controlled cyclic loading can increase the uptake of radiolabeled tracers to tumors in rat bone, and poroelastic finite element (FE) analysis has demonstrated that applied mechanical loading can overcome the increased tumor interstitial pressure and induce convective fluid flow within the tumor [**3**]. The amount of solute delivered to tumor is a function of fluid flow and solute-solvent molecular interaction; however, poroelastic analysis does not model the solute-solvent interactions. Multiphasic models allow the inclusion of solutes and can compute solute concentration [**4**]. In this study, we used a multiphasic model to compute interstitial fluid flow within an idealized tumor-bearing tibia under physiological compression without incorporating solutes and created a baseline for more refined future models.

Methods

The multiphasic analysis was conducted using FEBio software. The geometry of the idealized tumor-bearing tibia was obtained from a previous study, where characteristic dimensions of tumor-bearing tibia were measured (n=6) and averaged based on in vivo micro-PET/CT scans of human breast cancer cell (MDA-MB-231)-injected nude female rats [**3**]. Material properties utilized in the multiphasic model are shown in **Table 1**. A physiological displacement curve was defined on the proximal surface, utilizing cubic polynomial interpolation, where the maximum displacement was 0.1% (1000 microstrain) applied at 2 Hz. The z-axis displacement for all distal surface nodes and x- and y-axis displacement for nine central nodes were constrained to restrict translation. Increased tumor interstitial fluid pressure was modeled as a prescribed fluid pressure of 40 mmHg (~5.3 KPa) at tumor core nodes [**5**]. Cortical bone, bone marrow/ cancellous bone, and tumor were modeled as three separate objects, and they interacted only through interfaces where two objects were in contact (i.e., contact surfaces). Tied-multiphasic contact was introduced between objects, which restricts sliding with respect to each other and ensures continuous contact traction (i.e., contact stress) and fluid flux. Every other surface except contact surfaces were defined as impermeable (i.e., no fluid flux).

Results

Increased fluid pressure in the tumor core caused outward interstitial fluid flow from the tumor when no compression was applied to the bone. The physiologically relevant applied strain reversed the outward flow and led to convective interstitial fluid flow into the tumor, with a maximum fluid flux of 0.84 µm/s (**Fig. 1**); the inward fluid flux due to the applied compression was greater than the tumor-pressure induced outward flux.

Discussion

This multiphasic model of an idealized tumor-bearing tibia showed that physiological compression of the bone can reverse the outward flow of interstitial fluid typically caused by high interstitial pressure within the tumor. This reversal leads to convective fluid flow into the tumor, highlighting the potential of mechanical loading to improve drug transport. In future studies, we will expand this model by incorporating solutes of varying molecular sizes and analyzing drug transport under different loading conditions. The impact of tumor location and bone pathologies (e.g., cortical bone disruption) on drug transport will also be explored using this model. Ultimately, this research seeks to improve understanding of how drugs are transported within bone tumors to develop better treatment strategies for bone metastasis.

References

[1] Weilbaecher et al. Nat. Rev. Cancer 2011; [2] Nia et al. Science 2020; [3] Guerra et al. Trans. ORS 2024; [4] Mauck et al. J. Biomech. Eng. 2003; [5] Zachos et al. Clin. Orthop. Relat. Res. 2001.

Table 1. Material properties of multiphasic solid objects were chosen based on the previous poroelastic finite element analysis conducted in our lab [**3**].

Material Properties	Bone	Marrow/ Cancellous bone	Tumor
Solid fraction	0.96	0.20	0.80
Young's modulus (MPa)	17E+03	2.0	4.5E-03
Poisson's ratio	0.325	0.167	0.260
Permeability (mm^4/Ns)	630	0.01	0.59

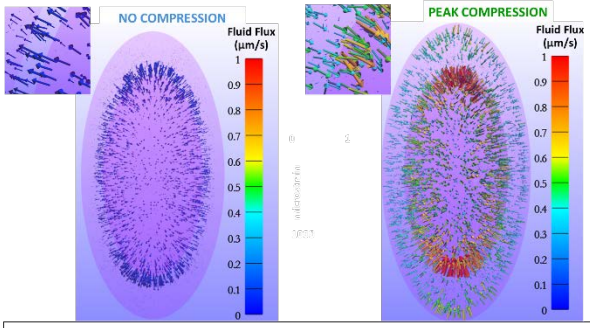

Figure 1: Distribution of fluid flux vectors in tumor compartment in no compression **(left)** and at peak 0.1 % compression **(right)** conditions.

ABSTRACT #07

A Novel Platform to Interrogate Osteocyte Endocytosis with Intravital Imaging

Melia D. Matthews[1], Nuzhat Mukul[1], Alexander Saffari[1], Nada Naguib[1], Ulrich B. Wiesner[1], Karl J. Lewis[1]

[1]*Cornell University, Ithaca, NY*

Osteocytes use transmembrane proteins to mediate mechanotransduction during physiological fluid flow stimulation and contribute to skeletal homeostasis[1]. Transmembrane proteins like integrins are maintained via endocytosis and are dynamically trafficked and recycled in numerous cell types *in vitro*[2]. However, to our knowledge, there has been no systematic study of endocytosis in osteocytes. We previously validated the use of functionalizable fluorescent nanoparticles as a novel *in vivo* tool for studying osteocyte uptake dynamics[3]. Here, we report use of this platform to test the hypothesis that pharmacological perturbation of dynamin or cholesterol, components affecting distinct endocytic-mechanisms, impairs uptake and trafficking of nanoparticles in osteocytes *in vivo*.

Isoflurane anesthetized C57BL/6J mice (16-18weeks, M/F) were injected subcutaneously above the third metatarsal (MT3) with Dyngo-4a to disrupt dynamin (Abcam), Methyl-β-cyclodextrin to disrupt cholesterol (Sigma), or PBS control for 30 minutes. Silica nanoparticles with Cy5 dye (C'Dots), created as previously described[4], were then injected and incubated for either a short (5 minute) or a long (45 minute) period. We tested PEGylated (control), RGD functionalized (integrin-targeted), and membrane penetrating TAT-functionalized (positive control) C'Dot types. The MT3 was then surgically isolated, stabilized, and submerged in a PBS bath in preparation for imaging. Fluorescent C'Dot signal was observed using 2-photon *in vivo* microscopy (ThorLabs). Ten 35µm z-stacks were taken over 30 minutes (short) or 2.5 hours (long) at 1090nm. Number of osteocytes with C'Dot signal was quantified in ImageJ (NIH) using 3D cell segmentation. 2-Way ANOVAs between drugged and control data were run on GraphPad Prism software (Error bars = SEM, *p≤0.05).

Dyngo4a administration impacted integrin-targeted C'Dots, but not PEG or TAT, as indicated by 2-Way ANOVAs. Males had a higher cell count while females had lower compared to control, suggesting a sexually dimorphic role for dynamin in integrin endocytosis. MβCD increased long-term uptake across PEG and RGD C'Dots, with males and females displaying improved signal retention. Interestingly, MβCD reduced uptake and slope in TAT positive control groups, indicating that the impact of cholesterol perturbation does not depend on C'Dot functionalization. Our platform is a novel method to interrogate and perturb cellular endocytosis *in vivo* and can be translated to other tissues. Sexual dimorphism in endocytosis is also a novel paradigm that deserves attention within the field.

1) Thi+ *PNAS* (2013). 2) Moreno-Layseca+ *Nat Cell Bio* (2019). 3) Matthews+ *Bone* (2023). 4) Erstling+ *Adv Materials* (2021).

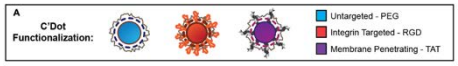

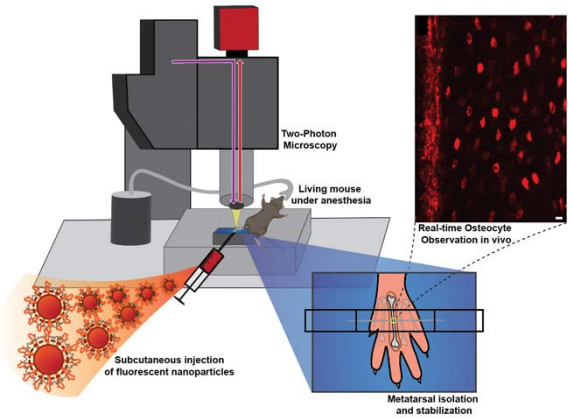

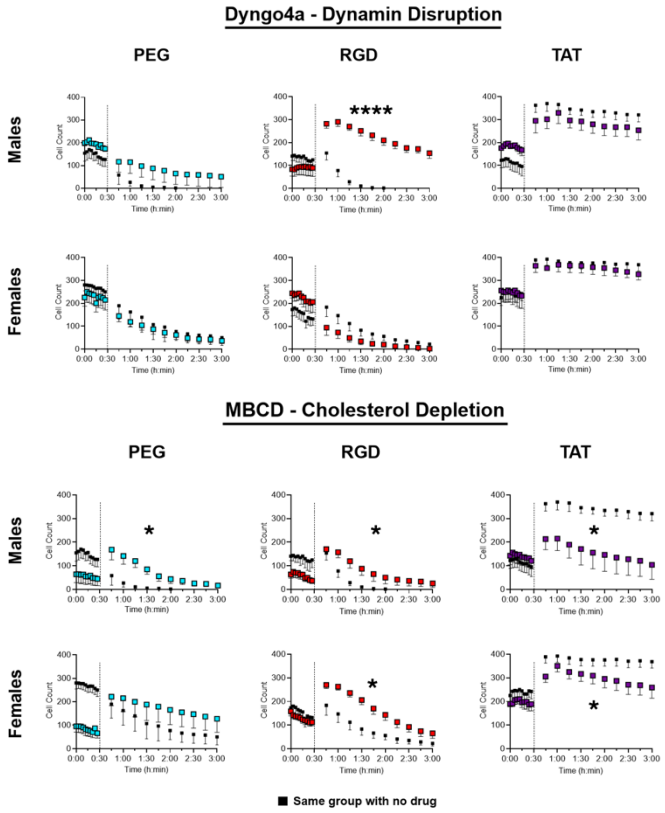

Changes in shape but not curvature: Distal femoral response to an introduction of bipedal walking in rats

Christopher O'Connor-Coates[1], David E. Komatsu[2], Christopher J. Percival[1]

[1]Stony Brook University Department of Anthropology, Stony Brook, NY, [2]Stony Brook University Department of Orthopaedics and Rehabilitation, Stony Brook, NY

INTRODUCTION: Chondral modeling theory (CMT) hypothesizes that consistent cyclic loading of a joint surface will result in the flattening of the condylar curve as a mechanism to maintain joint congruency. In humans, distal femur epiphyseal shape and flattened, elliptical femoral condyles are hypothesized to be adaptive responses to bipedal locomotion that improved knee joint function while maintaining congruency. Notably, children develop flatter femoral condyles in conjunction with the acquisition of bipedal walking, indicating that bipedal locomotion itself may contribute to these morphologies. However, the effects of changes in joint biomechanics, as brought about by an introduction of bipedalism, upon epiphyseal shape remain largely unresolved. We evaluated if distal femoral shape responds plastically to novel loading patterns generated by an introduction of bipedal exercise in rats when compared to quadrupedal controls. We hypothesized that the lateral femoral condyle (LFC) curvature of rats would become distally flatter and anteroposteriorly longer in response to an introduction of bipedal load compared to unexercised controls.

METHODS: We placed 17 anatomical and 80 curve-defining landmarks on femora from 20µm resolution CT scans of 4 juvenile female Sprague Dawley rats that were forced to walk bipedally on a treadmill for 1 hour per day for 12 weeks, as well as the femora from 5 unexercised controls. The CT images were collected at Penn State University at 160kV and 70µA with a 0.2mm aluminum filter. We identified 6 landmarks and estimated 60 sliding curve semilandmarks along the anterior and posterior aspects of the lateral and medial condylar surface curves. Procrustes superimposition and ANOVA quantified the impact of experimental group (Biped, Control) and centroid size on femoral shape. LFC curve lengths were calculated as the sum of the linear distances between the anatomical and semilandmarks along the curves. Distal LFC curvature flatness was estimated as the sagitta of the arc for the anterior and posterior aspect of the curve, and for the entire curve. All length measures were standardized by centroid size (CS) as an estimate of individual scale and were tested for significance via Wilcoxon Rank Sum tests.

RESULTS: Bipedal exercise resulted in a significant effect on distal femoral shape ($p = 0.02$), including relatively wider condylar flaring in the mean posterior epiphyseal shape. No significant differences in LFC curvature length relative to CS (anterior length $p = 0.56$, posterior length $p = 0.91$, total length $p = 0.29$) or sagitta of the distal curvature relative to CS (anterior curve $p = 0.29$, posterior curve $p = 0.91$, total curve $p = 0.41$) were identified between experimental groups.

CONCLUSION: The significant epiphyseal shape change could be a response following CMT, as wider flaring may indicate an expansion of the articular surface. Our analyses did not identify significant differences in LFC curvature length or sagitta length. As such, the epiphyseal shape change is not associated with differences in the length or LFC curve angulation. Thus, identifying a significant contributing factor, increased articular cartilage proliferation, and concomitant increased ossification would be required to confirm a differential chondral modeling pattern is occurring in the bipedally exercised rats. The lack of significant difference in the curvature measurements could affect how we understand the response of joints to novel loading conditions, like during changes in gait pattern and conditions where joint biomechanics are altered, such as osteoarthritis and joint injuries. Importantly, our findings could be due to limitations of the model, and assessing the effects of differential loading periods could provide more insight into developmental influences on femoral morphology. Regardless, our results indicate that the development of the distal femoral epiphysis is a complex process with limited ability to respond to external forces. We plan to expand our sample size and include comparative groups of rats forced to exercise quadrupedally or stand on their hindlimbs for 1 hour per day to further parse out the effects of bipedal load from exercise. We also plan to conduct similar morphological measurements upon the medial femoral condyle to determine the effects of introducing bipedal loading here.

SIGNIFICANCE: Prior research has hypothesized that the development of a flat LFC curvature in humans knee joints is a mechanism to maintain congruence during the acquisition of bipedal locomotion in early childhood. Clinically, our results could indicate that certain joint surfaces may have a predetermined shape that does not easily adapt to new loading conditions, which is important in understanding how joints might respond, or fail to respond, to altered biomechanics arising from congenital disorders, injuries, surgery, or changes in activities.

ACKNOWLEDGEMENTS: Thanks to Adam Foster for sharing his samples and insight; Thanks to America Campillo and Tim Ryan for sharing CT scans.

ABSTRACT #09

Characterizing Human Enthesis Development

Angel Moonilall[1], Saswati Kar[1], Dylan Gordon[1], Damien Laudier[1], Fei Fang[1]
[1]Leni and Peter W. May Department of Orthopaedics, Icahn School of Medicine at Mount Sinai, New York, NY

Disclosures: None

Introduction: The enthesis is a fibrocartilaginous connective interface and plays a crucial role by transferring mechanical force in different joints (i.e., shoulders) during movement [1-2]. This interface at the rotator cuff is particularly susceptible to injury and unfortunately, cannot regenerate naturally [1-3]. To guide the development of better treatments, significant progress has been made in exploring the mechanisms underlying rotator cuff development and etiology using mouse models [4-7]. However, the knowledge gap in conservation and divergence of these processes between mouse and human remains a crucial hurdle to translate research findings into clinical application. Therefore, this study aimed to take a fresh view on understanding human enthesis development by employing fetal tissues. Furthermore, enthesis structure, function, and cell types would be compared between mouse and human.

Methods: Human fetal tissues were provided from elective abortions obtained from the Developmental Origins of Health and Disease Biorepository at the Icahn School of Medicine at Mount Sinai (ISMMS). The consent process, treatment, and disposal of human fetal tissues were in full compliance with the human subjects protocol, New York State Laws, and ISMMS regulations. Fresh fetal shoulders of 12-23 weeks after conception were received in cold saline. Due to challenges keeping both shoulders intact after abortion, seven fetal shoulders were used for tissue evaluation and three for in vitro treatment. scRNA-seq: Fetal enthesis cells from 16 and 18 weeks were isolated for scRNA-seq analysis UMAP plots revealed distinct cell clusters and trajectory analysis highlighted differentiation paths. scRNA-seq data was processed and analyzed using R and Python. Histology and immunohistochemistry (IHC): The supraspinatus tendon-bone assembly was dissected, fixed, cryosectioned, and stained by safranin O [4-5]. Since progenitor cells expressing both Sox9 and Scx form the prenatal enthesis and later differentiate into Gli1-positive cells with Pdgfra expression [5-6], protein expression of SOX9, SCX, GLI1, and PDGFRA was examined by IHC. *In vitro* treatment to knockdown *NFIA*: Nfia is expressed in the tendon enthesis and regulates stem cells in hair follicles [8-10]. We identified Nfia as a transcription factor candidate that may mediate stem cell function and osteogenesis in the enthesis [5]. Its role in musculoskeletal tissues remains unclear. To explore this, we conducted *in vitro NFIA* knockdown in fetal enthesis cells and evaluated cellular changes transcriptionally and translationally. Cells from fetal entheses (14, 18, and 23 weeks) were expanded *in vitro,* treated with scrambled siRNA (Control) or NFIA-targeted siRNA, and validated for transfection efficiency. Cells were fixed for IHC or mRNA extraction for RNA sequencing. Bulk RNA-seq was done via Galaxy platform.

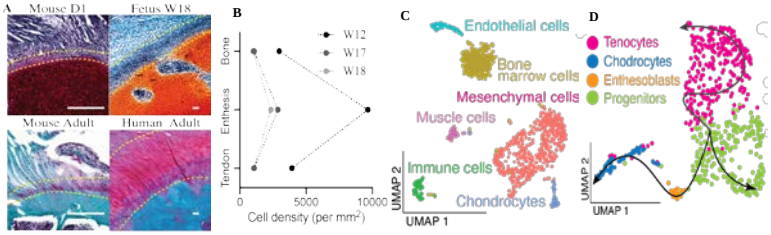

Figure 1. Human enthesis begins as a condensed primordium and matures into graded fibrocartilage, similar to mouse development. (A) Histological images of mouse and human entheses stained with safranin O [4]. Scale bar: 200 µm. D1, postnatal day 1; W18, week 18 after conception. Entheses are highlighted between two yellow lines. (B) Cell density quantification in fetal tendon, enthesis, and humerus head. (C)UMAP plot of six distinct cell types in fetal human supraspinatus enthesis. (D) Differentiation trajectory from progenitors to enthesoblasts and chondrocytes, showing stages of cellular progression.

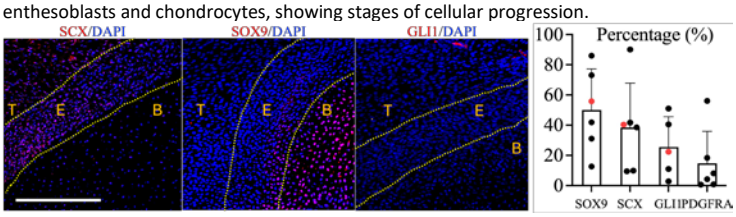

Figure 2. Expression of SCX, SOX9, and GLI1 in human entheses varies across fetal stages. Left: Immunostaining of SCX, SOX9, and GLI1 in fetal entheses. T, tendon; E, enthesis; B, bone. Scale bar: 200 µm. Right: Percentage of cells expressing each protein, with red dots calculated from the left images.

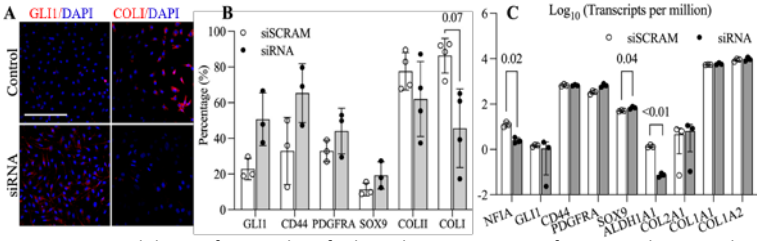

Figure 3. Knockdown of *NFIA*, identified as a key transcription factor regulating enthesis progenitors, reduces chondrogenic capacity in fetal cells. (A) Representative images of NFIA-siRNA treated fetal cells. Scale bar: 200 µm. (B) Quantification of cells expressing the listed proteins after NFIA-siRNA treatment. (C) Bulk RNA-seq analysis of genes related to enthesis stemness and chondrogenesis with NFIA-siRNA.

Results: The supraspinatus tendon enthesis was identified as histologically distinct from the neighboring bone and tendon by 12 weeks in the fetus (Fig. 1A). Cell density was greater in the enthesis than in the bone or tendon with variation across fetal stages (Fig. 1B). scRNA-seq identified distinct progenitor and enthesoblast populations (Fig. 1C). At gestational weeks 16 and 18, progenitor cells (PDGFRA, CD44), tenocytes, and enthesoblasts (low CD44, high SOX9, COL2A1) were identified. Trajectory analysis revealed differentiation paths from progenitors to enthesoblasts and chondrocytes (Fig. 1D). IHC from 13 to 22 weeks showed high expression of progenitor markers SOX9 and SCX, but lower levels of GLI1 and PDGFRA, consistently with the findings from scRNA-seq analysis. The enthesis expressed less SOX9 than bone and less SCX than tendon (Fig. 2) with GLI1 and PDGFRA expressed in both human and mouse samples. scRNA-seq (Fig. 1C) identified distinct progenitor and enthesoblast populations, confirming IHC expression patterns. At gestational weeks 16 and 18, progenitor cells (PDGFRA, CD44), tenocytes, and enthesoblasts (low CD44, high SOX9, COL2A1) were identified. Trajectory analysis (Fig. 1D) revealed differentiation paths from progenitors to enthesoblasts and chondrocytes, aligning with histological progression. Tenocytes had higher pseudotime than chondrocytes, suggesting more transcriptional changes in line with increased cell density in the enthesis. NFIA knockdown increased GLI1 and decreased COL1 expression (Fig. 1B), although sequencing data did not capture these changes. NFIA knockdown also significantly altered SOX9 and ALDH1A1 expression supporting their role in chondrogenesis [10].

Discussion: Our histological evaluation of human enthesis development and comparison between mouse and human demonstrated the conservation between the species: (1) a distinguished enthesis eminence from the surrounding tendon and bone was found in human and mouse; (2) similar expression patterns of enthesis progenitor markers across both species were observed. Consistently, *NFIA* knockdown in fetal cells led to increased GLI1 and SOX9. This suggested that NFIA might maintain stem cell identity, consistent with our findings of the role of NFIA in mouse enthesis [5, 8-9]. We did not exclude the fetuses with genetic diseases and all the experiments were conducted on a wide developmental range from 12 to 23 weeks with different morphologies at both the tissue and cell-levels, which led to high variation in the data.

Significance: Our findings offer valuable insights into human enthesis development and will help translate discoveries from animal models into clinical therapeutic strategies. **References:** [1] H. Lu et al. *Annu Rev Biomed Eng* 2013 [2] T. Moran et al. *Clin Sports Med* 2023 [3] L. Galatz et al. *J Bone Joint Surg Am* 2004 [4] F. Fang et al. *Sci Adv* 2020 [5] F. Fang et al. *Cell Stem Cell* 2022 [6] M. Killian et al. *Semin Cell Dev Biol* 2022 [7] A. Schwartz *Bone* 2013 [8] R. Adam et al. *Nat Cell Bio* 2020 [9] S. Kult et al. Elife *2021* [10] A. Unguryte et al. *Osteoarthritis Cartilage* 2016.

ABSTRACT #010

Determining the Role of Mechanosensitive PIEZO1 Ion Channel in Directing Skeletal Muscle Fibro-Adipogenic Progenitor Function

Kasoorelope Oguntuyo[1], Britney Chin-Young[1], Larion Santiago[1], Charlene Cai[1], Woojin Han[1]

1. *Department of Orthopaedics, Icahn School of Medicine at Mount Sinai*

Introduction: Fatty and fibrotic infiltration into muscle following chronic injury or disease is detrimental to muscle quality, leading to progressive decreased function. Fibro-adipogenic progenitors (FAPs) are the mesenchymal stem cell population that are the source of these degenerative tissues that embed within the muscle.[1] During normal muscle regeneration, these FAPs transiently proliferate to play a supportive role before being cleared.[2] In chronic conditions, FAPs persist and differentiate into adipocytes and/or myofibroblasts.[3] However, the cues that drive this response in FAPs is not well understood. We propose that mechanical cues that change over the course of muscle regeneration, such as the matrix stiffness,[4] contribute to FAPs pathologic function. While it is known that FAPs do respond to changes in matrix stiffness,[5] the underlying mechanism remains unclear. PIEZO1, an ion channel that has been shown to respond to matrix stiffness, stretch, and other mechanical cues,[6,7] that has been identified in cells across the musculoskeletal system, but not yet in FAPs. We hypothesize that PIEZO1 senses the dynamic matrix stiffness and is essential for FAP function during muscle regeneration.

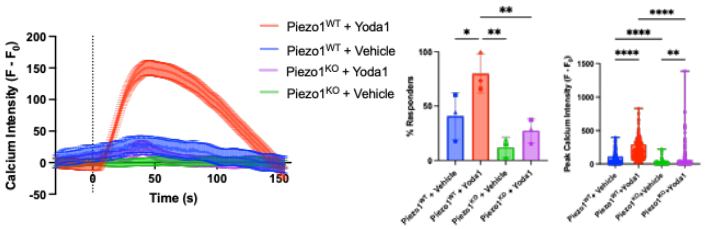

*Figure 1: Calcium Intensity in FAPs with PIEZO1 wild-type or knockout. * p < 0.05, ** p < 0.01, **** p < 0.0001 by one-way ANOVA.*

Brief Statement of Methods: To test our hypothesis, we confirmed the expression of PIEZO1 in FAPs by tracking intracellular calcium changes using Cal520, a calcium sensitive dye, in response to Yoda1, a PIEZO1-specific agonist. We also established a method to knockout PIEZO1 in FAPs *ex vivo* using lipid nanoparticles (LNPs) delivering Cre mRNA (Cre-LNPs). Finally, we evaluated the role of PIEZO1 activation on FAP function by assessing spontaneous adipogenesis following Yoda1 administration *in vitro*.

Results: Following administration of Yoda1, a greater percentage of wild-type FAPs showed increased intracellular calcium signals than those that treated with vehicle or Yoda1 in FAPs where PIEZO1 was knocked out by Cre-LNP (**Figure 1**). Additionally, Yoda1 administration decreased spontaneous differentiation of FAPs into adipocytes, as indicated by a decrease in perilipin area. A decrease in cell density following PIEZO1 activation by Yoda1 was observed, where we determined that this is due to reduced cellular proliferation, not a change in cell viability (**Figure 2**).

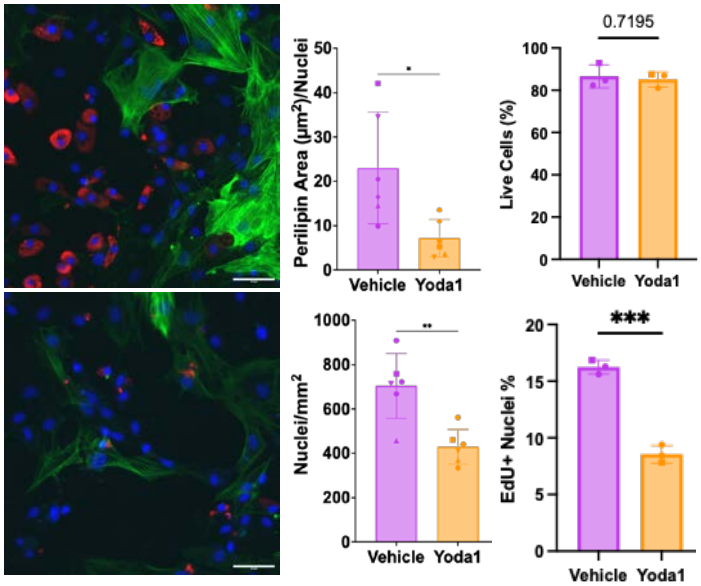

*Figure 2: PIEZO1 Activation Inhibits Adiopogenesis and Proliferation in FAPs. Perilipin in red, α smooth muscle actin in green, DNA in blue. * p < 0.05, ** p < 0.01, *** p < 0.001 by unpaired t-test.*

Conclusions: Our findings show that FAPs express PIEZO1, which can be knocked out *ex vivo* using Cre-LNP delivery, thereby attenuating their response to Yoda1. Additionally, PIEZO1 activation inhibits FAP proliferation, suggesting that mechanical activation of PIEZO1 during muscle regeneration may regulate FAPs quantity and prevent their persistence and differentiation.

Significance: This work identifies PIEZO1 as a potential mechanosensor in FAPs during muscle regeneration. This work may also identify potential therapeutic targets to prevent degenerative fatty and fibrotic infiltration in diseased states or following chronic muscle injury.

References: [1] Garcia+ 2023 bioRxiv, [2] Lemos+ 2015 Nat Med, [3] Uezumi+ 2014 Cell Death Dis, [4] Silver+ 2021 Sci Adv, [5] Loomis+ 2022 Sci Rep, [6] Atcha+ 2021 Nat Commun, [7] Savadipour+ 2023 PNAS.

ABSTRACT #011

Treatment with Parathyroid Hormone Following a Single Bout of Loading Does Not Attenuate Post-Traumatic Osteoarthritis Progression

Ana Witkowski[1], Adrien Y. Antoinette[1], Soph Ziemian[1], Miguel Otero[2,3], Marjolein C. H. van der Meulen[1,2]
[1]Cornell University, Ithaca, NY [2]Hospital for Special Surgery, New York, NY, [3]Weill Cornell Medicine, New York NY

Early-stage osteoarthritis (OA) is characterized by increased bone remodeling, leading to initial bone loss[1]. Thus, increasing bone mass early after a damaging loading event may attenuate post-traumatic OA (PTOA) progression. Parathyroid hormone (PTH) is an FDA-approved osteoporosis treatment used to increase bone formation. 6 wks of PTH pretreatment increased cartilage thickness and bone mass, and attenuated cartilage damage following subsequent daily loading[2]. Here, we asked whether PTH treatment also would attenuate damage after a single damaging loading event. We hypothesized that PTH treatment would improve cartilage damage outcomes in load-induced PTOA regardless of treatment initiation, and that changes in cartilage gene expression would mirror the differences in the treatments.

Under IACUC approval, the left hindlimbs of 26-wk-old male C57BL/6J mice underwent a single bout of cyclic tibial loading (9N peak load, 1200 cycles, 4Hz)[3]. The right hindlimbs were used as contralateral controls. To examine the tissue-level effects, mice were injected with: (a) saline (VEH, SQ, n=3-7, 5d/wk); (b) PTH (40µg/kg/day, SQ, n=3-7, 5d/wk) immediately following loading for 3 or 6 wks; or (c) PTH treatment delayed 2 weeks and given for 1 or 4 weeks. Mice were euthanized at 3 or 6 wks following loading, and knees were processed for Safranin-O staining and OARSI scoring[2]. Treatment differences were determined using a linear mixed effects model. To characterize changes in gene expression, mice were injected with saline (VEH, IP, n=8, 5d/wk) or PTH (40µg/kg/day, SQ, n=8, 5d/wk) immediately following loading. Mice were euthanized at 1 wk post loading, and tibial cartilage was dissected and isolated for 3' RNA sequencing (RNA-seq)[4]. We compared loaded and control limbs for differentially expressed genes (DEGs, EdgeR, FDR<0.05) and determined the top enriched biological pathways (GSEA, FDR<0.05)[2].

At 3 or 6 wks after the single bout of loading, cartilage damage was not attenuated with immediate or delayed PTH treatment (Fig 1). RNA-seq identified 775 DEGs between loaded and control VEH-treated limbs, and 704 DEGs with loading in PTH-treated limbs. 481 DEGs were common to the VEH and PTH groups, including genes with known association to OA progression, such as *Gdf5, Sox11, Il11, Piezo2,* and *Postn*. With loading, VEH-specific DEGs included *Adamts4, Trpv4, Ngf, Wnt5a,* and *Col1a,* whereas *Col10a1, Fgfr3,* and *Dact1* were differentially expressed only in PTH-treated cartilage (Fig 2). Our pathway analysis identified overlapping and unique pathways to each treatment group, with chondrocyte differentiation and endochondral bone morphogenesis enriched only in the VEH group, and skeletal system morphogenesis and limb development enriched only in the PTH group (Fig 3).

PTH pre-treatment attenuated joint damage induced by daily loading through beneficial effects on bone and cartilage[2]. However, here PTH treatment immediately after a single bout of loading did not modify subsequent cartilage damage. This discrepancy can be driven by differences in the PTH treatment regimen (pre-treatment prior to loading or post-loading bout) or by the loading protocol. The current study relied on a single loading bout that leads to more rapid and severe damage than daily loading at the same magnitude[5]. Interestingly, our RNA-seq analyses identified genes that are unique to PTH treatment, including upregulation of genes associated with OA attenuation (*Dact1, Fgfr3*) and recapitulation of developmental processes in response to cartilage damage and injurious stimuli (*Col10a1, Gdf5*). However, the severity of tissue damage due to the single bout of loading exceeded the potential chondroprotective effects of PTH treatment. Investigating earlier time-points and additional loading magnitudes would help to better define the potential ability of PTH treatment to prevent joint damage associated with PTOA. Promoting bone formation is insufficient to attenuate cartilage damage and PTOA development following a single bout of damaging load.

References: [1]Yuan+ 2014 [2]Antoinette & Ziemian+ 2024 [3]Ko+ 2013 [4]Culley+ 2021 [5]Ziemian et al. 2024 ORS

Acknowledgments: Funding provided by DOD W81XWH-17-1-0540, NIH R01-AR081943, NIH T32-AR078751, Cornell Genomics Core

B

Figure 1: A) Safranin-O-stained sections depicting cartilage damage, scale = 1 mm; B) OARSI Scores (posterior compartment)

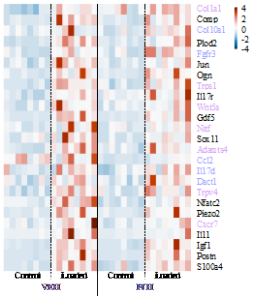

Figure 1: Heatmap representation of normalized OA-related DEGs. Significant in: Both or only VEH, PTH

Figure 3: Top 10 upregulated biological pathways in VEH- and PTH -treated mice, represented by normalized enrichment score

Evaluating the Role of Klotho Deficiency in Intervertebral Disc Health: No Evidence of Accelerated Degeneration in Mice

Veeraj Shah[1], Justin Hong[1], Ravi Krishnan[1], Chitra L Dahia[1, 2]
[1] HSS Research Institute, Hospital for Special Surgery, New York, NY, [2] Weill Cornell Medicine, New York, NY

Introduction:
Aging is a key risk factor for many chronic conditions, including lumbar intervertebral disc (IVD) degeneration, which is major cause of chronic low back pain. Disc degeneration typically involves the progressive loss of nucleus pulposus (NP) cells, disorganization of the annulus fibrosus (AF) lamellae, reduced disc height, and decreased extracellular matrix (ECM) integrity, all of which impair the disc's function. The ECM is critical for maintaining disc hydration, structural support, and biomechanical properties. The anti-aging gene Klotho (*Kl*) has been implicated in age-related pathologies. *Kl*-deficient mice (Kl^{Kl}/Kl^{Kl}) show accelerated aging phenotypes of several tissues including kidney, pancreas, brain, bone, liver, and cardiovascular system, multi-organ failure, and significantly reduced lifespan of about nine weeks. However, role of *Kl* impacts IVD homeostasis remains unexplored. We hypothesized that loss of *Kl* would accelerate IVD degeneration in the Kl^{Kl}/Kl^{Kl} mutants. Hence, the goal of this study is to characterize whether Kl^{Kl}/Kl^{Kl} mice have an accelerated phenotype in the IVD compared to wild-type (WT) control, and how it resembles to age-related IVD degeneration observed in naturally aging mice.

Methods:
We performed a comprehensive analysis of lumbar IVDs from eight-week-old Kl^{Kl}/Kl^{Kl} (n=3) and WT control (n=3) mice. Histological analysis using Hematoxylin and Eosin (H&E) staining was conducted to evaluate disc morphology and cellular organization, with particular focus on NP and AF structures, and histopathological scoring by two blinded raters. Morphometric measurements, including disc height and width, were taken to quantify potential structural differences between the Kl^{Kl}/Kl^{Kl} and WT groups. Immunostaining (n=3/cohort) for key markers of NP cell health, such as sonic hedgehog (SHH) and cytokeratin 19 (KRT19), was performed to assess the health of the NP cells. Additionally, immunostaining for major ECM components—collagen type I (COL1A1) and chondroitin sulfate proteoglycan (CSPG) was used to evaluate ECM integrity. Finally, multiplex quantitative PCR (qPCR) (n=4/ tissue) using TaqMan probes specific to each isoforms of *Kl* (secreted and receptor) and *Gapdh* as internal control was performed to detect its isoforms at mRNA level in the NP and AF cells. Kidney, pancreas, brain, bone, liver, muscle was used as positive controls. Statistical analysis was carried out using GraphPad Prism Vs 10, and unpaired two-tailed student's *t* test was used to determine differences between cohorts.

Results:
Histopathological and morphometric analyses revealed no significant differences in the lumbar IVDs of Kl^{Kl}/Kl^{Kl} mice compared to WT controls. Although the vertebral bone of the Kl^{Kl}/Kl^{Kl} mice were shorter with dense trabecular bone, as previously reported. Immunofluorescence analysis showed no change in expression of NP cell markers SHH and KRT19, and ECM markers COL1A1 and CSPG between the IVDs of Kl^{Kl}/Kl^{Kl} and WT mice. Furthermore, Multiplex qPCR analysis did not detect expression of any isoform (secreted and receptor) of *Kl* mRNA expression in NP or AF cells of the lumbar discs while kidney, pancreas, brain, bone, liver, and muscle showed robust expression of all *Kl* isoforms relative to *Gapdh* as internal control, suggesting that the absence of *Kl* in these cells does not directly impact disc health.

Conclusion:
Our findings show that Kl^{Kl}/Kl^{Kl} mice do not exhibit accelerated IVD degeneration at eight weeks of age, which can be attributed to the absence of KL and its receptor expression in both NP and AF cells of the mouse IVD. As a result, KL deficiency does not impact disc homeostasis or contribute to age-related degenerative disc pathology.

Acknowledgement/Funding Source: The research was supported by NIAMS (AR077145), NIA (RAG070079) and OD (1S10OD026763) of NIH.

Effect of bisphosphonates on the middle ear ossicles in brittle bone disease

Maialen Ugarteburu[1], Luis Cardoso[1], Claus-Peter Richter[2], Alessandra Carriero[1]
[1]The City College of New York, [2]Northwestern University Feinberg School of Medicine

Progressive hearing loss is a prevalent feature among people with osteogenesis imperfecta (OI), commonly known as brittle bone disease, a genetic disorder largely stemming from collagen type I mutations. Currently, no cure exists for OI, and hearing loss treatments are generally adapted from standard interventions, showing limited effectiveness in OI patients. The underlying mechanisms of hearing impairment in OI remain poorly elucidated. Similarly, the impact of bisphosphonate therapy – the standard treatment for children with OI – on auditory ossicle bones is still largely unexplored. This study examines the morphometric and volumetric characteristics of the middle ear ossicles in the bisphosphonate treated *oim/oim (oim)* mouse model of OI.

The middle ears of 14-week-old phosphate-buffered saline (PBS) and Alendronate (ALN) treated *oim* and wild-type (WT) mice (N=10/group) were imaged using synchrotron microtomography at 1.6 µm resolution. We measured the volume of the malleus, incus, and stapes, as well as the total ossicle volume. Specific measurements included the volume of the malleus' processus brevis, lamina area, and manubrium length, the long process length in the incus, and total height, footplate height and area, and crura height in the stapes. We also calculated the area convergence ratio and lever arm ratio, key parameters of middle ear function. Additionally, we measured the volume of interconnected canals in the incus and malleus and assessed cellular porosity across all ossicles, evaluating lacunar porosity, mean lacuna volume, lacunar density, and sphericity. Fractures or abnormalities were visually inspected and quantified.

The total ossicle volume and malleus volume were significantly smaller ($p < 0.05$) in ALN-treated mice compared to PBS-treated mice in both genotypes. Additionally, the PBS-*oim* group showed significantly smaller total ossicle volume, malleus volume, incus volume, and footplate area compared to PBS-WT, with a higher lacunae number density and porosity than PBS-WT. In ALN-WT mice, lacunar sphericity was higher in both the incus and stapes compared to PBS-WT, but there were no changes in the ALN-*oim* group compared to PBS-*oim* group. Lacunar porosity was greater in the incus of PBS-*oim* mice compared to PBS-WT. We observed a fused incudostapedial joint with a deformed head of the incus in one single PBS-WT mouse. In the PBS-*oim* group, we observed a fusion in the incudostapedial joint in one sample, a deformed head of the incus in another sample, and an incudomalleal fusion with a deformed incus in another sample. Both fusions seen in the PBS-*oim* happened in localized areas rather than in the entire joint surface. Similar abnormalities were also found in ALN-*oim* mice, indicating the presence of malformations regardless of the treatment. Specifically, in the ALN-*oim* group, we observed three abnormalities in three different samples. One ALN-*oim* mice exhibited a partly fused incudomalleal joint. Another ALN-*oim* mouse exhibited a localized bone formation in the interior surface of the stapes footplate, and another ALN-*oim* had a localized bone formation in the facet for the malleus at the head of the incus.

In conclusion, alendronate treatment reduces total ossicular volume, but does not prevent morphological abnormalities in *oim* mice. Interestingly, control *oim* mice showed smaller ossicle volume, with smaller malleus and incus, and smaller footplate area, but higher lacunar number density and total porosity density than WT. Abnormalities, including joint fusions and deformed ossicles, were more frequent in the *oim* group, and were found in both PBS and ALN-treated *oim* mice, indicating that ALN treatment did not prevent these abnormalities.

ABSTRACT #014

3D Bone Composition and Fiber Alignment at fracture sites to explain Crack Path

Aimar Silvan, Asier Muñoz, Alessandra Carriero
The City College of New York, New York, NY, USA

Bone fragility is primarily determined by bone toughness, which significantly develops during crack growth in a healthy bone. Brittle bones have a shorter, less rough crack surface than healthy bone. Analyzing the bone crack propagation from a notch inform on the mechanisms of bone fracture. Prior research has explored this phenomenon in cortical bone using techniques such as environmental scanning electron microscopy (ESEM), synchrotron computed tomography, high-resolution optical microscopy, and digital imaging correlation [1]. These studies have demonstrated that healthy bone employs mechanisms like deflection, splitting, and bridging to prevent catastrophic fractures, potentially increasing bone toughness by 4-6 times during crack propagation [2]. In contrast, brittle bone, such as those affected by osteogenesis imperfecta (OI), exhibits rapid, straight-line crack propagation [3]. Bone's hierarchical structure, primarily composed of mineral and collagen, is known to dictate its mechanical properties. Toughening mechanisms, such as crack deflection, arise from the interaction of cracks with micrometer-scale structural features, including intracortical porosity, collagen lamellae, and mineral heterogeneity. However, the exact impact of OI-induced changes in composition and structure, and their specific effect on crack behavior remains unclear. This study aims to directly correlate variations in crack path with the microstructural and compositional features of bone tissue. We employ 3D Raman spectroscopy to identify localized compositional changes in bone mineralization, and Second Harmonic Generation (SHG) microscopy to assess collagen fiber organization in both healthy and OI-affected bone (Figure 1).

Femurs from 14-week-old *oim* mice (B6C3Fe-a/a-Col1a2*oim/oim*, N=4/group) and their WT counterparts were micro-notched and subjected to controlled 3-point bending to measure fracture toughness. Post-fracture, samples were embedded in polymethyl-methacrylate, sliced, and polished to expose stable crack growth sites. 3D Raman micro-spectroscopy (WiTec Confocal Raman Microscope alpha300R) was used to map bone composition around the cracks, capturing mineral-to-matrix ratio, carbonate-to-phosphate ratio, and crystallinity in 1 x 1 x 2.5 µm resolution. Spectra were analyzed using Project 5 software and custom MATLAB scripts. Comparisons were made between 3D Raman micro-spectroscopy and single-point Raman spectroscopy to assess volumetric representation. SHG microscopy images (Prairie Technologies Ultima IV) were obtained to analyze collagen orientation and interaction with crack paths using *FiberO* software [4]. Statistical analyses were conducted with mixed-effects models to count for between- and within-sample variations in composition.

Compared to WT bone, *oim* bone showed higher mineralization and reduced carbonate substitution. SHG images also revealed lower collagen content and organization in *oim* bone. For both groups, there was not a major change in the bone near the crack path that could indicate a change in the path. Instead, organized collagen fibers were present and aligned along the crack path in WT bone but not in *oim* bone, potentially explaining a direct interaction between crack path progression and underlying collagen contents, as well as the difference between healthy and fragile bones

3D Raman micro-spectroscopy, applied for the first time to study bone composition in a volumetric manner, identified significant compositional differences between WT and *oim* bones, such as reduced carbonate substitution, higher mineralization, consistent with previous findings [1,3]. In 3D Raman micro-spectroscopy of bone fracture, the region closer to the crack path was consistently less mineralized that the other regions, indicating that the matrix either loses mineral as a consequence of fracture, or that the interface with the PMMA was creating an artifact, as previously reported in previous FTIR studies. 3D Raman micro-spectroscopy more accurately represented the inherent heterogeneity of bone composition compared to traditional single-point accumulations, which often failed to capture volumetric bone composition accurately. Arising from this work, future studies could use this new methodology to link fracture toughness and crack deflection to microstructural and compositional characteristics of bone in disease and inform on success and progression of treatment strategies to improve bone resistance to fracture.

REFERENCES:
[1] Muñoz et al, Curr Osteop Rep, 19(5):510-531, 2021
[2] Ritchie, Ann NY Acad Sci, 1192(1):72-80, 2010
[3] Carriero et al, JBMR, 29(6):1392-1401, 2014
[4] Muñoz et al, NEBEC 2022

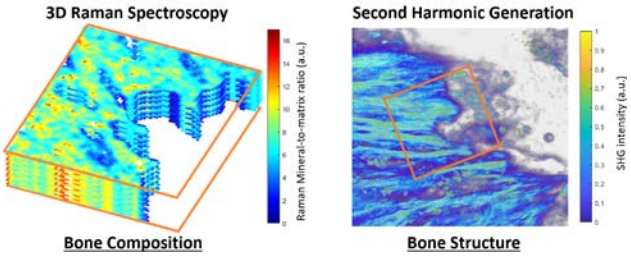

Figure 1. 3D bone composition (Raman) and fiber organization (SHG) along the crack path

ABSTRACT #015

Intraoperative Second Harmonic Generation Imaging Diagnoses Acute Median Nerve Injury Linked to Long-term Dysfunction and Neuroma-Formation in Rats

Christoph A. Schroen[1], Philip Nasser[1], Damien Laudier[1], Paul J. Cagle[1], Michael R. Hausman[1]
[1]Leni & Peter W. May Department of Orthopaedic Surgery, Icahn School of Medicine at Mount Sinai, NY, USA

Objective: In-continuity nerve injuries pose a major clinical dilemma to orthopedic surgeons as natural recovery remains inherently unpredictable. This study investigates whether intraoperative Second Harmonic Generation (SHG) Imaging effectively detects and distinguishes acute and chronic damage to the major anatomical sub-structures of the rat median nerve and if this damage is associated with functional impairment. A detailed intraoperative assessment of peripheral nerve injuries could potentially identify structural damage predictive of poor long-term outcomes and thus provide orthopedic surgeons with clear indications for or against surgical intervention.

Methods: This study was approved by IACUC. 33 one-year-old male Sprague-Dawley rats were randomly assigned to one of four groups: two mild-strain injury (MS) groups with follow-up timepoints at 6 and 12 weeks (n=8 rats per group), and two high-strain injury (HS) groups with follow-ups at 6 weeks (n=8) and 12 weeks (n=9). Left median nerves were injured, right nerves served as sham controls (SC). Median nerves were surgically exposed and secured under 2 metal pins 1 cm apart. A hook was attached to a load cell and raised from beneath the nerve at a speed of 0.2mm/s using an Instron Material testing system until induction of the respective injury severity was observed on a load-time-curve. MS-injury was achieved with detection of a first rapid loss of resistance-force and HS-injury was reached at a second steep decrease in force. SC-nerves were held in place for 5 minutes without being stretched. Immediately after induction of the nerve injury and at the respective follow-up time points, rats were placed under an Olympus FVMPE-RS multiphoton microscope with 1.5cm of the median nerve exposed to a laser-wavelength of 910 nm to visualize neural collagen. Multiple z-stack images with a depth of 54 micrometers were acquired along the nerve from proximal to distal at a filter-wavelength of 455 nm. Conductivity was assessed using an electrical nerve stimulator to induce digit movement before and after injury, as well as at the respective follow-up timepoints.

Results: At the day of injury, SHG-Microscopy of both strain levels revealed three distinct zones of injury from proximal to distal: a zone showing exposed endoneurial tubes without a surrounding epineurium, an area exhibiting the rupture edge of the epineurium, and a zone with disorganized but continuous epineurial collagen fibers (Figure 1, SHG-images at 25x magnification). Both MS- and HS-nerves exhibited complete epineurium rupture. The SHG-Signal of endoneurial fibers was substantially weaker than that of the epineurium, requiring higher filter-voltage for effective visualization. MS-nerves revealed exposed but grossly intact and aligned endoneurial tubes. HS-nerves exhibited larger areas of exposed endoneurium, exposing highly malaligned endoneurial tubes and breaks in endoneurial fibers. Epineurial collagen of all injured nerves was heavily disorganized, with short fiber fragments near the tear zone and wavy, misaligned fibers distal to the zone of epineurial tear. SC-nerves exhibited normal nerve architecture. At 6- and 12-weeks, MS-nerves exhibited similar zones of injury on SHG Imaging, indicating a lack of structural recovery and no closure of the epineurial gap (Figure 2). HS-injury revealed heavily disorganized epi- and endoneurial collagen fibers at the previous site of epineurium rupture, forming a tumorous structure with no clear fiber trajectory. The appearance of HS-nerves at 6- and 12-weeks was similar to and indicative of a traumatic neuroma-in-continuity with intense scar-formation within the nerve. Uninjured MS- and HS-nerves induced digit movement at electrical stimulator settings of 28.75±8.8 nC and 25.0 nC, respectively (p=0.21). Nerve conductivity was severely reduced in both injury severities on Day 0 (p<0.01 for both). HS-nerves required higher stimulator settings than MS-nerves, with 266.7±103.3 nC compared to 150±75.6 nC (p=0.04). Conductivity of MS-nerves improved at 12 weeks, with paw movement at 87.5±18.9 nC (p=0.04), but remained significantly reduced compared to pre-injury values, indicating only partial functional recovery (p<0.01). HS-nerves did not exhibit signs of recovery at 12 weeks, requiring 233.3±103.3 nC (p=0.77), and were less conductive than MS-nerves at 12 weeks (p<0.01).

Conclusions: Intraoperative SHG-Microscopy effectively detects structural damage associated with long-term dysfunction and neuroma-formation. It provides precise differentiation between damage to the epineurium and endoneurium, accurately detecting disruption of both structures as well as more subtle forms of damage, such as fiber disorganization and tear of individual endoneurial tubes. While epineurium rupture persisted in MS-nerves at 12 weeks, nerve function significantly improved. HS-injury severely impacted endoneurial tube alignment and trajectory on day 0, which resulted in unsuccessful recovery attempts and ultimately led to traumatic neuroma formation. Consequently, HS-injury led to a long-term impairment of conductivity without functional improvement at 12 weeks.

Significance: In the future, SHG-Microscopy could enable orthopedic surgeons to differentiate nerve lesions requiring immediate surgical intervention from those that have a high chance of natural recovery.

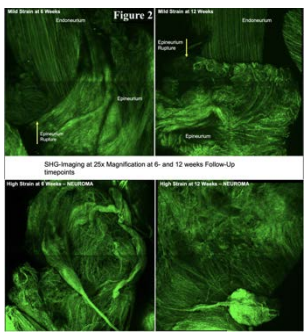

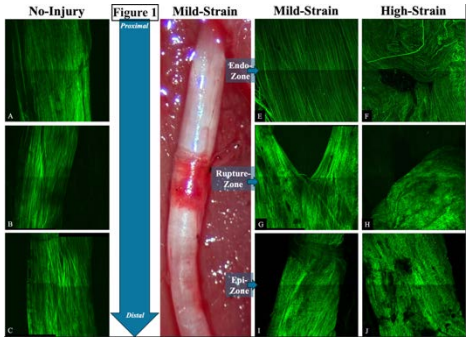

ABSTRACT #016

Activation of Hedgehog Signaling in Fibroadipogenic Progenitors Causes Pseudoarthrosis

Ezgi Aydin[1], Mark Bubnovich[1], Ugur Ayturk[1]
[1]Hospital for Special Surgery, New York, NY

INTRODUCTION: The molecular mechanisms involved in fracture healing and its failure remain incompletely understood. Emerging studies show that a diverse group of stem and progenitor populations repair bone following injury[1,2]. However, the specific signaling mechanisms that drive the activation and differentiation of these cells are unclear. Muscle-resident fibroadipogenic progenitors (FAPs) are among the populations that are mobilized to become osteoblasts in response to nearby fractures[3]. To characterize the functional significance of FAPs in bone repair, and the mechanisms regulating them, we have recently developed the novel Clec3b^{CreERT2} mouse allele that can be used to selectively track and manipulate FAPs. Our results indicate that FAP loss of function reduces fracture callus mineralization. Importantly, conditional activation of hedgehog signaling results in severe fibrosis and osteolysis, leading to pseudoarthrosis. These data show that abnormal hedgehog signaling in FAPs can recruit osteoclasts for pathologic bone resorption and suppress the bone-forming capability of other skeletal stem and progenitor populations in the periosteum and marrow.

METHODS: All experiments were approved by IACUC.

Mice: Clec3b^{CreERT2} mice were developed with CRISPR-Cas9. Ai14.R26^{tdTom} and R26$^{SMO/EYFP/+}$ mice (that conditionally express a Smoothened transgene harboring a missense mutation, resulting in constitutive activation of hedgehog signaling[4]) were purchased from Jackson Laboratories. Between 3 and 4 weeks of age, Clec3b^{CreERT2} R26^{tdTom} (control) and Clec3b^{CreERT2}, R26^{tdTom}, R26$^{SMO/EYFP/+}$ mice (SMO) were administered with tamoxifen (75mg/kg) intraperitoneally, receiving 3 injections in total, to activate Cre recombinase. For conditional *Ctnnb1*-deletion experiments, *Clec3b$^{+/+}$ Ctnnb1$^{fl/fl}$* (control) and *Clec3b^{CreERT2} Ctnnb1$^{fl/fl}$* mice were similarly treated with tamoxifen.

Stabilized Fracture Repair: Six weeks after tamoxifen injections, mice underwent stabilized fracture surgeries. Under anesthesia, the right femoral diaphysis was subjected to full osteotomy with a high-speed drill. The fractured bones were stabilized with a sterile 25G pin. Three weeks after surgery, mice were euthanized and both right and left femurs were collected.

Micro-CT: Fracture callus mineralization was determined with μCT analysis at 7.4μm resolution (μCT 45, Scanco Medical, Switzerland). The region spanning 1 mm (135 slices) on either side of the fracture line was selected as the region of interest (ROI). The native femoral bone was excluded from the analysis to disregard the differences that might be caused by baseline cortical bone.

Immunofluorescence: Frozen sections were stained with primary (CD31, BD Biosciences/553370) and secondary antibodies. Immunofluorescence imaging was conducted using Zeiss Axioscan7 Slide Scanner.

RESULTS: To quantify the contribution of FAPs to different cell types during fracture repair, we histologically evaluated femoral fracture calluses of Clec3b^{CreERT2}, R26^{tdTom} mice at multiple timepoints (6, 10, 14 and 21 days) **(Figure 3).** Although some FAPs undergo chondrogenesis during fracture repair, we found very little contribution by FAPs to the avascular cartilaginous portion of the callus compared to other compartments ($p < 0.001$). Thus, we decided to test whether we can induce chondrogenesis of FAPs by activating hedgehog signaling.

To promote hedgehog signaling, we generated Clec3b^{CreERT2}, R26^{tdTom}, R26$^{SMO/EYFP/+}$ mice (SMO) and performed stabilized fracture surgery on them, as well as their wild type littermates lacking Cre expression (control). Surprisingly, SMO mice developed pseudoarthrosis by 3 weeks post-surgery, indicated by fibrotic nonunion at the osteotomy site. A Chi-square analysis revealed significant nonunion risk in mutant mice (9/14 vs 1/11 in controls, scored blindly by 3 independent reviewers, p= 0.0052). Further, μCT analysis showed reduced callus bone volume (BV) even in the small group of mutant mice that did not develop nonunion (p=0.006) **(Figure 1a).** TRAP staining showed substantial bone resorption inside and around the callus, indicating the ability of dysregulated FAPs to mobilize osteoclasts for pathologic bone resorption **(Figure 1b).**

To test how genetic loss of function in FAPs affects fracture callus mineralization, we conditionally deleted the WNT-pathway transcription factor β-catenin by generating *Clec3b^{CreERT2}; Ctnnb1$^{fl/fl}$* mice and performing fracture surgery. μCT analysis confirmed decreased bone volume fraction (BV/TV) in conditional knockout mice compared to same-sex littermate controls (p=0.009) **(Figure 2).** However, this phenotype was not as severe as that triggered by hedgehog pathway activation, as the mice appeared to develop a callus, even if it is less mineralized.

DISCUSSION: The contributions of FAPs to fracture callus formation and calcification have been recently recognized. We have shown that FAP loss of function impairs callus mineralization, indicating the physiologic importance of FAPs in bone healing. However, aberrant hedgehog signaling leads to a much more severe nonunion phenotype. Thus, although FAPs are important participants in bone repair, they are also capable of promoting fibrosis and driving osteolysis when they are dysregulated, demonstrating their ability to determine whether a fracture will heal or not. Further, our findings indicate that hedgehog signaling could be a driver of fracture healing failure and could potentially serve as a therapeutic target in patients at risk.

REFERENCES: (1) Debnath S et al., *Nature*, 2018, (2) Perrin S et al., *Curr Osteoporos Rep.*, 2022 (3) Julien A et al., *Nature Comm.*, 2021 (4) Xie J et al., *Nature*, 1998

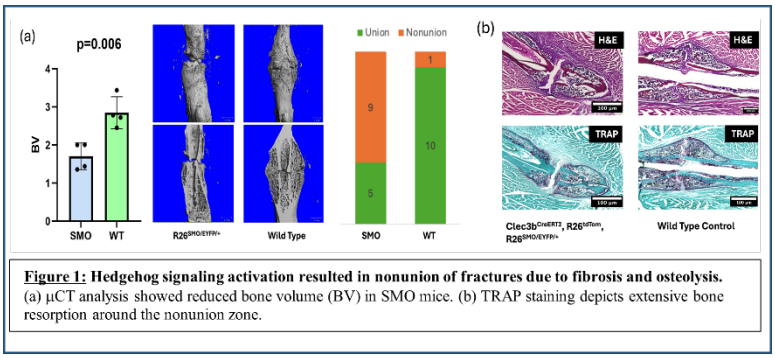

Figure 1: Hedgehog signaling activation resulted in nonunion of fractures due to fibrosis and osteolysis. (a) μCT analysis showed reduced bone volume (BV) in SMO mice. (b) TRAP staining depicts extensive bone resorption around the nonunion zone.

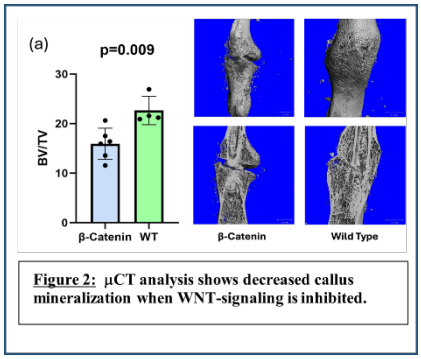

Figure 2: μCT analysis shows decreased callus mineralization when WNT-signaling is inhibited.

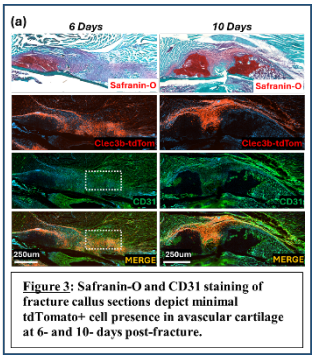

Figure 3: Safranin-O and CD31 staining of fracture callus sections depict minimal tdTomato+ cell presence in avascular cartilage at 6- and 10- days post-fracture.

Preliminary characterization of an *in vivo* model for investigating the role of mechanical tension on muscle stem cell behavior in regeneration

Josh A. Grey[1], GaYoung Park[1], Britney Chin-Young[1], Charlene Cai[1,2], Woojin M. Han[1]

1. Department of Orthopaedics, Icahn School of Medicine at Mount Sinai
2. Department of Biology, The College of New Jersey, Ewing, New Jersey, USA.

Introduction: Muscle stem cells (MuSCs) are essential for the long-term regenerative capacity of skeletal muscle. Intrinsic cellular cues and extrinsic environmental cues in the niche actively control cell fate and behaviors of muscle progenitor cells during regeneration in a tightly regulated manner for functional tissue restoration after exercise and injury. The biophysical properties of muscle tissue such as stiffness are known regulators of MuSC activation and expansion[1,2], but less is known about the role of other dynamic mechanical signals in the niche such as tensile forces transferred through the extracellular matrix (ECM) from intramuscular connective tissue (IMCT) that confer a state of tensional homeostasis across the tissue. The objective of this study is to determine the role of IMCT tension in muscle regeneration. We hypothesize that the absence of tensional homeostasis in acute skeletal muscle injury delays the regenerative response in myogenic progenitor cells.

Brief Statement of Methods: To test the hypothesis, we introduce a novel injury model that couples acute chemical injury using $BaCl_2$ with transection of the distal tibialis anterior to investigate regeneration dynamics in the absence of tensional homeostasis *in vivo*. 8-12-week old C57Bl6/J mice were randomized into 4 experimental groups for which the injury was performed on one hindlimb each: saline/sham, saline/tenotomy, $BaCl_2$/sham, and $BaCl_2$/tenotomy. The tissues were then allowed to regenerate for 5- and 7-days post injury (dpi) before sacrifice. Experimental and contralateral control TA tissues were then harvested, cryosectioned, and analyzed via histological and immunofluorescent staining.

Results: A preliminary cohort at 5 and 7 dpi show delayed regeneration in the absence of tension as indicated by increased retention of eMyHC expression and decreased myofiber CSA in $BaCl_2$/sham vs $BaCl_2$ tenotomy groups. Additionally, qualitative observations of obliquely shaped myofibers in the tenotomized groups indicates a heterogenous distribution of the loss of tension radiating out from the myotendinous junction.

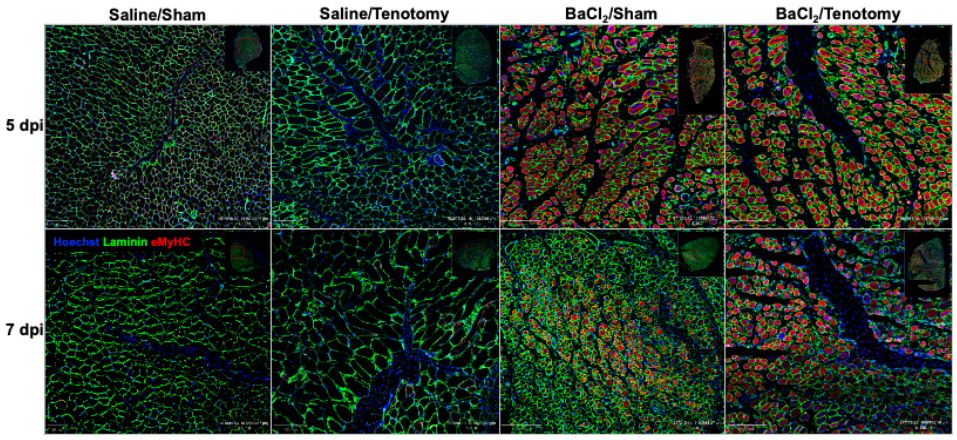

Figure 1. Representative immunofluorescent images of tibialis anterior muscle cross sections at 5 and 7 dpi.

Conclusion: This work begins to elucidate the mechanical contribution from connective tissue to the regenerative environment at the niche and whole tissue scale. Further experiments are required to determine the contribution of tensional homeostasis on MuSC and myogenic progenitor function during regeneration by performing tenotomy at distinct stages of myogenesis. This includes expansion of timepoints as well as further mechanistic interrogation comparing markers of myogenic progression such as MyoD, Myf5, and myogenin. Additional experiments are required to determine spatial variability of tension loss following tenotomy at a whole tissue scale.

Significance: These findings provide a mechanistic foundation for understanding the role of tension in MuSC function that may inform advancements in rehabilitative treatments and *in vitro* manipulation of muscle progenitors.

References: [1] Silver, J. S. *et al.* Injury-mediated stiffening persistently activates muscle stem cells through YAP and TAZ mechanotransduction. *Sci. Adv.* 7, eabe4501 (2021). [2] Gilbert, P. M. *et al.* Substrate Elasticity Regulates Skeletal Muscle Stem Cell Self-Renewal in Culture. *Science* 329, 1078–1081 (2010).

Biomechanical Comparison of Glenohumeral Stability Before and After Superior Labrum Anterior-Posterior Tear and Repair versus Biceps Tenodesis

Hayk Stepanyan, MD; Aaron T. Hui, BS; Victor T. Hung, BS; Michelle H. McGarry, MS;
Charles Long, MD; Gregory J. Adamson, MD; Thay Q Lee, PhD

Orthopaedics Biomechanics Laboratory, Congress Medical Foundation, Pasadena, CA USA

Purpose

The purpose of this study was to compare the biomechanical stability of the glenohumeral joint before and after a type II superior labrum anterior-posterior (SLAP) tear, and following treatment with a SLAP repair or biceps tenodesis.

Methods

8 male cadaveric shoulders were tested using a custom testing system. Twenty-two N glenohumeral compressive force and 5N biceps load was applied. All testing was performed in 30° and 60° of glenohumeral abduction. Humeral rotational range of motion was measured with 2.2 Nm torque. Glenohumeral anterior-posterior (AP) and superior-inferior (SI) translation was measured in 45° and 90° external rotation (ER) with 10 and 15 N loads. Six conditions were tested: Intact; SLAP tear (10:00 to 2:00 o'clock); Posterior SLAP repair (two anchors at 10:30 and 11:30); Posterior+Anterior SLAP repair (an additional anchor at 1:30); Simulated Biceps tenodesis with superior labral repair; Simulated Biceps tenodesis without superior labral repair. Repeated measures ANOVA with Tukey post hoc test was used for statistical analysis.

Results

There were no significant differences with SLAP tear or repair in AP/SI translation or range of motion compared to intact. Both simulated tenodesis conditions increased max ER compared to intact ($P<0.006$). Simulated tenodesis with SLAP repair significantly increased AP translation (6/8 positions) and SI translation (2/8 positions) compared to intact. Simulated tenodesis without SLAP repair significantly increased AP translation (all positions) and SI translation (3/8 positions) compared to intact.

Conclusion

The long head of the biceps has a major role in glenohumeral stability regardless of the condition of the superior labrum. The addition of an anterior anchor for SLAP repair did not restrict external rotation in this cadaveric model.

Clinical Relevance

In surgical treatments for SLAP lesions or biceps pathology, the long head of the biceps should be preserved when possible as it has a major role in glenohumeral stability.

Table 1. Maximum external rotational range of motion for all conditions.

	30° Glenohumeral Abduction	60° Glenohumeral Abduction
Intact	110.7 ± 6.3°	109.8 ± 6.3°
SLAP Tear	111.3 ± 6.7°	110.5 ± 6.8°
Posterior SLAP Repair	111.5 ± 6.6°	110.3 ± 6.8°
Anterior + Posterior SLAP Repair	110.2 ± 6.8°	111.0 ± 6.8°
Simulated Tenodesis with SLAP Repair	112.5 ± 7.0° *	113.8 ± 6.6° *
Simulated Tenodesis with SLAP Tear	113.8 ± 7.0° *	114.0 ± 6.5° *

Data are presented as mean ± Standard Deviation. (* $P < 0.05$ vs. Intact; SLAP: superior labrum anterior-posterior)

Defining the epigenetic signature of fate reprogramming in ligamentocytes after joint injury in zebrafish

Authors : Safiyah Ali[1,2,3], Troy Anderson[1,2,3], **Joanna Smeeton**[1,2,3,4]
Columbia University Irving Medical Center[1], Department of Genetics & Development[2], Columbia Stem Cell Initiative[3], Department of Rehabilitation and Regenerative Medicine[4]

Ligaments are dense connective tissues that provide stability to our joints and show little ability to regenerate following injury. Injuries to ligaments result in joint instability which can lead to impaired movement and the development of osteoarthritis (1). Mammals have a limited capacity to regenerate their ligaments following injury and instead heal with a biomechanically and biologically inferior fibrotic scar (2). Since there are limited effective treatment options for ligament injuries, it is crucial to understand mechanisms that drive scar-free regeneration to enhance ligament healing. In contrast to the poor healing of mammalian ligaments, we find that adult zebrafish can regenerate their interopercular-mandibular (IOM) ligament following transection injury (3). The IOM ligament functions to support the jaw joint and is composed of mature ligamentocytes that are packed within an ECM-rich environment. Following ligament transection, we discovered that pre-existing ligamentocytes dedifferentiate to rebuild and regenerate the new ligament tissue (3). The mechanisms that drive ligamentocytes to dedifferentiate after injury are unknown. Here, we used single nuclei Assay for Transposase Accessible Chromatin (snATAC) sequencing to define how the epigenetic landscape of ligamentocytes and joint cells change in response to ligament injury. We found that ligamentocytes have an increased number of accessible chromatin regions after injury compared to uninjured ligamentocytes. Within these newly accessible regions, we found enrichment of activator protein 1 (AP-1) transcription factor motifs, specifically belonging to Fos and Jun proteins. Together, results from our snATAC-seq analysis suggest that injury signals induce large-scale changes in the epigenetic landscape that may be responsible for driving dedifferentiation of pre-existing ligamentocytes following ligament injury. Additionally, the enrichment of AP-1 transcription factor motifs suggests a potential role for AP-1 in driving the dedifferentiation of ligamentocytes during ligament regeneration. Future work will help us determine if AP-1 transcription factors are expressed during regeneration and their requirement for driving dedifferentiation during ligament regeneration.

References:

(1) Blalock, D. et al. Joint Instability and Osteoarthritis. *Clin. Med. Insights*: *Arthritis Musculoskelet. Disord.* **19**, (2015).
(2) Howell, K. et al. Novel Model of Tendon Regeneration Reveals Distinct Cell Mechanisms Underlying Regenerative and Fibrotic Tendon Healing. *Sci. Rep*. **7**, (2017).
(3) Anderson, T. et al. Ligament injury in adult zebrafish triggers ECM remodeling and cell dedifferentiation for scar-free regeneration. *Npj Regenerative Medicine* **8**, (2023).

Dynamic Changes in Bone Cellular and Sub-Cellular Porosity Across Reproductive Phases in C57BL/6 Mice

Asier Muñoz[1], Tengteng Tang[2], Aurelien Gourrier[3], Kathryn Grandfield[2], and Alessandra Carriero[1]

1. The City College of New York, City University of New York, New York, NY, USA
2. McMaster University, Hamilton, ON, Canada
3. Université Grenoble Alpes, Grenoble, France

Osteocytes orchestrate bone remodeling and maintain calcium homeostasis through the process of osteocytic osteolysis (a reversible local mineral resorption around osteocytes and canaliculi) [1]. Current research on calcium transport focuses on lacunar-canalicular porosity. Yet, a complex subcellular pathway exists at the nanoscale length that could facilitate ions and moleculae diffusion within the extracellular matrix. Here, we combine advanced imaging to explore the cellular and sub-cellular porosity in lactating C57BL/6 mouse femurs, known to experience osteocytic osteolysis that recovers after weaning [2,3].

Bone cellular porosity of the femoral mid-shaft was acquired using synchrotron microtomography (beamline I13-2 at Diamond Light Source). Female C57BL/6 mice were mated at 11w.o. and randomly allocated to 3 groups (N=10/group): 1) Pregnancy (euthanized at 14w.o. after parturition); 2) Lactation (sacrificed at 16w.o. after 2 weeks of lactation); 3) Recovery (euthanized at 17w.o., after 2 weeks of lactation and 1 week of weaning). Age-matched nulliparous mice were used as controls (N=10/group). Cortical thickness, vascular, and lacunar porosity in the entire midshaft, and in its 4 anatomical quadrants, were examined. Focused-ion beam scanning electron microscopy (FIB-SEM) was utilized to assess subcellular porosity density in the femoral anterior site.

Synchrotron microtomography reveals that cortical thickness increases in pregnant mice in the posterior and medial regions, then decreases in lactating mice in the anterior, medial, and lateral regions, while canal volume density remains unchanged throughout pregnancy, lactation, and recovery. Lacunar density increased in the posterior and lateral regions at various stages of reproduction, but a decrease was noted in the anterior region of recovery mice. During lactation, a decrease in mean lacunar volume was observed in the anterior region, which remained unchanged after forced weaning. Lacunae were also less axially oriented, less elongated, and flatter during lactation, with only flatness returning to normal levels after recovery. FIB-SEM imaging showed about a fourfold increase in nanoporosity volume density in the anterior endocortical region of lactating mouse bone (Fig. 1), with only partial reduction following recovery.

Our findings show recoverable changes in the cortical bone cellular and sub-cellular porosity extending from the meso- to the nanoscale length following pregnancy and lactation. Our 3D-synchrotron microtomography did not show evidence of osteocytic osteolysis in lactation bone as previously reported in the literature [2,3]. Changes in the lacunae orientation and shape might explain the increased cross-sectional area noted in prior 2D-SEM studies [2,3]. FIB-SEM imaging reveals a post-lactation increase in nanoporosity volume density, concentrated in the anterior endocortical region, which may facilitate calcium transport in bone during periods of high mineral demand. Future research should target this area in C57BL/6 lactating mice to better understand its impact on bone.

REFERENCES:

[1] Tsourdi, J Musculoskelet Neuronal Interact., 18(3), 292.
[2] Qing, JBMR, 27(5), 1018-1029
[3] Kaya, JBMR, 32(4), 688-697

Figure 1. Segmented cellular (yellow) and sub-cellular (pink) bone porosities from FIB-SEM images

Differential Effects of Continuous Salt-Inducible Kinase Inhibition on Cortical and Cancellous Bone Responses to Mechanical Loading

Muyin (Mia) Huang[1], F. Patrick Ross[2], Marc N. Wein[3], Marjolein C.H. van der Meulen[1,4]
[1]Cornell University, Ithaca, NY, [2]FPR Scientific Consulting, Amherst, MA,
[3]Endocrine Unit, Massachusetts General Hospital, Boston, MA, [4]Hospital for Special Surgery, New York, NY

Disclosures: MH (N). FPR (N). MNW has received research funding from Radius Health, is a co-inventor on pending patents regarding the use of SIK inhibitors and serves as a consultant for Relation Therapeutics, Sitryx Therapeutics, Aditum Bio & GLG. MCH v/d M (N)

Introduction: Primary hyperparathyroidism (PHPT) is characterized by elevated parathyroid hormone (PTH) levels and has been associated with cortical bone loss, but the impact on cancellous bone is unclear[1]. PTH regulates bone formation and bone resorption by inhibiting Salt-inducible Kinases (SIKs). Continuous SIK inhibition via genetic knock-out in the mouse results in increased cancellous bone and decreased cortical bone in male mice[2]. Previously our lab found that short-term continuous SIK inhibition decreased metaphyseal shell cortical bone mass in adult female mice, whereas loading mitigated the loss. However, minimal effects were observed at the cancellous bone and mid-diaphysis cortical bone. Here, we explored the effect of long-term SIK inhibition at multiple skeletal sites and the therapeutic potential of mechanical loading as a treatment for PHPT-induced bone loss.

Method: Following IACUC approval, 16-week-old female C57BL/6J mice (n=10/grp) were administered the SIK inhibitor SK-124 (40 mg/kg, IP) or a vehicle solution (sterile water, IP, VEH) for 6 weeks (5d/wk). Concurrently, daily in vivo cyclic mechanical loading was applied to the left tibia (5d/wk, 9N, 4Hz, 1200 cycles)[3], and the right limb served as the contralateral control (C). On day 41, the animals were euthanized, and blood was collected for serum analysis. Tibiae were dissected and prepared for microCT imaging (n=9-10 per group) at the cancellous core and cortical shell of the metaphysis, and the mid-diaphyseal cortex. Statistical significance was determined using a linear mixed model (loading & treatment: fixed effects; mouse: random effect) with significance at $p<0.05$. A Tukey HSD post-hoc test was conducted when the interaction term was significant. The 2-week data, obtained previously, are included for comparison in Fig. 1b, 2, 3b.

Results: *Systemic effects:* Residual serum SK-124 levels were elevated in SIK inhibited mice 24 hours after the final injection, confirming continuous treatment (p=0.004). SK-124 increased bone volume fraction (BV/TV) and decreased tissue mineral density (Cn.TMD) in cancellous bone compared to vehicle mice (p=0.0041 & p=0.0054). Metaphyseal shell cortical bone area (Ct.Ar, p<0.0001) and thickness (Ct.Th, p<0.0001) decreased after 6 weeks of SK-124 treatment (Fig. 2). Mid-diaphysis Ct.Ar (p=0.02), Ct.Th (p<0.0001) and tissue mineral density (Ct. TMD, p=0.022) decreased, and marrow area (p=0.0008) increased (Fig. 3b&c). *Loading effects:* In cancellous bone, BV/TV (p<0.0001), trabecular thickness (p<0.0001) and Cn.TMD (p<0.0001) increased in the loaded limbs (Fig. 1a). In the metaphyseal shell, loading increased Ct.Ar, Ct.Th, I_{max} and I_{min} (all p<0.0001). Loaded limbs of VEH had the highest I_{max}, followed by loaded limbs of SK-124-treated animals. I_{max} was lowest in control limbs of both treatments (Tx*Load: p=0.0026). In the mid-diaphysis, loading decreased marrow area (p=0.024), and increased Ct.TMD (p=0.043), Ct.Ar, Ct.Th, I_{max} and I_{min} (all p<0.000, Fig. 3). Loading had more impact in SK-124-treated animals, showing a greater increase in Ct.Ar (p=0.02) and returning Ct.Th to baseline compared to VEH loaded limbs (p=0.01, Fig. 3a&d).

Discussion: Metaphyseal shell bone mass decreased further at 6-weeks compared to 2-week SIK inhibition (Fig. 2). Two-week SIK inhibition had a minimal effect on cancellous and mid-diaphysis cortical bone mass; however, 6-week SIK inhibition increased cancellous bone mass and decreased mid-diaphyseal cortical bone mass (Fig. 1b&3b). Mechanical loading was essential to maintaining cortical bone mass at both the cortical metaphyseal shell and mid-diaphysis. The increase in cancellous bone mass after 6 weeks of SIK inhibition occurred following significant bone loss in the metaphyseal shell observed at 2 weeks, emphasizing the importance of mechanical loading to rescue cortical bone loss and maintain bone mass. Future work should study the mechanism underlying the differential response to PHPT in cortical and cancellous bone and the increased mechanoresponsiveness at all sites examined.

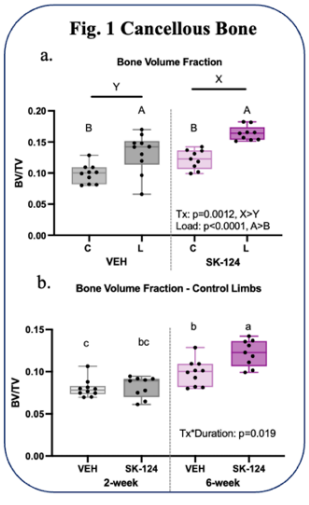

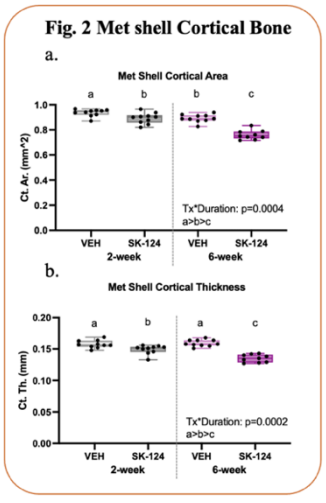

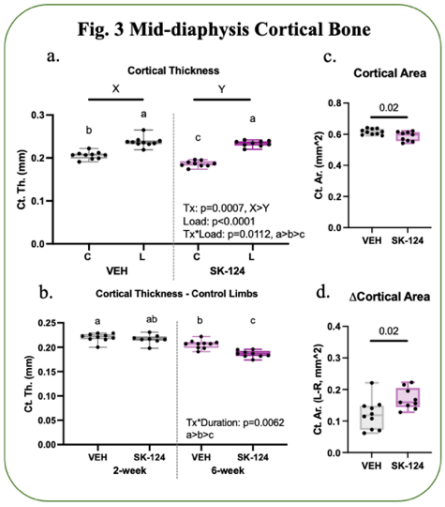

References:
[1]Khan et al. 2000. [2]Sato et al. 2022. [3]Fritton et al. 2005.

Acknowledgments: We thank the Cornell CARE Staff. Funding provided by Robert & Helen Appel Fellowship, and NIH R01-AR081943.

ABSTRACT #022

Inhibition of Fibroblast Activation Protein Restores the Homeostatic Phenotype of Mechano-activated Synovial Fibroblasts

Elizabeth R. Bernstein[1, 2, 3], Brendan Stoeckl[1,2,3], Rachel Flaugh[2, 3], Robert L. Mauck[1, 2, 3], Liane Miller[2, 3]
Depts. of [1]Bioengineering and [2]Orthopaedic Surgery, University of Pennsylvania; [3]CMC VA Medical Center, Philadelphia, PA

Introduction: Osteoarthritis (OA) is a major source of pain and disability and current treatments are limited to symptom management. Recently, synovial fibrosis has been identified as a potential driver of disease. Pro-inflammatory cytokines and extracellular matrix (ECM) stiffening in the synovium activate fibroblast-like synoviocytes (FLS), priming them to differentiate into myofibroblasts. These activated cells secrete additional ECM and inflammatory mediators, creating a vicious cycle of stiffening, inflammation, and degeneration. Fibroblast activation protein (FAP) is expressed in the synovium of patients with OA and contributes to disease progression, but the mechanisms by which it does so are undefined. This study sought to determine whether FAP inhibition can reverse the activation of FLS seen in OA.

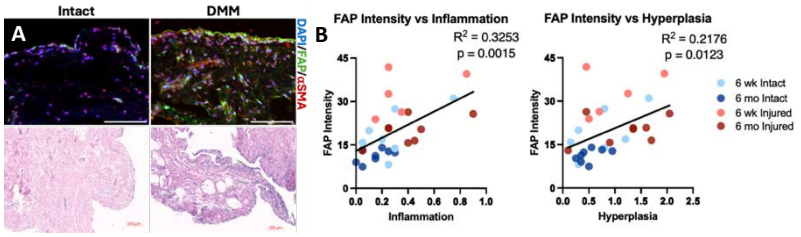

Figure 1. (A) Images of porcine synovium. Scale = 100μm. (B) Correlation of FAP staining intensity and synovial scoring.

Methods: Minipigs underwent destabilization of the medial meniscus (DMM). Synovium was harvested at 6 weeks and 6 months and scored or analyzed for FAP and αSMA expression. An *in vitro* model of FLS activation was established by culturing bovine FLS on glass with TGFβ-1. FAP inhibitor (FAPi) and Fasudil, a Rho/ROCK inhibitor that inhibits cell contractility, were added to activated FLS. After 6 days, cells were stained for actin, αSMA, paxillin, and FAP. Cell area, actin:αSMA colocalization, and focal adhesions were quantified, as was the expression of FAP, ACTA2, FN1, and CCN2. To assess contractility, FLS were seeded in collagen gels and percent initial area was quantified over time. Correlations between IF and synovitis scores were determined by linear regression. Other outcomes were compared by two-way ANOVA.

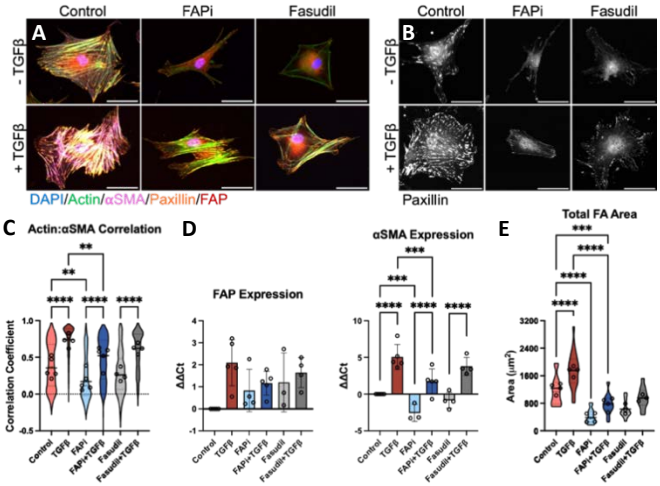

Figure 2. Images of (A) bovine synoviocytes (B) focal adhesions. Scale = 50μm. (D) Actin:αSMA colocalization. (E) RT-qPCR. (E) Total focal adhesion area per cell. **p<0.01. ***p<0.001. ****p<0.0001.

Results: <u>FAP expression correlates with αSMA, inflammation, and hyperplasia in OA synovium.</u> FAP and αSMA staining intensity increased in DMM synovium at both 6 weeks ($p<0.01$, $p=0.0004$) and 6 months ($p<0.05$, $p<0.0001$) (**Fig 1A**), with a positive correlation between FAP and αSMA staining intensity for individual donors ($R^2= 0.4294$, $p<0.001$). FAP intensity was also correlated with synovial inflammation ($R^2= 0.33$, $p<0.01$) and hyperplasia ($R^2= 0.22$, $p<0.05$) (**Fig 1B**). <u>FAP inhibition rescues mechano-activated FLS.</u> Activation of FLS on glass with TGFβ increased cell spreading, actin:αSMA colocalization ($p<0.0001$), and expression of FAP, αSMA ($p<0.0001$), CTGF ($P<0.0001$), and FN ($p<0.001$) (**Fig 2A,C,D**). Treatment with FAPi significantly reduced actin:αSMA colocalization ($p<0.01$) and αSMA expression ($p<0.001$) and decreased cell area and expression of FAP, CTGF, and FN (**Fig 2A,C,D**). FAP inhibition also reduced focal adhesion number ($p<0.0001$) and area ($p<0.0001$) (**Fig 2B,E**) and contraction of FLS-embedded collagen gels ($p<0.05$) (**Fig 3**).

Discussion: Our findings show that FAP inhibition can rescue the transcriptional and functional profile of activated FLS. Our *in vivo* porcine data indicate that the upregulation of FAP seen in human OA synovium is replicated in our large animal model and is correlated with progression of synovial pathology. The correlation of FAP and αSMA suggests that more mechano-activated cells express higher levels of FAP. *In vitro*, FAPi reversed the activated FLS phenotype, and did so to an equivalent or greater extent than Fasudil. FAPi's reduction of focal adhesion quantity and size implies that FAP may contribute to FLS activation by promoting focal adhesion initiation and maturation.

Significance: These data reveal a role for FAP in FLS mechanobiology, offering a potential mechanism by which this protein contributes to OA. The finding that FAPi effectively rescued the homeostatic phenotype of activated FLS indicates that it is a promising therapeutic for treating OA.

Figure 3. Quantification of collagen gel contraction. *p<0.05. ***p<0.001.

ABSTRACT #023

A mouse model for study of mechanisms and alleviation of osteoarthritis (OA) pain

Giulia DiRaimo[1], Hassan Ainani[2], Susan Mcnamara[3], Sylvia O Suadicani[3,4], Mia M Thi[1,4], David C Spray[2]

Departments of [1]Orthopedic Surgery,[2]Neuroscience, [3]Urology and [4]Molecular Pharmacology. Montefiore Medical Center and Albert Einstein College of Medicine, Bronx, NY

PURPOSE: Osteoarthritis (OA) is a chronic degenerative disease affecting >500 million individuals worldwide (WHO). OA substantially impacts patient quality of life through limited mobility and chronic joint pain, yet effective pain management strategies remain limited. Lack of curative treatments emphasize the need for translational and clinical research, combined with better fundamental understanding of the disease.

METHODS: To implement mechanistic studies on osteoarthritis pain and movement compromise, we are developing a mouse OA model induced by Monoiodoacetate (MIA). This drug is known to disrupt chondrocyte glycolysis leading to cell death, neovascularization, subchondral bone necrosis and collapse, as well as inflammation. In these studies, 3-6 month old mice received single intra-articular injections of MIA (1 mg/mL, in 10µL of saline solution) or the same volume of saline into one knee joint. Fluorescent dye FM-143FX was co-injected to allow identification of dorsal root sensory neurons innervating the tissue. Contralateral knee joints served as naïve controls. Pain was assessed through expression of pain biomarkers (including tumor necrosis factor alpha (Tnf-α), interleukin-1 beta (Il-1β), calcitonin gene-related peptide (CGRP), and components of the NLRP3 inflammasome. Pain sensitivity was evaluated through tactile hypersensitivity measurements on plantar surfaces of the ipsi- and contralateral hindlimbs (Von Frey test). At 4 weeks post-injection, knee joints were harvested for subsequent histological assessment of bone and cartilage damage. Dorsal root ganglia (DRG; L2-L6) corresponding to each side of the knee were collected for electrophysiological and qPCR analysis to evaluate biochemical and molecular alterations in sensory neurons innervating the knee. Intracellular Ca^{2+} imaging of DRG neurons and satellite glial cells was performed using both the ratiometric Ca^{2+} indicator Fura-2AM and the genetically encoded indicator GCaMP6 expressed in neurons or glia driven by Pirt or PLP promoters, respectively. All experiments were performed under IACUC approval.

RESULTS: Expression of pain biomarkers in DRGs innervating MIA-injected knees was upregulated when compared to that of DRGs innervating saline-injected or naïve knees, indicating enhanced pain sensitivity following MIA injection. Preliminary Von Frey assessments suggested that pain tolerance might be reduced post-MIA injection, although very high variability in responses necessitates further investigation. Electrophysiological recordings from dissociated cultures containing retrograde labeled FM-143FX DRG neurons revealed that the labeling did not negatively impact excitability properties. Preliminary results indicate sex differences in baseline neuronal excitability. Ca^{2+} imaging experiments performed using either ratiometric or genetically encoded Ca^{2+} indicators, neurons and glia were shown to respond to KCl induced depolarization and to bath applied ATP with robust increase in intracellular Ca^{2+} concentration.

CONCLUSIONS AND SIGNIFICANCE: Implementation of this mouse model now provides the opportunity to expand behavioral testing to include evaluation of both thermal and tactile pain and overall behavior with behavioral spectrometer, to assess mobility through gait/catwalk and extension testing. Next, electrophysiological studies of sensory ganglia from control and MIA-induced OA mice will be evaluated for neuronal hyperexcitability and dye coupling of glia and neurons, and histopathology and by µCT will be used to evaluate cartilage integrity. Additionally, we can now investigate the expression levels of several key targets associated with pain signaling in mice, and correlate their altered expression levels with measured changes in neuronal excitability in order to identify novel targets for alleviation of OA pain.

ACKNOWLEDGEMENTS: Supported in part by Montefiore Orthopaedic Seed Grant.

Potential Role of Irisin in the Association of Diabetic Neuropathy with Bone Loss

Hassan Ainani[1], Giulia DiRaimo[2], Marcia Urban-Maldonado[3], Sylvia O Suadicani[3,4], David C Spray[1], Mia M Thi[2,3]

Departments of [1]Neuroscience,[2]Orthopedic Surgery, [3]Molecular Pharmacology and [4]Urology, Montefiore Medical Center and Albert Einstein College of Medicine, Bronx, NY

PURPOSE: Peripheral neuropathy and osteoporosis are common diabetes complications resulting in long-term bone and joint pain, motor dysfunction and greater chance of fractures. Prior studies have recognized the importance of neural control in skeletal development, homeostasis, repair and bone pain, and point to "signaling molecules" acting as messengers between these systems, offering novel therapeutic targets for future approaches to manage diabetic neuropathy and skeletomuscular disorders. One such molecule is irisin, an adipomyokine released from muscle during exercise that has anti-inflammatory, cell survival and glucose-stabilizing properties. In previous studies we demonstrated that in T1D mice the exercise-induced bone anabolic response is impaired and is accompanied by both local bone inflammation and blunted exercise-induced increase in circulating irisin levels. We have now investigated the potential role that dysregulated irisin signaling plays in exercise-induced inflammatory response not only in the bone but also in the nervous system, whereby contributing to diabetic neuropathy and bone loss.

METHODS: We used the Akita (C57BL/6J<Ins2Akita>) mouse model of T1D and age-matched wildtype (Wt) mice (8 wk old, male, n=6/group) that were submitted to mechanical loading by treadmill running (1, 2 and 4 wk; 5 days/wk, 300 m/day) during their active phase (nighttime). All animals were euthanized immediately after the last running bout, and femur, blood and sensory dorsal root ganglia (DRGs; L2-L6) were collected. Serum irisin levels were quantified using ELISA. Levels of inflammatory mediators in DRG were quantified by qPCR. All experiments were performed under IACUC approval. A second set of Wt and Akita mice was used to prepare DRG cultures that were maintained in normal (1 g/dL; NG) and high glucose (4.5 g/dL, HG) respectively. Ca^{2+} imaging using ratiometric Ca^{2+} indicator Fura-2 AM and electrophysiological studies were performed on cultured DRG neurons and satellite glial cells (SGCs) in the absence and presence of irisin (100nM).

RESULTS: We found that in healthy mice the exercise-induced changes in circulating irisin levels followed a time course that paralleled that of the exercise-induced bone anabolic response, and inversely correlated with the levels of exercise-induced inflammatory mediators (*Cgrp, Tnfa, Nlrp3, Il1b*) in the DRGs. Notably, these associations and pattern of responses to exercise were lost in diabetic mice. Electrophysiological recordings from cultured DRG neurons showed that while irisin had no effect on the action potential (AP) properties of Wt neurons, it reduced the AP amplitude in T1D Akita neurons. Moreover, irisin decreased the excitability of diabetic Akita neurons. Ca^{2+} imaging experiments revealed that irisin decreased the sensitivity to stimulation with ATP in neurons alone, SGCs attached to neurons and SGCs alone in Wt mice cells cultured in both normal and high glucose media. However, in T1D neurons and SGCs, irisin blunted ATP sensitivity only when cells were cultured in high glucose medium.

CONCLUSIONS: Based on these initial findings, we hypothesize that irisin plays a key role in modulating the exercise-induced inflammatory responses in DRG, the DRG neuron excitability, neuron-SGC interactions and ATP signaling. In this context, dysregulation of irisin signaling in the DRG might be one of the factors contributing to diabetic peripheral neuropathy and consequent dysregulation of neural regulation of the bone, which can ultimately contribute to diabetic bone loss. These findings provide initial evidence that irisin signaling can provide a novel target to develop more effective management of diabetic neuropathy and skeletomuscular disorders.

ACKNOWLEDGEMENTS: Supported in part by Montefiore Orthopaedic Research Seed Grant

A New Mouse Model to Understand Pathogenesis of Heterotopic Ossification in Tendon

Julia Robbins[1], Matthew Casserly[1], Saswati Kar[1], Fei Fang[1]
[1]Icahn School of Medicine at Mount Sinai, New York, NY

Disclosures: None

Introduction: Heterotopic Ossification (HO) is the abnormal ectopic formation of bone in soft tissues, such as tendons and ligaments.[1,2] The exact mechanism governing HO development remains elusive. Our previous studies have shown that transplantation and then retention of cells with activated hedgehog (Hh) signaling leads to HO in tendon, which indicates the potential role of Hh signaling in driving HO formation.[3,5] The cellular origin of HO is also fairly complex, involving many different progenitor cells such as mesenchymal stem cells, tendon cells, and connective tissue cells (i.e. peritenon and epitenon).[4] The objective of this study is to build a new mouse model of tendon HO by activating Hh signaling to further understand HO pathogenesis. We hypothesize that activation of Hh signaling causes HO formation.

Methods: All animal procedures were approved by the Icahn School of Medicine at Mount Sinai IACUC. Animal Models: We used C57BL/6J mice to determine the effectiveness of Hedgehog Agonist (Hh-Ag 1.5, Cellagen Technology) in inducing HO via over-activation of Hh signaling.[5] Inducible Gli1Cre^{ERT2};Ai14 mice (Gli1, a Hh effector) were bred to determine the role of Hh-responsive cells during HO development.[3] Heterotopic Ossification Model: HO was induced by injecting 7.6 mM Hh-Ag 1.5 into the right Achilles tendons twice per week.[5] Saline was injected into the left Achilles tendons to serve as controls. For the C57BL/6J mice, injections were performed from 9 to 11 weeks and were sacrificed at 14 weeks. For Gli1Cre^{ERT2};Ai14 mice, Hh-Ag 1.5 injection was performed from 7 to 9 weeks, and the mice were sacrificed at 11, 12 and 14 weeks. Tamoxifen was administrated for lineage-tracing right after Hh activation.[3] µCT Analysis: Hindlimbs from the mice were dissected and analyzed by µCT (ScancoMed). The samples were imaged at a voltage of 70 kVp, current of 114 µA, voxel size of 4.9 µm per voxel, and a low resolution. The images were reconstructed and analyzed to determine bone volume and tissue mineral density. Histology: Tissue specimens were fixed overnight, decalcified, and embedded in OCT. The samples were sectioned and stained with Safranin O-Fast Green and imaged on a Zeiss Axiolmager 2 microscope. Immunohistochemistry (IHC): The sample sections were incubated with hyaluronidase, permeabilized with Triton X, blocked with goat serum, incubated with primary antibodies (Sox9 or Osterix (OSX)), and corresponding secondary antibodies. The stained samples were imaged on a Leica DM6 microscope and analyzed using Image J.

Results: In the C57BL/6J mice, mineralized tissue was found within all the samples that received Hh-Ag 1.5 injection. There was a statistically significant difference in bone volume, as well as tissue mineral density between the control and the group with Hh activation. Based on these results, we successfully created a Hh-induced HO model *in vivo*. In the Gli1Cre^{ERT2};Ai14 lineage-tracing reporter mice, a sex-dependent difference was observed. More mineralized tissue was found within the Achilles tendons of male mice (average bone volume = 0.1835 mm^3), compared to female mice (average bone volume = 0.01315 mm^3) (Fig. 1A & B). There was a statistically significant difference in terms of bone volume between the control and treated groups in the male but not the female mice (Fig. 1B). Histological findings corroborated the µCT results, indicating greater cartilage and ectopic bone formation in the male mice, compared to the female mice. IHC revealed that Sox9 and OSX were both expressed within the HO region of the Achilles tendons. Co-localization of Gli1 and Sox9 (Fig. 2A & B), as well as Gli1 and OSX (Fig. 2C & D) was observed, indicating that Gli1-lineage cells contribute to chondrogenesis and osteogenesis during HO pathogenesis. Furthermore, the Safranin O-Fast Green stains monitoring the progression of HO development indicate that HO tissue contained chondrocyte-like cells at 3 weeks after Hh activation and similar structure to trabecular bone (i.e lacunae) was found at 5 weeks after Hh activation. These observations indicate that Hh-induced HO within the Achilles tendon is generated through endochondral ossification (Fig. 3).

Discussion: We developed a new *in vivo* model, which is free of trauma or injury, to track cell phenotype shifts during HO development. This *in vivo* model demonstrates that Hh signaling plays an essential mechanistic role in HO progression. Through the use of lineage-tracing mice, we were able to track the involvement of specific Gli1-lineage cells within HO pathogenesis. Consistent with our previous studies, Gli1-lineage cells appear to be the main cell population involved in HO formation. Once activated, these Gli1-expressing cells functions as stem cells, displaying both chondrogenic and osteogenic potential. Furthermore, our µCT and histology results indicate that tendon HO develops through a cartilage intermediate, and undergoes endochondral ossification.[2,3] Our future work will explore the sources of Gli1-lineage cells for driving HO formation and identify molecular factors responsible for cell differentiation during HO pathogenesis.

Significance: A better understanding of the mechanism and cellular origins of HO will provide insights into the development of more effective and specific therapeutic strategies to prevent HO initiation.

References: [1] C. Meyers et al. *JBMR Plus* 2019 [2] Y. Xu et al. *Front. Cell Dev Biol.* 2022 [3] F. Fang et al. *Cell Stem Cell* 2022 [4] J. Yea et al. *Bone Res* 2023 [5] J. McKenzie et al. *J Orthop Res* 2019 [6] A. Schwartz et al. *Development* 2015 [7] A. Schwartz et al. *Development* 2017

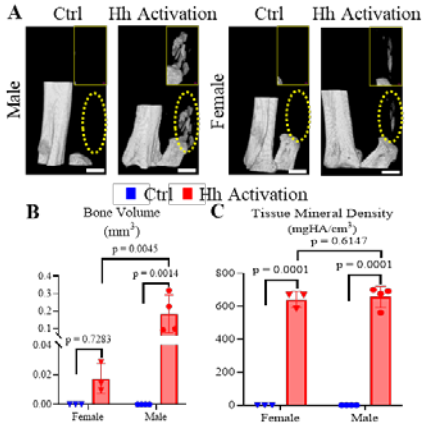

Figure 1. Hh-induced HO is sex-dependent. **(A)** The µCT reconstruction of the limbs of Gli1Cre^{ERT2};Ai14 mice sacrificed at 14 weeks. Ossified tissues are encircled in yellow. The scale bar is 500 µm. **(B)** Bone volume of HO tissues. **(C)** Tissue mineral density of HO tissues.

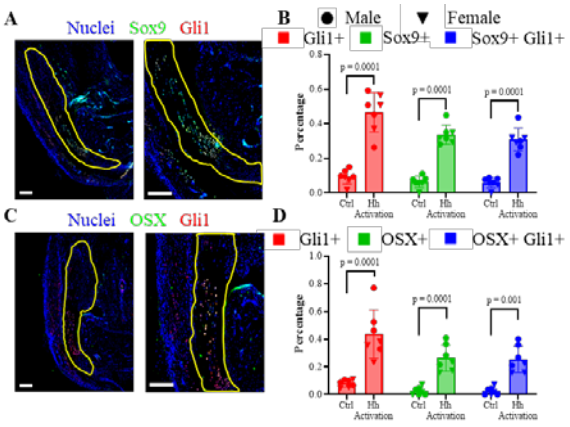

Figure 2. Hh-lineage cells form HO tissues. **(A)** Chondrogenic marker Sox9 is present within HO regions of the Achilles tendon after Hh activation. The scale bar is 200 µm. **(B)** Most Gli1-lineage cells express the chondrogenic marker Sox9. **(C)** Osteogenic marker OSX is present within HO regions of the Achilles tendon after Hh activation. The scale bar is 200 µm. **(D)** Most Gli1-lineage cells express the osteogenic marker OSX.

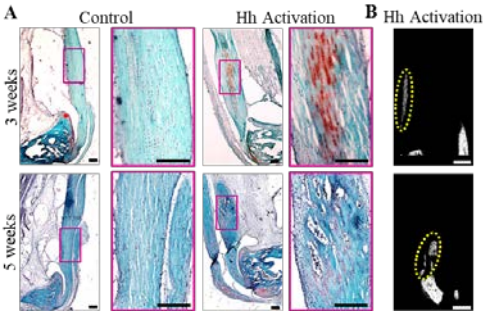

Figure 3. HO tissue is identified first as chondrogenic process, followed by osteogenic progress. **(A)** Representative Safranin O-Fast Green image indicates cartilaginous and osteogenic tissue in HO region. (**B)** Representative µCT imaging correlates with histology. The scale bar is 200 µm.

ABSTRACT #026

Microenvironment-specific transcriptomic changes in OS metastasis

Shimara Gunawardana-Zeigler[1], Dan Peng, PhD[2], Yuqi Tan, PhD[3], Patrick Cahan, PhD[2], David Loeb, MD PhD[1]

[1]Department of Developmental and Molecular Biology / Department of Pediatrics, Albert Einstein College of Medicine, Bronx, NY.

[2]Department of Biomedical Engineering, Johns Hopkins University School of Medicine, Baltimore, MD.

[3]Department of Microbiology and Immunology, Stanford University, Stanford, CA.

Osteosarcoma (OS) is the most common primary malignancy of bone in children and adolescents. While conventional chemotherapy has improved 5-year survival rates for localized disease to 70%, metastatic disease remains at 20-30%. Failure of modern treatment options to improve survival reflects the failure of agents that appear promising in preclinical models to demonstrate clinical efficacy in human patients. We hypothesize that this is because most preclinical testing is performed on tumors implanted subcutaneously in immune deficient mice. Our previous work has shown that tumors implanted subcutaneously do not metastasize, whereas genetically identical tumors implanted orthotopically (in the tibia) metastasize to lungs and bones. Thus, to better understand non-genetic drivers of metastasis, we implanted patient-derived xenografts (PDXs) either orthotopically or subcutaneously into NSG mice. Once tumors reached 1.5cm, tumors were extracted along with distant metastases and analyzed by single-cell RNA sequencing. Transcriptomic analysis reveals 1) that fragments of the same tumor implanted subcutaneously have a vastly different transcriptome than fragments implanted orthotopically, 2) the transcriptome of distant metastases is dramatically different from the transcriptome of the primary tumor, and 3) the gene expression profile of metastases is different in different metastatic sites. In all 3 of these circumstances, these differences reflect differences in differentiation status, signaling pathway activation, and immune cell infiltrate. Thus, we conclude that the environment in which a tumor grows significantly alters its gene expression and phenotype. Our study highlights the need for careful consideration of the tumor microenvironment when designing pre-clinical studies to ensure accurate representation of human osteosarcoma and may help to explain the dismal record of translating novel agents from preclinical studies into standard therapy.

Investigating the role of mechanical stimulation in guiding stem cell activation and differentiation during scar-free ligament regeneration post-injury in adult zebrafish

Maryam Kamel[1,2 3], Troy Anderson[1,2 3,4], **Joanna Smeeton**[1,2 3,4]
Columbia University Vagelos College of Physicians and Surgeons[1], Columbia Stem Cell Initiative[2], Department of Rehabilitation and Regenerative Medicine[3], Department of Genetics and Development[4]

Ligament and tendon tears are common musculoskeletal injuries that often lead to long-term complications, including scar formation, recurrent tears, and osteoarthritis. This significant clinical burden highlights the need to enable scar-free connective tissue regeneration. Previously, we found that unilateral transection of the jaw joint-stabilizing interopercular-mandibular (IOM) ligament in adult zebrafish heals without scarring through the activation of endogenous skeletal progenitors that differentiate into mature ligament cells.[1] Moreover, tenocytes have been shown to respond to mechanical stimulation in exercise and acute injury contexts.[2,3,4] Recognizing the crucial role of mechano-transduction in skeletal tissue healing, this study investigates the role of mechanical stimulation and biomechanical signaling during scar-free regeneration.

In-silico analysis of chromatin accessibility in ligament progenitors suggests that the transcription factors Nfatc4 and Tead4, involved in transducing Calcineurin and Yap/Taz mechano-signaling pathways respectively, are active during regeneration. To assess the activity of these biomechanical signaling pathways *in vivo*, we employed fluorescence *in situ* hybridization for *nfatc4*, *piezo1*, and *tead4*, as well as pathway target genes, such as *cyr61*, in histological sections of injured ligaments at 1-7 days-post-ligament-transection (dplt). We find that mechanosensitive pathway activity is downregulated immediately following injury but recovers by 3 dplt, coinciding with the re-expression of mature ligament marker *thbs4a*. These data suggest a correlation between mechano-sensation and the regulation of ligamentocyte differentiation during scar-free ligament regeneration in adult zebrafish.

Ongoing research tests the requirement of mechano-signaling by contrasting normal ligament healing with healing in the absence of mechanical stimulation. Ultimately, these foundational studies not only have critical translational implications for the use of physical therapy following ligament tears but also lay the groundwork for future research aimed at understanding mechano-signaling mechanisms and applying these findings to stimulate regeneration in analogous cells in human patients.

This research was funded by an AR[3]T Regenerative Rehabilitation Pilot Grant.

References:

1. Anderson, T. *et al.* Ligament injury in adult zebrafish triggers ECM remodeling and cell dedifferentiation for scar-free regeneration. *Npj Regenerative Medicine* **8,** (2023).
2. Jones, D. L. *et al.* Mechanoepigenetic regulation of extracellular matrix homeostasis via Yap and Taz. *Proceedings of the National Academy of Sciences* **120,** (2023).
3. Nakamichi, R. *et al.* The mechanosensitive ion channel PIEZO1 is expressed in tendons and regulates physical performance. *Science Translational Medicine* **14,** (2022).
4. Passini, F. S. *et al.* Shear-stress sensing by PIEZO1 regulates tendon stiffness in rodents and influences jumping performance in humans. *Nature Biomedical Engineering* **5,** 1457–1471 (2021).

Novel Analgesic ART26.12 as a Fatty Acid Binding Protein 5 Inhibitor for Osteoarthritic Pain

Kai L. Bou[1], Adam J. Bruzzese[2], Chris Gordon[1], Kaitlin M. Farrell[2], David E. Komatsu[2], Martin Kaczocha[1]
[1]*Department of Anesthesiology, Renaissance School of Medicine, Stony Brook University*
[2]*Department of Orthopaedics and Rehabilitation, Renaissance School of Medicine, Stony Brook University*

INTRODUCTION: Knee osteoarthritis (OA) is a prevalent, degenerative joint disease characterized by loss of articular cartilage, subchondral bone damage, and inflammation of synovial tissues, contributing to the onset of chronic pain. Current treatments resort to non-steroidal anti-inflammatory drugs (NSAIDs) or opioids to treat OA-induced pain, however, the lack of short term efficacy of both in addition to the adverse effects of elevated blood pressure and gastrointestinal ulcers in NSAIDs and development of tolerance and addiction in opioids fail to treat OA-induced pain efficaciously in the long term. The need to develop a non-opioid analgesic to treat pain in the setting of OA with long term efficacy is pressing. Previous preclinical models have shown that fatty-acid binding protein 5 (FABP5) inhibition demonstrates analgesic activity through modulating its role as a chaperone to transfer fatty acids within the endocannabinoid system (ECS). ART26.12 (Fig. 1), a FABP5 inhibitor, demonstrates selective binding to FABP5 rather than to known FABP family isoforms; ART26.12 has anti-nociceptive properties, less off-target liabilities, and increased oral bioavailability, thus having potential to prevent and/or reduce OA-induced pain. This study investigates the efficacy of the novel drug, ART26.12, in reducing OA pain using a rat model.
METHODS: Experiments were conducted under approval by the Stony Brook University Institutional Animal Care and Use Committee (#277150). Female Sprague Dawley rats (n = 51) underwent surgical destabilization of the medial meniscus (DMM). X-ray imaging was conducted to visualize progression of OA (Fig. 2) throughout eight weeks post-surgery. On the eighth week, rats were subdivided into five groups, and acute dosing was carried out via oral administration of vehicle (n = 10), 8 mg/kg naproxen (n = 10), and three concentrations of ART26.12 (10 mg/kg [n = 10], 25 mg/kg [n = 10], 50 mg/kg [n = 10]) at a volume of 2 µl/g. Static incapacitance was measured post-administration at 1 hour and 4 hours. To measure incapacitance, rats were gently positioned into the IITC incapacitance test meter (IITC Life Science Inc, USA), and six readouts of ten-second hind leg recordings were collected. Incapacitance is reported as an averaged ratio of ipsilateral to contralateral hindlimb weight bearing. Results are presented as dot plots with mean and 95% confidence intervals overlaid. Normality was confirmed with Shapiro-Wilk tests. Subsequently, comparisons between groups were made using one-way repeated measures ANOVA followed by Dunnett's multiple comparisons with the baseline data as the control group. All analyses were performed using Prism (Ver. 10.3.0, GraphPad).
RESULTS: X-ray images show progression of osteoarthritis through observing shortening of the knee joint space and subchondral bone damage (Fig. 2). As expected, no differences in incapacitance were found for the vehicle group (Fig. 3). In the ART26.12 groups, significant increases in weight bearing on the ipsilateral (arthritic) limb were observed compared to the contralateral limb, indicated by the increased weight bearing ipsilateral/contralateral ratios between baseline and post-dose timepoints in the treatment groups. Specifically, rats dosed with 10 mg/kg ART26.12 showed a significant increase in weight bearing on the ipsilateral limb only at the 1-hour post-dose time point, while the 25 mg/kg and 50 mg/kg ART26.12 groups showed significant increases at both 1-hour and 4-hour post-dose timepoints (Fig. 3). The 8 mg/kg naproxen group showed a significant increase in weight bearing on the ipsilateral limb only at the 4-hour post-dose time point (Fig. 3).
DISCUSSION: The increases in weight bearing ratios between baseline and post-dose timepoints in the treatment groups suggest that ART26.12 reduced OA-induced pain in the ipsilateral limbs. In the naproxen group, there was only an increase in weight bearing on the ipsilateral limb at the 4-hour post-dose timepoint, resembling the 10 mg/kg ART26.12 group. This is consistent with previous studies showing the mild-to-moderate efficacy of nonsteroidal anti-inflammatory drugs (NSAIDS) in mediating OA. With higher ART26.12 concentrations, from 10 mg/kg to 25 mg/kg and 50 mg/kg, there was a more pronounced, statistically significant increase in weight bearing on the ipsilateral limb from baseline to 1-hour and 4-hour post-dose timepoints. The positive correlation between ART26.12 concentration and weight bearing on the arthritic limb suggests that ART26.12 may be a more responsive alternative to naproxen in treating OA-induced pain. Osteoarthritis (OA) affects over 500 million people worldwide most commonly in the knee (~60% of cases), leading to joint debilitation and persistent, extreme pain; yet, no established medication mitigates OA pain with long-term efficacy. ART26.12 is a promising treatment alternative for chronic OA pain given its efficacy with acute doses and its selective action upon a novel lipid-signaling pathway.

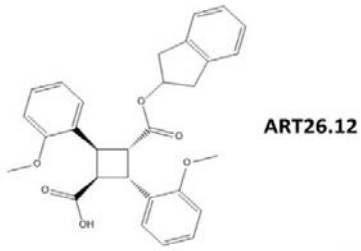

Figure 1. ART26.12 Chemical Structure

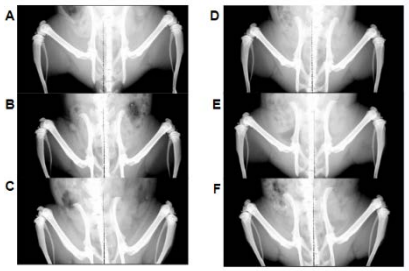

Figure 2. X-ray imaging of two pre-dose rats. (A) and (D) pre-DMM surgery. (B) and (E) 2 weeks post-surgery. (C) and (F) 8 weeks post-surgery.

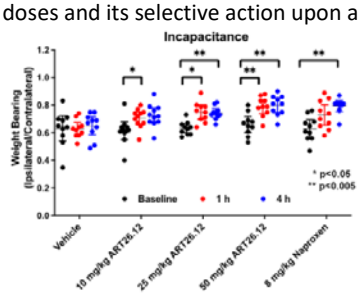

Figure 3. Acute Dose Weight Bearing on Arthritic Limbs Ipsilateral/contralateral weight bearing ratios were measured at baseline, 1-hour post-dose, 4-hour post-dose timepoints

A Multi-functional Small Molecule to Enhance Healing of Avascular Meniscus Tears

Meng Feng, David Pellei, HunJin Jeong, Vyshnavi Tallapaneni, Elen Zhu, Chang Lee
Regenerative Engineering Laboratory, Columbia University

Introduction: Meniscus injuries are a leading cause of weakened knee joint function, pain, and post-traumatic osteoarthritis. Simultaneously, the endogenous repair capacities of the meniscus are limited. Our previous studies demonstrated the efficacy of bioactive glue sequentially releasing connective tissue growth factor (CTGF) in meniscus healing and harnessing endogenous synovial mesenchymal stem cells (SMSCs). However, an approach involving multiple growth factors has suffered from several translational challenges. In this study, we repurposed a small molecule, 4-PPBP as an agonist for Sigma 1 receptor (σ1R) in endoplasmic reticulum homeostasis for meniscus healing. Our central hypothesis is that 4-PPBP delivery via an injectable bioglue may promote meniscus healing via inducing cellular proliferation, migration, and differentiation of endogenous meniscal fibrochondrocytes and SMSCs, as well as regulating proinflammation niche. We further investigated the profibrogenic and anti-inflammatory effects of 4-PPBP *in vitro* and *ex vitro*.

Methods: This study was approved by the IRB at Columbia University (project number #AC-AACB1704). *Cells:* Primary meniscus fibrochondrocytes were isolated from healthy bovine knee joints with type 2 collagenase enzyme digestion for 6 hours, followed by growing migratory cells for 24 hours. Human SMSC was isolated from a 56-year-old female patient and validated per our prior methods. Effect of 4-PPBP on *cell migration and proliferation*: We applied a wound scratch model for SMSCs treated with 4-PPBP and performed a CCK-8 assay at 24 and 48 hours. *Anti-inflammatory roles of 4-PPBP*: The anti-inflammatory effect of 4-PPBP was tested in bovine meniscus cells & human SMSCs treated with 10 ng/ml IL-1β and/or 10 μM 4-PPBP. In addition, pro-inflammatory marker expression was measured by qRT-PCR in SMSCs treated by 1) IL-1β, 2) 4-PPBP overnight and then IL-1β for 24 hours, or 3) IL-1β overnight and then by 4-PPBP for 24 hours. Immunofluorescence for σ1R, MMP-3, and CTGF was measured in SMSCs treated by 4-PPBP with or without σ1R, BD1047. Signaling of 4-PPBP was described using Western blotting. *Meniscus explant*: Per our established methods, a longitudinal tear was created in the inner 1/3 zone of fresh bovine meniscus explants (1.0cm×0.8cm×0.6cm). *Bioglue*: fibrin (100 mg/ml fibrinogen + 100U/ml thrombin) cross-linked with 2.5 mg/ml genipin (FibGen), was applied to the meniscus defects with or without 10 μM 4-PPBP and suspending 106/ml human SMSCs in the culture plate. The meniscus explants were then cultured in fibrogenic and chondrogenic medium for 28 days. The harvested tissues were analyzed using HE and Picrosirius red staining. *Statistical analysis* of gene expressions was performed using GraphPad Prism 5.0 with Student's *t*-test for two-group comparisons. $p<0.05$ was considered as statistically significant.

Results: Scratch wound healing and CCK-8 assays showed that 4-PPBP promoted migration and proliferation of human SMSCs and bovine meniscal fibrochondrocytes (Fig. 1A). Per CCK8 assay, IL-1β reduced proliferation of SMSCs but 4-PPBP attenuated the effect of IL-1β (Fig. 1B). Inflammatory cytokines in bovine fibrochondrocytes, IL-1β and IL-6, as well as an inflammation-associated transcription factor, NF-κB, stimulated with IL-1β were significantly attenuated by 4-PPBP treatment both before and after IL-1β application (Fig. 1C). Immunofluorescence showed that 4-PPBP elevated expressions of σ1R and CTGF while decreasing that of MMP3 in meniscal cells and SMSCs. This was notably attenuated by application of 100 μM BD1047, σ1R antagonist. Similarly, our Western blotting data showed that 4PPBP inhibited MMP3 expression and increased downstream expression of pERK and CTGF (Fig. 1D). In our meniscus explant healing model, a single application of 4-PPBP via FibGen enhanced healing of longitudinal tears in the inner avascular zone, demonstrated by minimal tissue gapping and newly formed collagen fibers (Fig. 2A & B). In addition, we noticed highly proliferative cells at the peripheral region of meniscus tears with 4-PPBP application, likely confirming the effects of 4-PPBP in stimulating cellular proliferation (Fig. 2A).

Conclusion: FibGen bioglue was activated by 4-PPBP to serve as an artificial matrix which can enhance healing and seal meniscal gapping within a torn meniscus. Our data may lead to the development of a novel, injectable, and *in situ*-forming bioactive glue with a single small molecule that can reduce inflammatory response-associated tissue damage and enhance avascular meniscus healing.

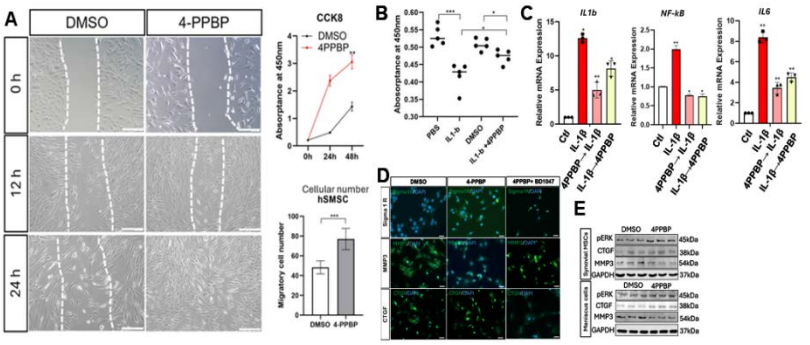

Fig. 1. (**A**) Effects of 4-PPBP on cell migration (left) and cell proliferation (right) in human SMSCs *in vitro*; (**B**) Effects of 10 μM 4-PPBP on cell proliferation in IL-1β stimulated condition (n=5 per group); (**C**) Expressions of proinflammatory markers with IL-1β with pre- & post-treatment of 4-PPBP on SMSCs (n=3 per group; *$p<0.05$, **$p<0.01$, ***$p<0.001$); (**D & E**) Effects of 4-PPBP and Sigma-1R antagonist (BD1047) on CTGF and MMP expression in primary meniscus fibochondrocytes per immunofluorescence and Western blotting. Scale bar=200 μm.

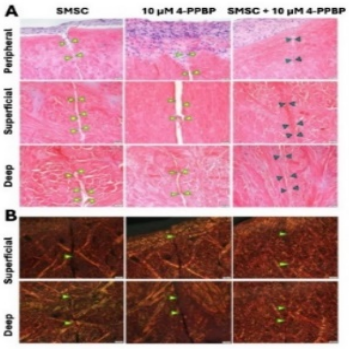

Fig. 2. The meniscus healing e*x vivo* model of longitudinal tears in bovine explants by a single injection of 10μM 4-PPBP via bioglue and SMSCs for 4 weeks: (**A**) Representative HE staining images of explant and (**B**) Picrosirius red staining with polarized microscopy (n=6 each group, scale bar=100 μm).

ABSTRACT #030

Elastin peptide-functionalized hydrogels support collagen production by bovine annulus fibrosus (AF) cells but are not conducive to cell proliferation or spreading in the absence of adhesive peptides: Implications for cell-instructive biomaterials for AF repair.

Sabrina Delva [1,2], Woojin Han[1], Steven Nicoll [2], James Iatridis[1], [1] Icahn School of Medicine at Mount Sinai, NY, [2] The City College of New York, NY sabrina.delva@mssm.edu, Disclosures: none

INTRODUCTION: Back pain is a major source of global disability with intervertebral disc annulus fibrosus (AF) defects being a specific and sensitive cause. The interaction of collagen and elastin preserves the structural integrity of the AF. Collagen deposition occurs in response to injury or degeneration, but if not sufficiently organized by elastin, tensile strength of the AF may not be functionality restored. [1, 2] Elastin also has bioactive properties stimulate cellular proliferation in fibroblasts[3], which may further enhance AF. Yet AF repair strategies disregarding the collagen-elastin interactions, and we believe incorporating these interactions in an AF repair biomaterial may better mimic healthy AF properties and could enhance reconstruction effectiveness. This study uses an elastin peptide-functionalized hydrogel, CGVGVAPG (VGV), to determine if it can serve as a cell-instructive biomaterial that enhances AF cell proliferation, cellular network organization, and collagen production. Moreover, we hypothesize that when VGV is used in combination with RGD, a cell adhesive peptide pervasively found on many matrix proteins, AF cells will have the balance cell proliferation, AF cell network organization, and collagen production.

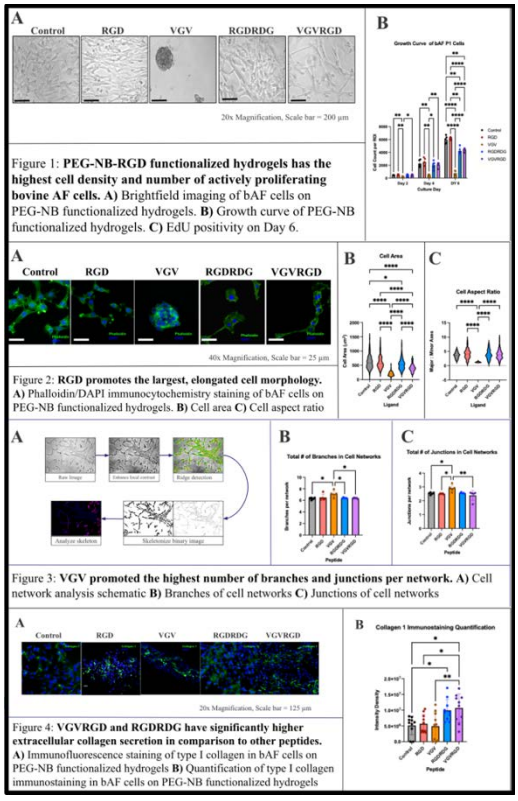

Figure 1: **PEG-NB-RGD functionalized hydrogels has the highest cell density and number of actively proliferating bovine AF cells. A)** Brightfield imaging of bAF cells on PEG-NB functionalized hydrogels. **B)** Growth curve of PEG-NB functionalized hydrogels. **C)** EdU positivity on Day 6.

Figure 2: **RGD promotes the largest, elongated cell morphology. A)** Phalloidin/DAPI immunocytochemistry staining of bAF cells on PEG-NB functionalized hydrogels. **B)** Cell area **C)** Cell aspect ratio

Figure 3: **VGV promoted the highest number of branches and junctions per network. A)** Cell network analysis schematic **B)** Branches of cell networks **C)** Junctions of cell networks

Figure 4: **VGVRGD and RGDRDG have significantly higher extracellular collagen secretion in comparison to other peptides. A)** Immunofluorescence staining of type I collagen in bAF cells on PEG-NB functionalized hydrogels **B)** Quantification of type I collagen immunostaining in bAF cells on PEG-NB functionalized hydrogels

METHODS: Thiol-functionalized 8 mm glass coverslips were used to promote adhesion with poly(ethylene glycol) norbornene (PEG-NB)-based hydrogels, synthesized using poly(ethylene glycol) dithiol (PEG-DT) as a crosslinker and lithium phenyl-2,4,6-trimethylbenzoylphosphinate (LAP) as a UV-activated photo initiator. RGD, VGV, RGDRDG, and VGVRGD were incorporated as cell-adhesive ligands, with bovine AF cells seeded on both hydrogels and thiol-functionalized coverslips (control) at 1,000 cells/cm^2. Hydrogels were crosslinked under UV for 1 minute, then cultured in DMEM with supplements at 37°C and 5% CO_2 to 70% confluency. Cell density, morphology, and proliferation (via Click-iT EdU Kit) were analyzed using ImageJ and FIJI, while collagen production was assessed with a type I collagen antibody. Statistical significance was determined by two-way ANOVA ($\alpha = 0.05$).

RESULTS: When incorporated into PEG-NB hydrogels, RGD significantly increased cell proliferation in comparison to the other peptides (Figure 1). VGV caused cells to aggregate into with clusters with small, rounded cells (Figure 2), while AF cells on RGD substates exhibited the largest, most elongated cells. VGVRGD substrates has cell area and aspect ratio that were similar to RGDRDG and approached RGD alone. Cell network analysis demonstrated that cells grown on VGV substrates had the highest number of branches and junctions per network, highlighting its potential role enhancing cell-cell interactions to create cell networks, while all other group were similar (Figure 3). Type I collagen expression was highest in VGVRGD and RGDRDG (Figure 4).

DISCUSSION: Results demonstrate elastin VGV- and RGD-functionalized hydrogels influence AF cell phenotype with VGV stimulating cell network formation and RGD enhancing cell proliferation and elongation. Specifically, AF cells grown on RGD-functionalized hydrogels exhibited the highest cell proliferation and growth rate with largest and most elongated cells, highlighting the excellent adhesion of AF cells to RGD ligands. [4] Meanwhile, AF cells did not bind well to VGV-functionalized substrates, which forced AF cells to organize and form the greatest numbers of cell networks. Interestingly the combination of VGV and RGD exhibited the greatest collagen I production which may suggest a balance between cell proliferation and matrix production. The VGVGRG hydrogel may more closely resemble the native collagen-elastin cell adhesion environment, and results this condition may balance cell proliferation, cellular organization, and matrix production which will future studies with functional assays to further evaluate.

CLINICAL RELEVANCE: This work aims to enhance our understanding of AF development and inform the design of cell-instructive biomaterials for improved strategies in repairing intervertebral disc degeneration.

CLINICAL RELEVANCE: To inform the design of cell-instructive biomaterials for AF repair.

REFERENCES: Diller RB, Tabor AJ, *Biomimetics* , 2022[1];Tavakoli J, Diwan AD, Tipper JL. *Int. J. Mol. Sci.* , 2020[2];Tajima et al., *Arch Dermatol Res*, 1996[3] Nettles et al., 2010[4]; Bax et al., *JBC,* 2009[5];Torre et al, *Ann N Y Acad Sci.*, 2019[6]

ACKNOWLEDGMENTS: Funded by NIH Grant R01-AR080096.

Characterization of ethanol post-treatment on collagen type I scaffolds for pathological tendon modelling

Authors: Arnold, KM[1]; Deymier, AC[1]
Affiliations: [1]Biomedical Engineering, School of Dental Medicine, UConn Health, Farmington, CT

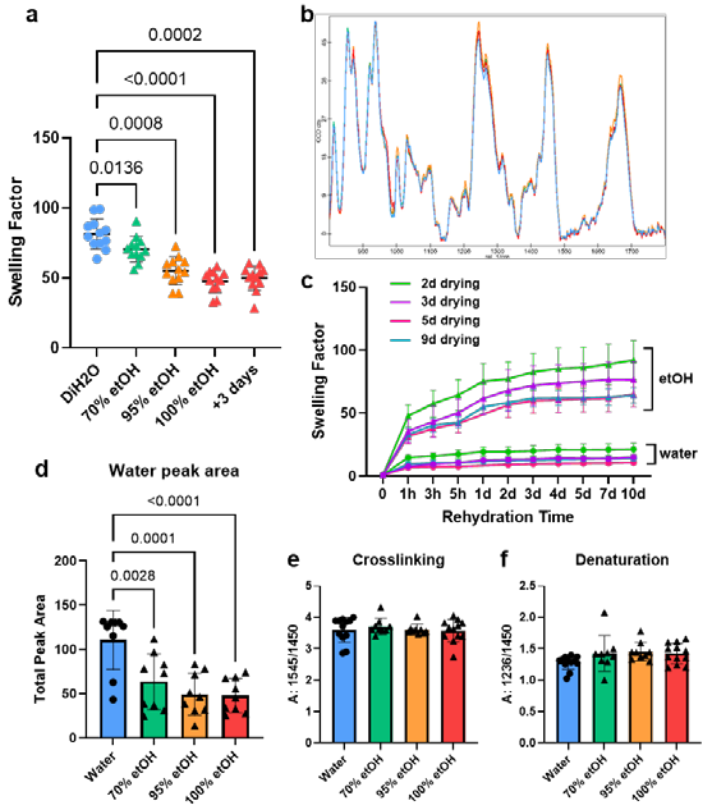

Figure 1: Effect of ethanol post-treatment on collagen 1 scaffolds. *(a) Swelling factor decreases with treatment in serial ethanol dilutions (b) Raman spectra overlapped, showing no differences between ethanol concentration (water = blue, 70% etOH green, 95% etOH orange, 100% etOH red). (c) Swelling factor during rehydration. Ethanol treated scaffolds = triangles, water scaffolds = circles. Colors indicate drying time prior to rehydration (d) FTIR analysis, area of water peak. (e) FTIR analysis, area ratio of peaks 1545/1450 cm^{-1} representing crosslinking. (f) FTIR analysis, area ratio of peaks 1236/1450 cm^{-1}, representing denaturation.*

Tendons are comprised almost entirely of type I collagen, making col1 scaffolds an ideal model for *in vitro* studies. To develop a model of tendon pathology, we are characterizing the behavior of collagen I scaffolds with ethanol (etOH) post-treatment and hydration. Ethanol dehydration is an extremely common step in both scaffold manufacture and tissue processing, and yet the influence of etOH on collagen is not well understood. Collagen I scaffolds were submerged in single etOH dilutions, serial dilutions, or deionized water overnight, at which point they were air dried completely to remove remaining solvent. At this stage Raman spectroscopy showed no significant changes to the structure of the collagen triple helix, but Fourier Transform Infrared spectroscopy (FTIR) indicated that etOH treatment altered the secondary structure, leading to increased fibrillogenesis. This was indicated by a downshift of the Amide II and III peaks (1540 and 1236cm^{-1} respectively), and a broadening of the Amide I peak at 1640cm^{-1}. All samples had a very broad series of peaks between 2500 and 3750cm^{-1} indicative of tightly bound water. The area of these peaks decreased with exposure to etOH. SEM revealed no differences in the macroscopic structure between water and etOH treated samples, with all scaffolds showing an extremely dense fibrillar structure, similar to that of tendon. These results indicate that the effect of ethanol is limited to the secondary structure of collagen, rather than the molecular or macroscopic levels. Thermogravimetric analysis (TGA) showed that ethanol treatment decreased the thermal stability of collagen scaffolds, causing them to break down at lower temperatures, and resulting in increased mass loss between key inflection points. The most profound differences caused by etOH exposure were found in the rehydration properties. Ethanol treatment, even up to two weeks prior, results in significantly increased swelling upon rehydration in deionized water. In both water and ethanol treated scaffolds, swelling stabilized after approximately 5 days, after which point scaffolds maintained their swollen state without degradation. To evaluate the suitability of these scaffolds for pathological tendon modelling, results of the above analyses will be compared to those of murine tendons, specifically the patellar and achilles tendons. This study is essential to understanding the interaction of collagen and ethanol, both from a basic science perspective and to improve scaffold modelling of tendon pathology.

Gli1 Function in Intervertebral Disc Development

Andrew Parker Hallmark[1], Harsh Alluri[1], Ravij Mehta[1], Nidhi Mahadevan[1], Ravi Krishnan[1], Chitra L Dahia[1,2]

Affiliations:

1 HSS Research Institute, Hospital for Special Surgery, New York, NY, USA

2 Department of Cell and Developmental Biology, Weill Cornell Medicine, New York, NY, USA

Background and Significance:

It is well documented that the *Gli1* gene downstream of hedgehog (Hh) signaling has many important effects relating to both embryonic development and cell proliferation. An important region where such effects play a role in development and functionality is that of the notochord. The notochord is a transient embryonic structure that forms the nucleus pulposus (NP) cells that exist within each intervertebral disc (IVD) of the spine. Sonic hedgehog (SHH) expression by the notochord has both cell autonomous and non-autonomous function in embryonic patterning. However, it is not known which GLI members downstream of SHH are crucial for notochord patterning and formation of NP cells within the IVD.

Methods:

To test the importance of *Gli1* downstream of SHH in NP formation, we employed the $Gli1^{LZ}$ knock-in allele where endogenous GLI1 function is abolished. Notochord cells were lineage traced using *ShhCre; R26TOM* alleles in the $Gli1^{Lz/WT}$ and $Gli1^{Lz/Lz}$ littermates in two-day-old pups to evaluate NP formation. Additionally, the effects of loss of *Gli1* on the postnatal lumbar IVD structure and function were evaluated during phases of rapid growth (one-week) and maturation (seven-week). Immunofluorescence stainings were performed to evaluate the expression of NP markers, cell proliferation, cell death, and extracellular matrix (ECM) expression within the NP and annulus fibrosus (AF) regions of the IVD. Further, morphometric data was measured to determine perceived physical changes to the IVD itself. Additionally, a histopathological scoring system and DEXA machine were used to further measure changes to the IVD region. GraphPad Prism 10 was used to perform statistical analyses of the data.

Results:

Findings highlight the notion that GLI1 does indeed play an important role in patterning of the mouse spine and particularly the development of the IVD region. A specific “fused IVD” phenotype was observed in $Gli1^{Lz/Lz}$ mice, in which the NP space was greatly diminished and occupied by AF. This observed phenotype was further supported by lineage tracing and immunofluorescence staining. Immunofluorescence staining also revealed that these fused IVD phenotypes lack important ECM and structural proteins and developmental markers typically found in the NP and AF. Morphological analysis and histopathological scoring additionally confirmed that observable deformities to the IVD region occurred in $Gli1^{Lz/Lz}$ mice with the “fused” phenotype. However, several IVDs in $Gli1^{Lz/Lz}$ mice did continue to have NP cells that were maintained in the postnatal stages.

Conclusions:

Results indicate that *Gli1* is critical for patterning of the mouse spine and formation of NP in the IVD. However, maintenance of NP cells and their markers in the $Gli1^{Lz/Lz}$ IVDs that were not fused suggests that GLI1 is not necessary for NP homeostasis, and that other GLI orthologs downstream of SHH may be critical in postnatal NP cells.

Acknowledgement/Funding Source:

The research was supported by NIAMS (AR077145), NIA (RAG070079) and OD (1S10OD026763) of NIH.

WNT7A mRNA-LNPs reduce skeletal muscle fibro-adipogenic progenitor adipogenesis

Larion Martin Santiago[1], Kasoorelope Oguntuyo[1], Britney Chin-Young[1], Angelo Amabile[2,3,4], Woojin M. Han[1]
[1]Department of Orthopaedics, Icahn School of Medicine at Mount Sinai, New York, NY
[2]Icahn Genomics Institute, Icahn School of Medicine at Mount Sinai, New York, NY
[3]RNA Nanoparticle Core, Icahn School of Medicine at Mount Sinai, New York, NY
[4]Department of Immunology and Immunotherapy, Icahn School of Medicine at Mount Sinai, New York, NY

INTRODUCTION: Myosteatosis, the infiltration of fat into skeletal muscle, is commonly observed in chronic skeletal muscle injuries and degenerative myopathies, correlating with increased disease severity, diminished function, and poor surgical repair outcomes.[1-3] Fibro-adipogenic progenitor (FAP) cells, crucial for muscle maintenance and regeneration, also contribute to fatty infiltration through unchecked differentiation into adipocytes.[4-6] We previously showed that recombinant, secretory protein wingless-type MMTV integration site family 7a (*WNT7A*) can prevent muscle degeneration by reducing FAP adipogenesis and fatty infiltration without fibrosis, making it a promising therapeutic candidate for muscle regeneration.[7] However, recombinant protein therapies face challenges related to production scalability and therapeutic efficacy.[8,9] Lipid nanoparticle (LNP) delivery of mRNA offers a promising alternative with scalable production and effective therapeutic delivery.[10] While systemic delivery has been explored for treating myopathy,[11] local intramuscular delivery of mRNA-LNPs for muscle regeneration has not been investigated. Here, we assess the feasibility of local LNP-mediated mRNA delivery and evaluate the efficacy of *WNT7A* mRNA-LNPs in reducing FAP adipogenesis, comparing it to recombinant *WNT7A* protein.

METHODS: We developed a *WNT7A* mRNA-LNP formulation, using the human *WNT7A* sequence as the template. All animal studies were performed following the approved IACUC protocol. *In vitro* feasibility studies were conducted by injecting cre mRNA-LNPs (15 µg/30 µL) into the tibialis anterior (TA) muscle of Ai14-tdTomato and R26-LSL-tdTomato mice. TAs were harvested 12-13 days post-injection and cryosectioned. LNP uptake and mRNA expression in skeletal muscle was assessed by visualization of fluorescent tdTomato expression in myofibers. *Ex vivo* dose-response studies were performed using FAPs isolated from C57BL/6J mice,[7] cultured in growth media, adipogenic differentiation media with/without recombinant *WNT7A* (200 ng/mL) or *WNT7A* mRNA-LNPs (1, 10, 100 ng/mL). Levels of adipogenesis were assessed using immunocytochemistry, staining for perilipin-1, a lipid-droplet associated protein.

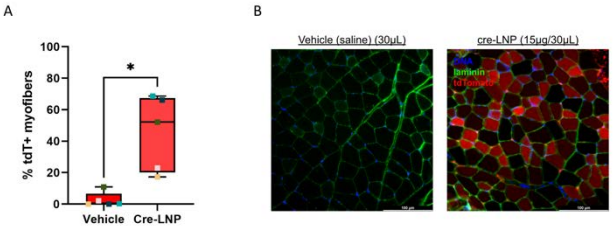

Fig. 1 A) Percentage of tdT+ myofibers after local cre-LNP injections (15 µg/µL). Paired t-test. *p < 0.05. n = 5. Colors represent biological replicates. B) Representative cross sections of TA muscles treated with cre-LNP or saline. Scale bar: 100 µm.

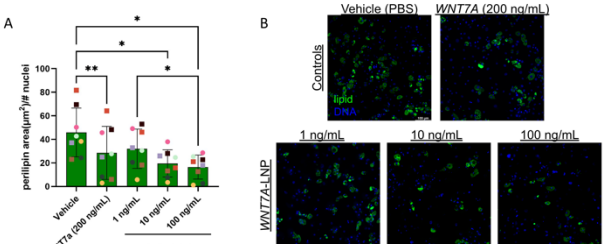

Fig. 2 A) Perilipin area normalized by nuclei quantity. Repeated measures one-way ANOVA, Tukey post-hoc analysis. Vehicle, PBS. n = 8. *p < 0.05, **p < 0.01. B) Representative immunofluorescence images of perilipin-labeled FAPs cultured in media ± WNT7A (200 ng/mL)/WNT7A-LNP (1/10/100 ng/mL). Scale bar: 100 µm.

RESULTS: *WNT7A* mRNA was encapsulated in LNPs with 92.60% efficiency, an average diameter of 86.59 ± 0.54 nm and polydispersity index of 0.0363. *In vitro* feasibility studies demonstrated significant expression of tdTomato following local injection of cre-LNPs to TA (Fig. 1). *Ex vivo* dose-response studies demonstrated significant reductions in FAP adipogenesis following treatment with both recombinant *WNT7A* protein and *WNT7A* mRNA-LNPs. Notably, lower doses of *WNT7A* mRNA-LNPs (10 ng/mL and 100 ng/mL) were sufficient to reduce FAP adipogenesis compared to recombinant *WNT7A* (Fig. 2).

CONCLUSION: We show that LNPs effectively deliver mRNA payloads to FAPs–cells implicated in adipogenesis and fatty infiltration in skeletal muscle–and suggest that these cells can successfully translate the delivered *WNT7A* mRNA, perform necessary post-translational modifications, and secrete the protein to activate signaling pathways that reduce adipogenesis. Our in vivo proof-of-concept study demonstrates that mRNA-LNPs delivered through intramuscular injection are successfully taken up by myofibers, confirming feasibility.

SIGNIFICANCE: This study highlights the potential of mRNA-LNP therapies for muscle regeneration, demonstrating that *WNT7A* mRNA-LNPs reduce adipogenesis at lower doses than recombinant *WNT7A* protein, potentially addressing challenges related to dose toxicity, scalability, and production costs. These findings also suggest broader applications for mRNA-LNPs in developing new therapies for chronic muscle injuries, myopathies, and related degenerative conditions.

REFERENCES: [1] Li+ *Neuromuscul Disord*. 2015; [2] Gladstone+ *Am J Sports Med*. 2007; [3] Park+ *Am J Sports Med*. 2015; [4] Joe+ *Nat Cell Biol*. 2010; [5] Uezumi+ *Nat Cell Biol*. 2010; [6] Wosczyna+ *Cell Rep*. 2019; [7] Fu+ *Stem Cell Reports*. 2023;[8] Niazi+ *Biologics*. 2023; [9] Vavilis+ *Pharmaceutics*. 2023; [10] Hou+ *Nat Rev Mater*. 2021; [11] Kenjo+ *Nat Commun*. 2021.

FiberO for an Automated Quantification of Fibers Orientation and Organization in Biological Tissues

Asier Muñoz, Anxhela Docaj, Julen Fernandez, and Alessandra Carriero

The City College of New York, City University of New York, New York, NY, USA

The hierarchical organization of collagen fibers plays a crucial role in determining the mechanical properties of connective tissues, such as bone and tendons. Understanding the orientation and organization of these fibers is essential for understanding their contribution to tissue mechanics. Traditional methods of analyzing fiber orientation and continuity have been limited in their ability to provide quantitative assessments, leading to challenges in accurately characterizing the structure of fibrous tissues. For the purpose, we developed *FiberO*, a novel open-source software designed for the automated and quantitative analysis of collagen fiber orientation and organization in tissue images showing fibers, such as in second harmonic generation (SHG) microscopy.

FiberO, developed in MATLAB, processes grayscale images of fibrous tissues through several steps. First, a 2D statistical filter removes noise and background artifacts. Next, adaptive thresholding differentiates collagen fibers from the background, and their orientation is calculated using morphological openings. The program analyzes fiber continuity by assessing the orientation across a grid of facets and connecting neighboring facets based on orientation similarity. The performance of FiberO was evaluated using second harmonic generation (SHG) microscopy images of bone and tendon from 14-week-old *oim/oim* mice, a mouse model of osteogenesis imperfecta (OI) characterized by disorganized collagen fibers. Tissue sections were imaged using a Prairie Tech Ultima IV Multiphoton Microscope with a 40X 0.8 N.A. water immersion objective, keeping them hydrated with saline. A titanium sapphire femtosecond laser tuned to 920 nm provided the excitation needed for SHG signals, while a 460/20 nm bandpass filter detected emitted signals within a spectral window of 440–480 nm. To validate *FiberO*, we created a dataset of 75 images featuring artificial fiber networks, comparing its accuracy with established ImageJ plugins, Directionality and OrientationJ.

FiberO allows for an automated, quantitative analysis of tissue fiber orientation and organization using our software. n our validation test on images with predetermined fiber orientation and organization, FiberO demonstrated an average angle error of 0.22 ± 0.12 degrees, surpassing the accuracy of OrientationJ (1.14 ± 0.78 degrees) and the local gradient Directionality method (2.00 ± 0.26 degrees) in measuring the known fiber orientation in these tissues. *FiberO* also excelled in quantifying the quantity of fibers aligned with the preferential orientation, exhibiting an error of 7.5% ± 2.3%, compared to 14.7% ± 3.7% for the Fourier Directionality, 23% ± 5.7% for local gradient Directionality, and 48% ± 3.8% for OrientationJ. Orientation maps demonstrated that *FiberO* provided detailed regional orientation color maps, while Directionality failed. The capabilities of *FiberO*, therefore, extend beyond SHG and collagen, making it applicable to a variety of fibrous tissues composed of non-collagenous proteins, thereby broadening its utility in the study of various biological and synthetic materials.

In summary, we have developed an open-source software, named *FiberO*, which utilizes morphological image openings to automatically and accurately quantify the primary regional orientations of fibers and assess their organization (continuity) in biological tissues from grayscale images, such as those of bone and tendon collagen fibers obtained through SHG microscopy. FiberO's quantification and visualization of fiber orientation surpass the performance of existing open-source methods used for tracking fiber orientations. Additionally, FiberO is currently the only free software that offers information on the continuity of fibers within tissues. This study introduces an innovative resource for researchers to explore fiber orientation and organization in various natural and synthetic fibrous materials.

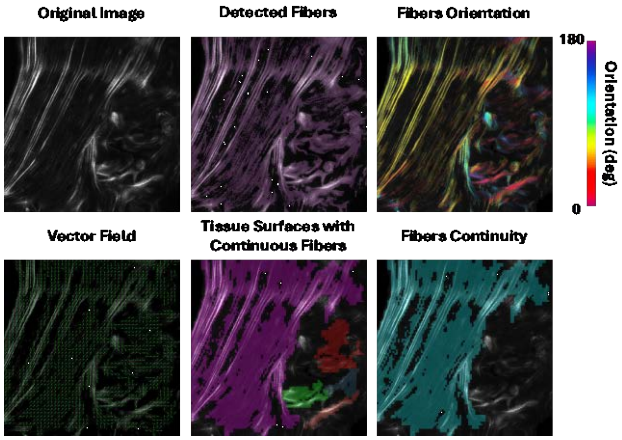

Figure 1. Processing pipeline of FiberO for a representative bone image using SHG

Short-Term Immobilization Using Semi-Rigid Casting Improves Early Tendon-to-Bone Healing in a Murine Model of Anterior Cruciate Ligament Reconstruction

Yuki Suzuki, Yuki Okazaki, Chia-Hung Hung, Xuewu Xing, Wataru Morita, Leonardo A Sanchez, Lauren Simonian, Julia S. Retzky, Alexander Piacentini, Hirotaka Iura, Matthew Covello, Laura Moore, Claire D. Eliasberg, Camila B. Carballo, Scott A. Rodeo
Laboratory for Joint Tissue Repair and Regeneration, Orthopaedic Soft Tissue research, Hospital for Special Surgery, New York, NY

INTRODUCTION: Functional recovery following anterior cruciate ligament reconstruction (ACL-R) requires secure healing of the tendon graft in the bone tunnel, and early post-operative immobilization may accelerate this process. However, there is a lack of consensus amongst clinicians with regard to use and duration of knee immobilizers post-operatively [1]. A three-dimensional printed, semi-rigid knee cast has been utilized previously for the mouse knee and represents a non-invasive, more clinically relevant method of knee immobilization [2]. The purpose of the current study is to elucidate the effects of short-term immobilization using semi-rigid casting following ACL-R in mice. We hypothesized that short-term casting would improve early tendon-to-bone healing and functional outcomes after ACL-R.

METHODS: Forty-five 12-week-old male C57BL/6J mice (average weight: 26 g) were used in this study, and underwent open ACL transection followed by immediate ACL-R surgery in the right knee using ipsilateral flexor digitorum longus tendon autograft as previously described [3]. The mice were randomly assigned to one of the three groups post-operatively: 1) no casting (free cage) group, 2) 5-day casting group followed by free cage activity, and 3) 14-day casting group. All mice were euthanized at two weeks post-surgery. The primary outcome measures were new bone formation and tendon-to bone interface healing within the bone tunnel, assessed by micro-CT and histology (tendon-to-bone tunnel healing [TBTH] score [4]). Secondary outcomes included biomechanical properties, knee range of motion (ROM), and gene expression related to pain (assessed in the lumbar dorsal root ganglia) and muscle atrophy markers (measured in the tibialis anterior muscle). Gait analysis was also performed using DigiGait. Histological and biomechanical assessments were conducted on 5 and 10 mice per group, respectively. qPCR was performed on 6 mice per group, while the other measurements were conducted on 15 mice per group. Statistical analysis was carried out using one-way ANOVA followed by multiple comparisons using the Bonferroni test, with statistical significance set at $p < 0.05$.

RESULTS: In both casting groups, bone volume formation (BV/TV) and bone mineral density (BMD) in the tibial tunnel were higher than in the free cage group. The TBTH score in the tibial tunnel was also higher in both casting groups compared to the free cage group (Fig 1). No significant differences were observed in biomechanical ultimate load to failure. All groups exhibited restricted ROM compared to the contralateral knee, with the 14-day casting group showing significantly less ROM than the other groups. However, the 5-day casting group had significantly greater ROM than the free cage group. Additionally, the variability in paw area and angle of the affected limb measured with gait analysis was significantly decreased in the 5-day casting group. There were no significant differences in pain marker gene expression among groups, but genes related to muscle atrophy (CAPN1 and CTSB) were significantly upregulated in both casting groups.

DISCUSSION: These findings suggest that postoperative casting improves new bone formation within the bone tunnel and tendon-to-bone healing in the tibial tunnel at 2 weeks after ACL-R. The 5-day casting group demonstrated better ROM and improvements in some gait parameters, while the 14-day casting group showed significantly decreased knee ROM. We hypothesize that the improvement in knee motion at 2 weeks following an initial period of casting is due to resolution of the postsurgical inflammatory process. However, genes related to muscle atrophy were upregulated in both casting groups, and muscle atrophy after ACL-R can be deleterious to recovery and return to sport. This study suggests that non-invasive short-term semi-rigid immobilization followed by free cage activity may be a key factor in accelerating early healing and facilitating an early return to sport after ACL-R.

REFERENCES: [1] Hiemstra et al., Clin J Sport Med. 2006. [2] Moore LK et al. J Orthop Res 2022. [3] Lebaschi A et al. J Knee Surg. 2017. [4] Liu PP et al. Anal Quant Cytol Histol 2011.

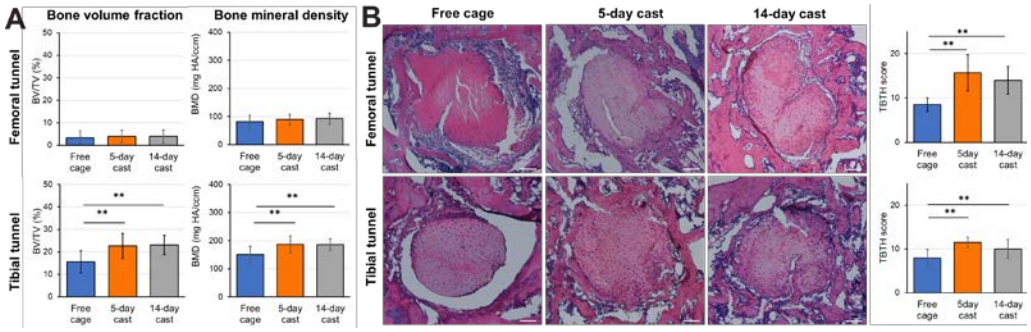

Figure 1: New bone formation and tendon-to-bone healing within the bone tunnel were higher in the casting groups. (**A**) Micro-CT analysis: New bone formation was assessed by bone volume fraction (BV/TV) and bone mineral density (BMD) in both the femoral and tibial tunnels. Scale bars: 200 µm. (**B**) Histological evaluation: Representative images and tendon-to-bone healing scores. *P < 0.05, **P < 0.01.

Biomechanical Impact of Simulated Microgravity on Osteoblasts and Osteoclasts

Isaiah T Taylor, Sardar MZ Uddin, David E Komatsu
Stony Brook University, Stony Brook, NY, 11974

With the Artemis missions rapidly approaching, and despite recent breakthroughs in space biology, sending the first humans to the moon remains a significant challenge. During space flight, astronauts lose 1-1.5% of their bone mass per month. Because of our inadequate understanding of the mechanisms causing microgravity-induced bone loss, as well as the difficulties in developing effective remedies, NASA has designated microgravity-induced bone loss as a high-priority knowledge gap. Lack of gravity-induced mechanical stress decouples osteoclasts and osteoblasts, increasing osteoclastic bone resorption and decreasing osteoblastic bone formation. Unfortunately, there are not yet any comprehensive studies describing effects of microgravity on osteoblast-osteoclast communication. Our hypothesis is that simulated microgravity will disrupt the activity of osteoblasts and osteoclasts.

Primary human osteoblasts and osteoclasts (25,000 cells/block) were seeded on tricortical human decellularized blocks and subjected to either microgravity or gravity using a rotary cell culture system (Synthecon®) for 28 days. The mechanical integrity of tricortical blocks was assessed using unconstrained uniaxial compression. Briefly, a monotonic load to failure was applied at 5mm/min, and data were analyzed for stiffness, energy to failure, yield force, ultimate force, and failure force.

The biomechanical integrity of osteoblast and osteoclast seeded blocks was significantly reduced in MG-exposed samples compared to samples experiencing normal gravity. Specifically, stiffness was 140% lower, energy to failure was 419% lower, yield force was 274% lower, ultimate force was 269% lower, and failure force was 269% lower in microgravity conditions compared to gravity. The biomechanical results for osteoclast-seeded chips were also decreased as osteoclasts were more active, therefore, resorbing bone at a much faster rate than control. Analysis from alkaline phosphatase staining indicates the presence of less osteoblast activity in the microgravity samples compared to gravity. Current analysis includes a LIVE/DEAD and DNA content analysis to determine the rate of cell proliferation on human tricortical blocks.

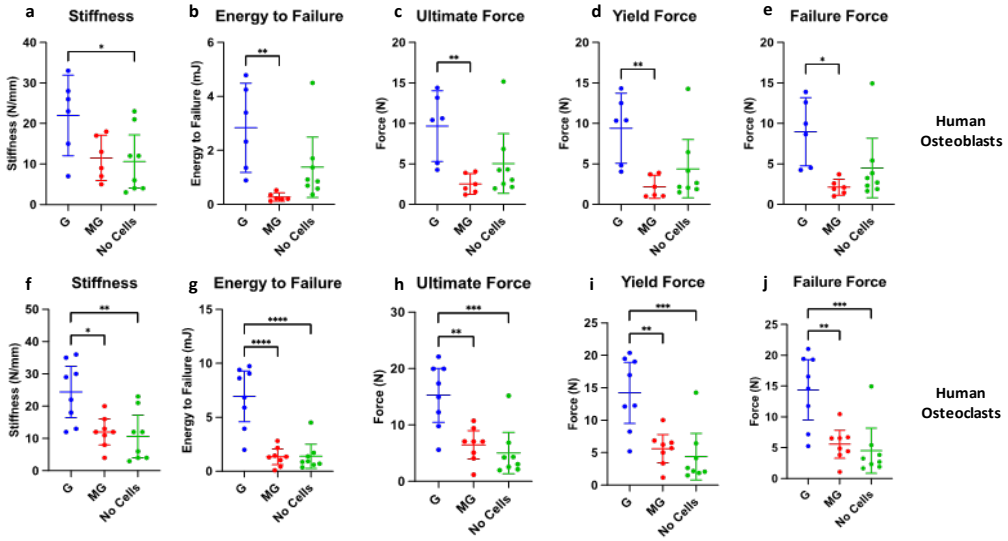

Figure 1: *Mechanical integrity of tricortical blocks seeded with primary human osteoblasts (a-e) and osteoclasts (f-j). The blocks were tested for (a, f) stiffness [N/mm], (b, g) energy to failure [mJ], (c, h) ultimate force [N], (d, i) yield force [N], and (e, j) failure force [N]. (n=10, *p<0.05)*

The use of primary human cells in their physiological environment makes our study highly translational. Subsequent signaling pathway analyses will allow us to determine the effects of microgravity on osteoblast-osteoclast communication leading to osteoblast-osteoclast decoupling and bone remodeling. The functional analysis will show effects of osteoblast-osteoclast decoupling on bone structure and mechanical integrity.

REFERENCES: [1]Komatsu, D. E., M. Hadjiargyrou, S. M. Udin, N. A. Trasolini and S. Pentyala (2015). "Identification and Characterization of a Synthetic Osteogenic Peptide." Calcif Tissue Int 97(6): 611-623.

ACKNOWLEDGEMENTS: Funding for the study was provided by the 2016-17 Space Biology NASA grant (ROSBio) 80NSSC18K1479.

Elastin Collagen Nanovesicles – A Novel Platform for Targeted and Controlled Drug Delivery

Ann Thomas[1], Sanjna Rao[1], Kristi Kiick[1], Christopher Price[1]
[1]*University of Delaware, Newark, DE*

INTRODUCTION: Post-traumatic osteoarthritis (PTOA) is a form of OA, induced by an acute traumatic injury to the knee, leading to progressive degeneration of the articular cartilage[1]. Currently, clinical PTOA treatments only focus on symptomatic relief (e.g., analgesics and NSAIDs), not the modification of underlying disease progression. Furthermore, systemic delivery of both symptom treating and putative disease-modifying drugs pose significant concerns regarding side effects, off-target interactions, and compliance. To enhance drug efficacy and reduce systemic exposure and the side effects of PTOA therapeutics, intra-articular (i.a.) injection approaches have been developed. Yet, these present challenges to efficacy, low joint drug retention time and poor targeting to cartilage's dense ECM[2]. Therefore, a need exists for drug delivery platforms that both localize and retain disease-modifying drugs within the joint space. In this arena, recent work from our team has shown that short synthetic elastin- and collagen-like peptide sequences (ELPs & CLPs, respectively) can be conjugated to form novel nanovesicles having 1) high binding affinity for tissues exhibiting collagen damage—thus actively targeting and binding damaged tissues; and 2) sequence-specific behaviors that allow tuning of drug loading efficiency, passive drug release, and thermoresponsive disassembly due to mild cooling[3]; attributes that collectively enhance the targeted delivery and prolonged retention of therapeutic agents in diseased cartilage. However, the retention, distribution, and targeting of these elastin-collagen nanovesicles (ECnVs) (and their cargo) *in situ* has yet to be established. In this study, we leveraged multiscale bioimaging approaches (*e.g.*, *in vivo*, epi-fluorescent, confocal, and super-resolution imaging) to characterize the retention and localization of fluorescently-labeled ECnVs (far-red) and their fluorescent cargo (near-IR), within intra- & peri-articular tissues of the mouse joint following i.a. injection.

METHODS: We synthesized ELP and CLP monomers, based upon the sequences (VPGWG)6G and (GPO)8GC, termed (W6) and (G8) respectively, using solid-phase peptide synthesis. 30% of the G8 CLPs were modified to allow fluorescent labeling via an EDC/sulfo-NHS reaction. W6 was conjugated to G8 using copper-catalyzed click chemistry to yield ~1mg/ml W6-G8 conjugates, which self-assemble into (empty-) ECnVs upon cooling from 80C to ~40C. These ECnVs were then surface-labelled with AZ647-NHS, a far-red fluorophore, to allow their *in vivo/in situ* visualization. ECnV particle size (~200nm diameter) and concentration (~10^{11} per ml) were determined via nanoparticle tracking analysis (NTA). Confocal and super-resolution imaging of ECnVs and their localization and interactions within target tissues necessitates their survival through optical tissue clearing and processing, involving tissue fixation, solvent-based clearing, and paraffin embedding. Initially, AZ647-labeled (empty-) ECnVs were introduced into intact rat muscle tissue (*ex vivo*), fixed, and optically cleared (using a number of tissue clearing approaches; e.g., THF-DBE, TDE[4]) for *ex vivo* multiscale imaging. After characterizing their stability to tissue processing/clearing, these same ECnVs were i.a. injected into 12-week-old BALB/CJ mice for macro-scale *in vivo* imaging (UVP iBox Scientia) and subsequent multiscale 3D confocal imaging of intact lower limbs following THF-DBE or PEGASOS[4,5] clearing (Andor Dragonfly and Zeiss CD7). Intact joints will be de-cleared and processed for decalcified paraffin embedding for histology and super-resolution imaging.

RESULTS AND DISCUSSION: AZ647-labeled (empty-) ECnVs were successfully synthesized and shown to be robust to temperature-controlled handling, fixation, and most clearing, and tissue processing approaches. *Ex vivo* ECnV injection into rat muscle tissue (vastus lateralis) substantiated their *in situ* stability and the optimization of both delivered particle numbers and clearing protocols, permitting the facile far-red fluorescent visualization of ECnVs *in situ* at tissue depths exceeding 500µm (to the objective limit;. Longitudinal *in vivo* tracking and localization of AZ647-ECnVs following i.a. administration into BALB/CJ mice joints exhibited a bi-exponential clearance, with a "slow" half-life of ~19-hours while also exhibiting significant fluorescent signal (compared to contralateral limb) out to 7-days post-injection. In the intact joint, deep-tissue imaging in THF-DBE cleared joints (R.I. 1.56; Fig 1 C) was superior to that of TDE and PEGASOS cleared joints (R.I. 1.47 & 1.54, respectively), while also establishing the stability of ECnVs to a wide range of tissue clearing and processing strategies. Localization, retention, drug delivery, and biosafety studies will be performed *in vivo* following IACUC approved i.a. injection of (empty-)ECnVs vs. (loaded-)ECnVs (e.g. Cy7.5- or Dex-CF) in mice knees. Overall, these results confirm our ability to directly characterize AZ647-labeled ECnV presence *in situ* across several translationally relevant length scales in murine musculoskeletal tissues.

CLINICAL SIGNIFICANCE: In this study, multiscale bioimaging, traversing size scales from millimeter to nanometer, was applied to characterize the presence of fluorescently-labeled AZ647-ECnVs within murine joint and muscle tissues. Multiscale analyses greatly improve our ability to directly study clinically translatable drug delivery characteristics using smaller sample sizes. Our data conclusively demonstrates the ability of our novel ECnV particles to survive the handling & imaging necessary for such interrogations and provide early characterization of the localized accumulation of ECnVs within the knee joint after i.a. injection. Future work will focus on the *in vivo* i.a. administration of empty- and cargo-laden- ECnVs to both healthy and injured (early PTOA) murine joints, followed by multiscale imaging and advanced bioimaging to comprehensively analyze nanovesicle retention and distribution in and around the joint, as well as to establish the biosafety and efficacy of ECnVs as a targeted and controllable delivery platform for PTOA therapeutics.

REFERENCES: [1] Little (2013) *Nature R Rheum;* [2] Mease (2011) *Lancet;* [3] Dunshee (2022) *Drug Deliv Sci Technol;* [4] Berke (2016) *PLoS One*; [5] Jing (2018) *Cell Res*.s

Bone toughens during skeletal growth. A study on healthy and osteogenesis imperfecta mouse bone

Anxhela Docaj[1], Asier Muñoz[1], Lukasz Witek[2], Deepak Vashishth[3], and Alessandra Carriero[1]
[1]*The City College of New York, NY, United States*
[2]*New York University, NY, United States*
[3]*Rensselaer Polytechnic Institute, NY, United States*

OBJECTIVE

In classical osteogenesis imperfecta (OI or *brittle bone* disease) mutations in collagen type I genes disrupt the collagen structure, leading to bone fragility [1]. Our studies using the homozygous *oim* mouse model of OI and their control wild type (WT), revealed that bone fracture toughness, *i.e.* bone resistance to crack initiation and propagation, increases during skeletal growth in both groups [2]. We also observed that OI bone fragility changes its mechanisms with skeletal growth. Young *oim* bones exhibited low resistance to crack initiation but not to propagation, whereas in more mature *oim* bones were more resistant to crack initiation and less to propagation. Notably, bone toughening mechanisms resisting crack growth, such as crack defection, splitting and bridging, were observed in very young 4-week-old (w.o.) OI bone [3]. This is the first time that we observed toughening mechanisms in brittle OI bone, and it was also the first time that very young bones were tested for fracture toughness. These mechanisms were absent in more skeletally mature bones from 12 w.o. OI mice [2], while they are present in WT bones at any age. To understand these mechanisms of bone fragility across different growth stages in *oim* mice, we examined the changes in bone tissue structure, collagen organization, matrix composition and mechanical properties of these tissues.

METHODS

Femora from 4 and 12 w.o. *oim/oim* (B6C3Fe-a/a-Col1a2$^{oim/oim}$) and their WT counterparts were scanned with synchrotron microtomography (Diamond Light Source, UK) to assess cortical thickness and intracortical porosity. Furthermore, collagen fiber orientation and organization were assessed using second harmonic generation (SHG) microscopy and our recently developed software *FiberO* [4]. Finally, bone matrix composition and mechanical properties (stiffness and hardness) were determined using Raman spectroscopy and nanoindentation, respectively. Enzymatic crosslinks and advanced glycation end-products (AGEs) at the nanoscale were quantified using Raman spectroscopy and molecular fluorescent assays.

RESULTS

Our study showed that the bone tissue of young mice is less organized compared to the nearly skeletally mature bone. Particularly, very young *oim* bone exhibits increased cortical porosity, both vascular and cellular, reduced collagen content, and disorganized mineralized fibers characterized by low mineral crystallinity. Additionally, there is a significant presence of carboxymethyl-lysine (CML), glycosaminoglycan (GAGs) and fluorescent AGEs in very young *oim* bones vs. more mature ones. These structural deficiencies, such as lacunar porosity and low plasticity due to poor collagen and mineral properties and packing, contribute to a heightened susceptibility to crack initiation. In brittle bones, osteocyte lacunae are smaller and more spherical (less elongated and flat). These characteristics are indicative of the high bone turnover, observed in *oim* bones [5], where osteocytes align randomly due to insufficient time to orient along the direction of the load. This misalignment is most pronounced in very young brittle bones, with the greatest deviation from the bone's longitudinal axis. Furthermore, the elevated ratio of AGEs to collagen, coupled with the reduced collagen content, highlights the potential controversial role that non-enzymatic crosslinks could have in *oim* bones – where they help provide stability to a bone that would otherwise break even more easily. Nearly mature *oim* bone have lower AGEs and increased mineralization, and the presence of lamellae as observed by SHG microscopy, that all together contribute to increase the fracture resistance to crack initiation but not to propagation as these lamellar regions are not mechanically functional in the almost mature *oim* mice, further confirmed by the lack of crack-growth toughening mechanisms observed at this age.

CONLUSIONS

This study enhances our understanding of how bone toughness evolves during skeletal growth in both healthy and brittle bone. The findings of this study indicate that OI bone fragility treatments should differ in young and older children, addressing the distinct mechanisms of bone fragility in each age group.

SIGNIFICANCE

Understanding *how* and *why* bone resistance to fractures changes during skeletal growth and in *brittle bones* will inform on what to target with therapies to restore age-appropriate tissue mechanical integrity.

REFERENCES

1. Carriero A., et al., JBMR 29(6) (2014) 1392-401
2. Docaj A., et al., ORS Meeting (2020)
3. Docaj A., et al., ASBMR Meeting (2020)
4. Muñoz A. et al. NEBEC Meeting (2021)
5. Kalajzic I., et al., Endocrinology 143(5) (2002) 1594-1601

Disparities in Education and Socioeconomic Status Are Associated with Increased Severity of Presentation of Early-Onset Blount Disease

Eduardo Valero-Moreno[1], Zachariah Samuel[1], Leila M. Alvandi[1], Edina Gjonbalaj[1], Melinda Sharkey [1]
Affiliations : [1]Montefiore Medical Center, Bronx, NY

Objective: Children's Opportunity Index (COI) measures the quality of resources and conditions at the zip code level and stratifies data into quintiles (very low, low, moderate, high, very high). Prior research at our institution, which primarily serves patients from very low/low COI neighborhoods, showed no differences in accessing timely orthopaedic care for infant hip dysplasia or adolescent ACL tears. Because of this, we hypothesized that patients from lower COI neighborhoods do not present later or with more severe disease in early-onset Blount Disease.
Methods: In this IRB-approved, retrospective study, demographic, clinical, and radiographic data were obtained through chart review for all patients presenting to a single academic institution with early-onset Blount Disease over 17 years. Overall COI 3.0 scores, as well as three subdomains: education, socioeconomic status (SES), and health were collected. Patients were separated into two groups based on COI quintiles: very low/low and moderate/high/very high. Chi-square and Fisher's exact tests were used to compare groups.
Results: Out of 98 patients, 88 came from low/very low COI neighborhoods, while 10 resided in moderate/high/very high COI neighborhoods. The average age at presentation was 3.39±2.32 years for the low/very low COI group and 2.92±1.90 years for the moderate/high/very high COI group (p=0.53) trending toward older presentation in the very low/low COI group. Significant differences in Langenskiöld stage and varus deformity (measured by mechanical axis deviation (MAD)) were found, with patients in the low/very low COI group presenting with more advanced disease than those in the moderate/high/very high COI group (p=0.034 and p=0.043, respectively). Sub-analysis revealed that the differences in Langenskiöld stage and MAD were primarily associated with the education and SES COI subdomains. The health COI subdomain could not be analyzed as all patients fell into the moderate/high/very high group, suggesting equitable access to medical care in our area.
Conclusion: Patients from very low/low COI neighborhoods presented with more advanced disease compared to those from higher COI neighborhoods. This difference in severity at presentation was associated with education and SES COI subdomains. The average age at presentation did not differ significantly between groups, however there is a trend toward older age at presentation in the very low/low COI group.
Significance: Despite similar access to care, patients from very low/low COI neighborhoods presented with more severe disease. This highlights the need for increased awareness among the public as well as primary care providers in our area for diseases like Blount Disease that primarily affect children of color.

Table 1: Demographics and Presenting Characteristics Stratified by Total COI

	Low/Very Low Total COI	Moderate/High/Very High Total COI	P Value
n	88	10	
Age at Diagnosis (mean (SD))	3.39 (2.32)	2.92 (1.90)	0.533
Female (%)	42 (48.8)	4 (44.4)	1
Race/Ethnicity (%)			0.139
Black or African-American	28 (31.8)	5 (50.0)	
Spanish/Hispanic/Latino	25 (28.4)	0 (0.0)	
Unknown	35 (39.8)	5 (50.0)	
BMI percentile (mean (SD))	91.69 (15.38)	95.29 (6.34)	0.543
Bilateral (%)	65 (77.4)	8 (88.9)	0.71
Initial Treatment (%)			0.493
Guided growth	27 (31.0)	5 (50.0)	
Osteotomy	8 (9.2)	0 (0.0)	
External Fixator	4 (4.6)	0 (0.0)	
Nonoperative	48 (55.2)	5 (50.0)	
Langenskiöld at Presentation (%)			**0.034**
1	43 (53.1)	5 (62.5)	
2	20 (24.7)	1 (12.5)	
3	2 (2.5)	2 (25.0)	
4	8 (9.9)	0 (0.0)	
5	8 (9.9)	0 (0.0)	
Drennan Angle at Presentation (mean (SD))	17.60 (9.71)	14.06 (5.94)	0.316
mLDFA At Presentation (mean (SD))	99.24 (9.87)	96.37 (8.42)	0.432
MAD At Presentation (%)			**0.043**
1	6 (8.1)	1 (14.3)	
2	14 (18.9)	4 (57.1)	
3	54 (73.0)	2 (28.6)	

Assessing The Relationship Between Spanish Language and Postoperative Outcomes in Elderly Hip Fracture Patients

Mohammed Bashier[1], Jessica Chao[1], Brandon Wang[1], Margaret Fagan[1], Megan Darrell[1], Dylan Horan[2], Leila M. Alvandi[2], Wanda Horn[2], Mani D. Kahn[2]

[1]Albert Einstein College of Medicine, Bronx, NY, [2]Montefiore Einstein, Department of Orthopaedic Surgery, Bronx, NY

Objective

Although research has demonstrated correlations between race and ethnicity with respect to unfavorable outcomes within orthopedic surgery, identifying and addressing traceable systemic barriers that contribute to disparities in care remains of utmost importance. The objective of this study was to examine the effect of primary language as a predictor of health and functional outcomes among elderly patients following hip fracture surgery.

Methods

This study was approved by the Institutional Review Board. This was a retrospective chart review of hip fracture patients over the age of 65 who underwent surgical management at a single academic tertiary care center between January 1, 2019 and September 30, 2022 and met our study criteria. Patients who sustained pathologic fractures or underwent nonsurgical treatment were excluded from the study. Primary outcomes included patient mortality during admission, within 30 days, and within one year of surgery. Statistical analysis was conducted using R (v. 4.2.1). Univariate analysis comparing English- and Spanish-speaking patients was conducted by Chi-squared (or Fisher's exact for $n < 10$) tests for categorical variables, and Mann-Whitney-U (non-parametric 2-sample t-test) for continuous variables. Benjamini-Hochberg correction was applied to account for multiple tests. To examine the effects of primary language independent of potential confounding patient characteristics, multivariate logistic regression with Benjamini-Hochberg correction was utilized to compare English- and Spanish-speaking patients. Outcome variables with a univariate corrected p-value less than 0.25 were included, and patients with missing data were excluded.

Results

Four hundred fifty-six patients met the study criteria; 342 were English-speaking and 114 were Spanish-speaking. Univariate analysis showed that patients in the English-speaking group were more likely to be White or Black ($p < 0.001$), whereas patients in the Spanish-speaking group were more likely to be of Hispanic ethnicity (94.7% vs 15.2%, $p < 0.001$). Following Benjamini-Hochberg correction, Spanish-speaking patients were significantly more likely to have diabetes ($p = 0.006$), chronic kidney disease ($p = 0.032$), and dementia ($p = 0.004$). Additionally, they had a significantly higher mean Distressed Communities Index (DCI) percentile compared to English-speaking patients (72.79 vs 65.95, $p = 0.002$) suggesting greater socioeconomic distress. Multivariate logistic regression adjusting for the aforementioned characteristics (aside from race/ethnicity) showed no significant differences in mortality (in-hospital, 30-day, or one-year) between the two groups. However, Spanish-speaking patients were more likely to experience postoperative delirium compared to English-speaking patients ($p = 0.003$). In addition, while not significant in the univariate analysis, multivariate analysis showed that Spanish-speaking patients were significantly more likely to experience postoperative VTE compared to English-speaking patients ($p = 0.028$).

Conclusion

The results of our study revealed that patients whose primary language was Spanish were more likely to have postoperative delirium and VTE compared to patients whose primary language was English. It is important to note that Spanish language was significantly correlated with Hispanic ethnicity among patients included in this study. However, the current literature suggests that Hispanic patients are at a decreased risk for VTE, whereas our univariate analysis did not show English- and Spanish-speaking patients to differ with respect to VTE occurrence. This may be due to the effect that Hispanic ethnicity is thought to have in decreasing risk of VTE among this patient group, as suggested by the literature. Thus, our results suggest that the language barrier itself may have a substantial effect on a patient's increased risk of VTE despite evidence for decreased risk among the Hispanic population. Similarly, the increased risk of post-operative delirium among Spanish-speaking patients (after controlling for delirium) is also suggestive of management-based differences in patient care greatly influenced by the presence of a language barrier.

Significance

Our results suggest that a language barrier may be implicated in the development of certain adverse postoperative outcomes among orthopedic patients. This underscores the importance of closely assessing the management of non-English-speaking patients for the presence of inequities in clinical care, so as to develop adequate interventions to address lapses in effective communication and mutual comprehension between patient and provider which may adversely affect patient outcomes.

Presentation and Outcomes of Pediatric Patients with Osteochondral Defects of the Knee

Edmund Corcoran[1], Zachariah Samuel[1], Leila Alvandi[1], Mauricio Drummond[1], Eric Fornari[1]

[1] *Montefiore Einstein Department of Orthopaedic Surgery, Division of Pediatric Orthopaedic Surgery, Bronx, NY*

Introduction: There is minimal literature regarding osteochondral defects of the knee, particularly in pediatric populations. This study aims to describe the presentation and outcomes of pediatric patients surgically treated for osteochondral defects (OCD) of the knee.

Methods: A retrospective chart review identified patients surgically treated for OCDs between January 2012 and December 2023. Demographic information, injury characteristics, and outcome information including time to return-to-sports and patient-reported outcome (PRO) scores were collected.

Results: A total of 133 patients (85 males, 48 females) with 149 OCD lesions were included, with 12 patients presenting with two ipsilateral lesions and three patients later developing four contralateral lesions. The mean age at initial diagnosis was 16.18±2.66 years, and the mean BMI was 26.46±6.22. Sixty-three patients (47.37%) sustained injuries during sports activities. Lesion locations were as follows: 54 (36.24%) on the lateral femoral condyle, 52 (34.90%) on the patella, 24 (16.11%) on the medial femoral condyle, 11 (7.38%) on the tibial plateau, and eight (5.37%) on the trochlea. The average lesion size was 2.30±1.94 cm^2. Patients had an average follow-up post-surgery of 1.47 years.

Primary treatments included 43 (28.86%) chondroplasties/abrasion arthroplasties, 39 (26.17%) microfractures, 35 (23.49%) fixations, 21 (14.09%) osteochondral allograft transfers (18 with De Novo cartilage), five (3.36%) osteochondral autograft transfers, and six (4.03%) loose body removals. Eleven (8.27%) patients required unplanned second surgeries, with two due to unresolved OCDs after primary surgery.

Concomitant ligamentous injuries were present in 74 patients (55.64%), including 38 MPFL tears, 22 lateral meniscal tears, 20 ACL tears, and 10 medial meniscal tears. Non-athletes accounted for 24 patients, while of the remaining 109 patients, 69 (63.30%) returned to sports with an average return time of 7.26±3.35 months. Nine patients (8.26%) did not return, and four (3.67%) were still recovering.

Postoperative outcomes demonstrated improvements in Tegner/Lysholm Knee Scores (TLKS), Pediatric IKDC scores, and KOOS-Child scores.

Conclusion: OCDs of the knee demonstrate complex pathology often involving ligamentous injuries and multiple sites of osteochondral injury. Despite this, a majority of patients returned to sports following surgery and PRO scores showed improvement from pre-operative values.

Significance: This research highlights the multifaceted nature of osteochondral defects of the knee in pediatric patients, revealing that though these injuries often coincide with various ligamentous pathologies, surgical intervention can enhance patient outcomes and facilitate a successful return to sports.

	Pre-Op Scores			6-Month Scores		
	Mean	SD	n	Mean	SD	n
TLKS	64.63	17.93	28	87.68	13.56	28
IKDC Score	50.28	20.23	29	75.79	15.64	29
KOOS Child Pain	69.05	22.27	27	90.5	11.05	27
KOOS Child Symptoms	70.13	19.15	27	86.24	14.19	27
KOOS Child ADL	72.14	24.26	26	94.62	9.96	27
KOOS Child Sport/Rec	50.48	30.30	22	72.82	25.40	24
KOOS Child QOL	40.62	27.88	26	62.44	23.68	27
	1 Year Scores			2 Year Scores		
	Mean	SD	n	Mean	SD	n
TLKS	88.38	17.08	32	75.33	24.04	24
IKDC Score	83.80	18.80	31	70.48	22.49	25
KOOS Child Pain	90.60	14.21	30	75.60	22.66	23
KOOS Child Symptoms	87.37	17.69	30	75.61	22.81	23
KOOS Child ADL	92.42	16.82	29	84.08	21.38	23
KOOS Child Sport/Rec	83.09	23.42	29	68.07	29.56	21
KOOS Child QOL	73.92	26.63	30	58.20	26.53	23

Figure 1: OCD Cohort PRO Score Mean Values and Standard Deviation at Four Time Points: Pre-Operation, 6 Months (0.42-0.75 years post-surgery), 1 Year (0.76-1.50 years post-surgery) and 2 Years (>1.50 Years post-surgery).

AI Patient Resources for Lumbosacral Radiculopathy: An Objective Analysis of Available Materials

Michael Birnhak[1,6], Rajwinder Singh[1], Hitangee Jain[2,7], Romona Ling[2,8], Mohammad Athar MD[3], Nakul V. Karkare MD[5], Vedant Vaksha MD[3]

[1]*Research Associate, Complete Orthopedics 2500 Nesconset Hwy 10D, Stony Brook, NY 11790*

[2]*Research Associate, Complete Orthopedics 52-21 Little Neck Pkwy, Queens, NY 11362*

[3]*Attending Orthopedic Surgeon, Complete Orthopedics 2500 Nesconset Hwy 10D, Stony Brook, NY 11790*

[4,5]*Attending Orthopedic Surgeon, Lenox Hill Hospital 100 E 77th St, New York, NY 10075*

[6]*Medical Student, Touro College of Osteopathic Medicine, 230 W 125th St, New York, NY 10025*

[7]*Medical Student, SUNY Downstate College of Medicine 450 Clarkson Ave, Brooklyn, NY 11203*

[8]*Undergraduate Student, Cornell University, 410 Thurston Avenue, Ithaca, NY 14850*

Abstract

As times change and the world around us advances, medical knowledge must adapt. Technology integration in healthcare has drastically advanced over the years with the advent of increasingly available public medical information. With the recent advent of public AI web interface tools, we aimed to determine whether the use of such provides a better platform for the general public to understand and access healthcare literature. We utilized three of the most well-recognized, and free-to-access, AI tools - ChatGPT, Google Gemini, and Meta AI. The focus of the study was regarding lumbosacral radiculopathy and our grading criteria were based on information quality, information accuracy, and the ability of the AI to alter readability appropriately. The quality of the responses was measured using indexes previously used to evaluate online articles, thus providing a validated source of evaluation. Overall, the mean quality of the response written at the college graduate level was significantly higher than the quality of the simplified response written at a seventh to ninth-grade level. In conclusion, if the AI models follow the given outlines of reading level criteria provided by the American Medical Association (AMA), Centers for Disease Control and Prevention (CDC), and/or National Institutes of Health (NIH) the quality of the response is compromised in exchange for better readability.

Introduction: The future of medical knowledge lies in our hands, both literally and figuratively, with the advent of internet-accessible smartphones. Additionally, with the advancement of free web-based AI interfaces people have the ability to access a powerful supercomputer that utilizes information from millions of sourced data points - developing what it considers to be the most appropriate response. We questioned the quality and readability of the AI interface responses to determine their viability as a source of healthcare information for the general public. Furthermore, we sought to understand the capabilities of the AI interface in differential diagnostics with regard to the terminology used by the general population - specifically regarding “radiating back pain” (lumbosacral radiculopathy).

Methods: Each of the three web-based AI interfaces was given a series of prompts to assess their abilities to both give orthopedic-based medical advice and to deliver such information for use by the general population. Each set of questions was asked in a new session with the AI, thereby avoiding bias from previous conversations and enabling the reproducibility of our results. The results were taken in two parts, as the original answers, and as “simplified” answers after prompting the AI interfaces to “simplify the previous response to a seventh grade reading level”. The responses were graded to determine the AI interface's ability to not only provide quality responses but also its ability to simplify the data to a level of understanding for the general public.

Results: The mean quality of unaltered AI-produced responses was not significantly higher than the adjusted versions (p-value = 0.85). The reading level of the original response is significantly higher than the simplified version (p-value = 0.037). The results (FK scores) indicated the AI was successfully prompted to change the reading comprehension level of its responses from a high reading level (college level) to the standard seventh grade reading level making medical information presented to the public easily comprehensible to a wider range of individuals.

Discussion: Our results indicate that the simplification of data to a seventh grade reading level did not significantly alter the quality of the results (p-value = 0.037). This is a positive result in that it indicates responses generated for the general population would not alter the quality of data initially presented by the AI. Additionally, we can see that the AI was successfully able to significantly simplify the data to a seventh grade reading level (p-value = 0.037). Such a calculation was based on a grading comparison in which we utilized a web-based Flesch-Kincaid calculator per AI interface conversation string.

Clinical Relevance: This paper seeks to bridge the gap between healthcare and the upcoming significance of free web-based AI interfaces. Many people do not, potentially due to monetary reasoning or time restraints, seek medical care concerning their healthcare questions, but increasing the availability of medical-oriented free AI interfaces may be a prospective solution.

Acknowledgments: We would like to thank Dr. Athar, Dr. Karkare, and Dr. Vaksha for their support and guidance throughout the creation and data collection of this paper. Their help in determining the quality of the data was greatly appreciated.

AI Patient Resources for Ankle Instability: An Objective Analysis of Available Materials

Rajwinder Singh[1], Hitangee Jain[1,2], Michael Birnhak[1,3], Romona Ling [1,5], Amritjot Dhillon [1,4] Vedant Vaksha MD[6], Mohammad Athar MD[6], Nakul V. Karkare MD[6,7]

[1]Research Associate, Complete Orthopedics 2500 Nesconset Hwy 10D, Stony Brook, NY 11790

[2]Medical Student, SUNY Downstate College of Medicine 450 clarkson Ave Brooklyn NY 11203

[3]Medical Student, Touro College of Osteopathic Medicine 230 W 125th St New York, NY 10025

[4]Medical Student, Touro College of Osteopathic Medicine 60 prospect ave Middletown, NY 10940

[5] Undergraduate Student, Cornell University, 410 Thurston Avenue, Ithaca, NY 14850

[6]Attending Orthopedic Surgeon, Complete Orthopedics 2500 Nesconset Hwy 10D, Stony Brook, NY 11790

[7]Attending Orthopedic Surgeon, Lenox Hill Hospital 100 E 77th St, New York, NY 10075

Abstract

As times change and the world around us advances, medical knowledge must too. The role of technology in healthcare has drastically advanced over the years with the advent of increasingly available public medical information. Worldwide access to medical knowledge via search engines - including Google, Bing, and Yahoo - has allowed the general public to become involved in their own healthcare. The quality, accuracy, and readability of the data provided via these search engines, with regard to orthopedic-related injuries, have been minimally studied, but initial data points toward poor quality and/or inadequate readability. With the recent advent of public AI web interface tools, we wanted to see if the use of such tools provides a better platform for the general public with regard to healthcare information. We utilized four of the most well-recognized, and free-to-access, AI tools - ChatGPT, Google Gemini, Meta AI, and Microsoft Copilot. The focus of the study was regarding ankle instability and our grading criteria were based on information quality and the ability of the AI to alter readability appropriately. Results indicated a successful and significant alteration from a high reading level response, e.g. college level, to the standard seventh grade reading level required for medical information presented to the public.

Introduction: The future of medical knowledge lies in our hands, both literally and figuratively, with the advent of the internet-accessible smartphones. Additionally, with the advancement of free web-based AI interfaces people have the ability to access a powerful supercomputer that utilizes information from millions of sourced data points - developing what it considers to be the most appropriate response. We questioned the quality and readability of the AI interface responses to determine their viability as a source of healthcare information for the general public. Furthermore, we sought to understand the capabilities of the AI interface in differential diagnostics with regard to the terminology used by the general population - specifically regarding “Ankle instability”.

Methods: The AI assistants were each given a series of prompts to assess their individual abilities to both give orthopedic-based medical advice and to deliver such information for use by the general population. Each set of questions was asked in a new session with the AI, thereby avoiding bias from previous conversations and enabling the reproducibility of our results

Results: The results of each AI’s response quality significantly differed between the original response and the simplified response. The average response quality in the original responses was 10.38 out of 18.00 and the average response quality of the simplified responses was 7.79 out of 18.00. The average response quality of the original was statistically higher than the average quality of the simplified response (P = 0.001; 95% CI = 1.40 to 3.77). Overall, Meta AI produced the best quality responses in both the original and simplified versions, with average quality scores of 11.33 and 8.67, respectively. ChatGPT had the lowest original average quality score of 9.67. Both Google Gemini and Copilot had the lowest simplified average quality scores of 7.33 All four AIs generated original responses written at a college or college graduate level, while the simplified responses varied between seventh through ninth grade levels. The mean F-K score of all original AI responses was lower than the mean score of their complementary simplified responses. The average F-K score of the original responses was 34.6, indicating a difficult, college reading level. While the average F-K score of all simplified responses was 69.2, indicating a standard, eighth to ninth grade reading level. The mean quality of the unaltered AI responses was significantly higher than the altered to seventh grade reading level responses (P = 0.001). The reading level of the original responses was significantly higher than the level of the simplified AI responses (P = 0.004).

Discussion: Our results indicate a significant and successful alteration from a high reading level response to a simplified 7th to ninth-grade level response. However, the overall quality of the responses decreased with the simplification. The reading level grades of the responses decreased; their qualities decreased as well. Overall, the mean quality of responses written at college-to-college-graduate level was much higher than the quality of the simplified responses written at a seventh-to-ninth-grade level.

Clinical Relevance: Ai webtools seem promising, at the current time it is very user dependent leading to variability in how much the user can obtain from its responses. Ai is still not as reliable as human interactions.

Acknowledgments: We would like to thank Dr. Athar, Dr. Karkare, and Dr. Vaksha for their support and guidance throughout the creation and data collection of this paper. Their help in determining the quality of the data was greatly appreciated.

The Sclerotic Hip Index in Patients with Sickle Cell Disease (SHIPS)

Hannah Kareff[1], Zeynep Seref-Ferlengez[2], Carlos Alvarado[2]
Albert Einstein College of Medicine[1], Montefiore Medical Center[2]

Objectives: Sickle Cell Disease (SCD) is an autosomal recessive condition that produces numerous Orthopedic manifestations. One of the most common conditions resulting from SCD is Avascular necrosis of the femoral head, affecting roughly 30% of patients with SCD. Due to this disease process, many SCD patients are required to undergo Total Hip Arthroplasty (THA). It has been previously documented that THA in this patient population is fraught with higher incidence of perioperative complications, making THA in the setting of SCD a challenging prospect. Although there is a known increased risk of perioperative complications in SCD, to our knowledge, no studies have attempted to stratify patients based on the extent of sclerotic changes throughout the proximal femur. Our study aimed to create a Radiographic classification system for SCD to help predict the risk of perioperative complications.
Methods: A new classification system was designed to be applied to standard AP Pelvis Radiographs to avoid the need for costly additional imaging. The Sclerotic Hip Index in Patients with Sickle Cell Anemia (SHIPS) classification was divided into three grades based on the distal extent of sclerotic changes within the proximal femur. Grade 1: sclerotic changes in the femoral head and neck, but not distal to the intertrochanteric line. Grade 2: sclerosis distal to the intertrochanteric line, but proximal to the subtrochanteric region. Grade 3: sclerotic changes into the subtrochanteric region of the femur. The patient cohort was obtained from electronic records review of all patients at our institution with a diagnosis code of SCD that received primary THA at a single institute between 2016 and 2023. After reviewing the preoperative radiographs, a final cohort (n=88) was developed. Radiographs were graded by two observers, an attending surgeon and an adult reconstruction fellow blinded to each other's gradings, grades were compared for inter-observer reliability. Cohorts were created based on the SHIPS grade, surgical outcomes (length of stay, blood loss, blood transfusion, intra-operative and post-operative complications, and 90-day readmission and infection rates) as well as longer term outcomes (revision and mortality) were collected and statistically compared between three groups by Chi-Square and ANOVA tests.
Results: The inter-observer reliability for the classification system was found to be 91%. 88 subjects were included, cohort sizes were 54,18 and 15 for grades 1,2 and 3, respectively. SHIPS Grade3 cohort had significantly longer LOS compared to groups 1 and 2 (mean LOS: SHIP1:3.63, SHIP2:4.5, SHIP3:10,$p < 0.01$). Patients with more severe SHIP grades had higher rates of pre-operative blood transfusion, higher blood loss (>500ml Blood loss: SHIP1:20%,SHIP2:39%,SHIP3:64%,$p<0.01$) and post-operative blood transfusions (SHIP1: 39%, SHIP2:%, 78%, SHIP1:93%, $p>0.01$). No significant difference was observed with regards to infection rates, readmission rates, or Emergency room visits within 90 days. In addition, there was no significant chronic postoperative findings. There was no significant difference between the SHIPS cohorts with regards to deep vein thrombosis (DVT), pulmonary embolism (PE), ED visits or readmission after 3 months, infection after 1 year, or all-time revision and mortality rates.
Conclusions: The SHIPS Classification demonstrated excellent inter-observer reliability in this study, indicating it can be used broadly between surgeons. The classification system was also able to show differences in length of stay outcomes and transfusion requirements with high statistical significance. Interestingly, SHIPS Grade 2 cohort demonstrated more complications than Grade 3 despite the lower extent of sclerotic changes. This is likely due to sclerosis extending to the intertrochanteric region, making THA more complicated. There were no long term findings between the SHIPS cohorts.
Significance: The SHIPS Classification is a simple classification that can be done at a patient's initial visit without any additional cost to the healthcare system. It provides valuable preoperative information to the surgeon and patient, allowing for improved pre-operative patient education and planning of the intra-operative and post operative course.

Influence of CD4 Count on Three-Month and One-Year Surgical Outcomes of Total Joint Arthroplasty in HIV Patients

Authors: Vishal Shankar[1], Carlos Salazar[1], Zeynep Seref-Ferlengez PhD[2], Carlos Alvarado MD[2], Eli Kamara MD[2]

Affiliation: [1]Albert Einstein College of Medicine, Bronx, NY 10461

[2]Department of Orthopedic Surgery, Montefiore Medical Center/Albert Einstein College of Medicine, Bronx, New York 10461

Background: The advent of new HIV antiretroviral therapies has not only improved the life expectancy of those living with the illness but has increased the prevalence of those undergoing total joint arthroplasty (TJA). Nonetheless, patients with lower CD4 counts still may be more vulnerable to post-operative complications and future revisions, returns to the operating room (OR), and other hospitalizations. Characterizing this relationship in HIV+ patients is crucial to improving prognosis of arthroplasty in this immunocompromised population. This study aims to assess the impact of CD4 count on three-month and one-year surgical outcomes in HIV patients undergoing TJA.

Methods: Patients who had a total joint arthroplasty (TJA) within the Montefiore Health Network in the years 2016-2024 were retrospectively reviewed for CD4 counts, infection rates, postoperative drainage, revisions, emergency department visits, readmissions, and length of stay. Based on past literature that has shown that CD4 counts under 500 indicate a weakened immune system and increased susceptibility to adverse outcomes, two groups were created based on CD4 counts: CD4 counts ≥ 500 (HIV Stage 1) and CD4 < 500 (HIV Stage 2).[1] All surgeries took place in the same academic institution. Patients lost to follow-up or without a completed 3 month or 1-year visit were excluded from the study. The rates of the outcome variables were compared between the two groups using Chi-Square and Student's t-tests with p-values and odds ratios (OR) reported.

Results: For the 3-month follow up group, the total cohort included 198 patients with 130 (66%) in the HIV Stage 1 group and 68 (34%) in the HIV Stage 2 group. Significant differences between the groups ($p < 0.05$) were found for smoking and drug use history, with HIV Stage 2 patients having higher rates of smoking history (82.4% vs 66.7%) and drug use history (51.5% vs 30%) than HIV Stage 1 patients. HIV Stage 2 patients also had higher rates of 30-day readmission (6.06% vs 5.38%), but lower rates of 30-day return to ER (14.7% vs 16.2%) and 3-month infection (1.5% vs 0.7%) compared to HIV stage 1 patients, though these associations were not statistically significant. There was no difference in 30-day DVT/PE occurrence or 3-month mortality. For the 1 year follow up group, a total of 159 patients met the inclusion criteria: 107 (67%) were classified as HIV Stage 1 (CD4 > 500) and 52 (33%) as HIV Stage 2 (CD4 < 500). A significant difference in drug use history was found between the two groups ($p < 0.02$), with HIV stage 1 and stage 2 patients having drug use history prevalences of 30.8% and 53.8% respectively. HIV Stage 2 patients had notably high rates of return to the operating room (OR: 2.63, $p = 0.04$) and revision (OR: 3.23, $p = 0.015$) compared to HIV Stage 1.

Conclusion: For the 3 month follow up group, there were statistically significant differences in drug history and higher rates of 30-day readmission for HIV Stage 2 patients compared to HIV Stage 1. Interestingly, the rates of 30-day ER visit and 3-month infection were lower in the HIV Stage 2 group compared to HIV Stage 1. For the 1-year follow up group, HIV Stage 2 patients exhibited higher odds of requiring return to the operating room and revisions to their prosthesis. This group also showed a significant difference in drug use history. These associations not only support extra precautions in severe cases of HIV, but it may also corroborate underlying influences of drug use on surgical outcomes. Future research should be done to quantify these relationships and contribute to better outcomes in this vulnerable population.

References:

1. Battistini Garcia SA, Guzman N. Acquired Immune Deficiency Syndrome CD4+ Count. [Updated 2023 Aug 14]. In: StatPearls [Internet]. Treasure Island (FL): StatPearls Publishing; 2024 Jan-. Available from: https://www.ncbi.nlm.nih.gov/books/NBK513289/

Short-term outcomes and complications in patients treated with a knee implantable shock absorber (ISA) system.

Janet Hsu, BS[1,2]; Ava G. Neijna, BA[1]; Andreas H. Gomoll, MD[1]; Sabrina M. Strickland, MD[1]
[1] Department of Sports Medicine, Hospital for Special Surgery, New York, NY, USA
[2] Albert Einstein College of Medicine, Bronx, NY, USA

Abstract

Introduction

In the last decade, the implantable shock absorber (ISA), also known as the MISHA Knee System (Moximed, Fremont, CA), was developed as another treatment option for medial knee osteoarthritis (OA). The ISA specifically helps patients who have failed non-operative treatments but are not ready for a total knee replacement. The implant was FDA-approved in April 2023, and this study aims to study short-term outcomes and complications since FDA approval.

Materials and Methods

Twenty-one patients who received the ISA since FDA approval between August 2023 and August 2024 were retrospectively reviewed. The surgery was done by two sports medicine-trained surgeons from our institution. Short-term outcomes included subsequent surgeries, complications, and range of motion. Patient-reported outcomes, including the International Knee Documentation Committee (IKDC) and Knee Injury and Osteoarthritis Outcome Score (KOOS) scores, for patients who had at least six months of follow-up were obtained.

Results

Twenty-one patients (mean age = 52 ± 9, BMI = 28.7 ± 5.6 kg/m2, 48% female) who received an ISA were analyzed. The patients had an average Kellgren and Lawrence grade of 2 ± 1 and Outerbridge grade of 3 ± 1. Medial meniscus surgery was the most common concomitant procedure, which 14 (67%) patients received. Knee flexion improved post-operatively from 6 weeks (115 ± 17 degrees) to 3 months (129 ± 11 degrees). Four patients (19%) had complications, which were deep vein thrombosis (DVT), arthrofibrosis, infection, and painful hardware. IKDC scores were 44.25 ± 14.58 pre-operatively and increased to 54.74 ± 16.64 post-operatively (p = 0.04). KOOS scores for activities of daily living (ADL), sports, and quality of life (QoL) were significantly increased after the surgery compared to before the surgery. KOOS scores for symptoms and pain were not significantly different.

Conclusion

The complication rate in this study (19%) is similar to the complication rate (16%) found in past studies before FDA approval.[1] Given the potential complications that may occur with the ISA, it is important to inform patients of the possible risks with the ISA surgery and potential dissatisfaction after surgery. There is also potential to investigate ways to optimize post-operative protocols to reduce complication rates.

References

[1] Diduch DR, Crawford DC, Ranawat AS, Victor J, Flanigan DC. Implantable Shock Absorber Provides Superior Pain Relief and Functional Improvement Compared With High Tibial Osteotomy in Patients with Mild-to-Moderate Medial Knee Osteoarthritis: A 2-Year Report. Cartilage. Jun 2023;14(2):152-163. doi:10.1177/19476035231157335

Table 1

PROMs (n=8)	Pre-Op	6-month Post-Op	Change	p-value
IKDC	44.25 ± 14.58	54.74 ± 16.64	10.49	**0.040**
KOOS				
Pain	62.50 ± 16.47	67.36 ± 17.87	4.86	0.057
Symptoms	70.09 ± 22.98	62.50 ± 20.20	-7.59	0.108
ADL	75.68 ± 16.33	77.77 ± 16.44	2.09	**0.039**
Sports / Recreation	28.13 ± 24.78	43.13 ± 24.34	15.00	**0.024**
QoL	17.97 ± 14.35	26.45 ± 23.56	8.48	**0.002**

Assessing Child Opportunity Index 2.0 as a Risk Factor for Patellar Dislocation

Authors: Eliana Weinstein, BS[1], Jason Brenner, BS[1], Leila Mehraban Alvandi, PhD[1,2], Steven M. Henick, MD[2], Edina Gjonbalaj[2], Benjamin J Levy, MD[1,2], Jacob Schulz, MD[1,2], Eric Fornari, MD[1,2], Mauricio Drummond, MD[1,2]
Affiliations: [1]Albert Einstein College of Medicine, Bronx, NY, [2]Montefiore Einstein Department of Orthopaedic Surgery, Division of Pediatric Orthopaedic Surgery, Bronx, NY

Introduction: Patellar dislocation (PD) is a common, debilitating pediatric knee injury with a multifactorial etiology. Social determinants of health (SDoH) can affect the time and ability for individuals to access specialty level care. The Child Opportunity Index 2.0 (COI) is a tool used to measure community conditions and access to resources that may affect health outcomes [1-2]. The time from MRI order to MRI completed represents an additional proxy for SDoH.

Purpose: To investigate whether SDoH is a risk factor for PD, and if so, whether SDoH is associated with recurrent patellar dislocations, in an urban, underserved setting.

Methods: Following institutional review board approval, we retrospectively reviewed (Level III) medical charts from pediatric patients at a single institution in an urban, underserved area who were treated for PD into two cohorts: recurrent patellar dislocators (RPDs) and one-time dislocators (OTDs). The OTDs were called to confirm their history of just one PD. Patients with prior surgery in the affected knee were excluded. Then, one-hundred age- and sex-matched controls were recruited from an internal database of patients treated for ACL injuries and a negative history of PD. Statewide COI 2.0 metrics including total COI, socioeconomic (SE) COI, health (HE) COI, education (ED) COI, and composite total COI scores were recorded, as well as categorical groups. Patients were grouped one through five (1=very low, 2=low, 3=moderate, 4=high, 5=very high) by the creators of the index for each metric; we further assigned patients into either very low/low or moderate/high/very high groupings based on prior literature [3]. We also recorded the following proxy for SDoH for all cohorts: time from MRI order to MRI completed (days). Comparative statistics included chi-squared tests for categorical variables and independent samples T-tests for continuous variables.

Results: A total of 270 knees were included in our analysis (172 PDs, average age = 15.13 ± 2.62; 100 controls, average age = 15.60 ± 1.41). Of the PDs, 105 were RPDs (average age = 15.29 ± 2.45) and 67 were OTDs (average age = 14.89 ± 2.70). Several measures of SDoH were worse in PDs than in controls (Table 1). SDoH was not useful as a predictor of RPD in this cohort (Table 1).

	PD (n=172)	ACL Controls (n=100)	P-value	RPD (n=105)	OTD (n=67)	P-value
COI SE (low / very low)	153 (89%)	91 (91%)	.435	93 (86%)	62 (93%)	.283
COI HE (low / very low)	**171 (99%)**	**94 (94%)**	**.038**	103 (98%)	67 (100%)	.371
COI ED (low / very low)	**139 (81%)**	**71 (71%)**	**.032**	82 (78%)	58 (87%)	.116
COI total (low / very low)	151 (88%)	90 (90%)	.401	93 (89%)	61 (91%)	.403
MRI order to MRI done (days)	**29.6 (±50.9)**	**15.5 (±14.3)**	**<.001**	30.0 (±49.7)	29.0 (±53.0)	.910

Table 1: Chi-squared tests and independent samples t-tests comparing metrics of social determinants of health between patellar dislocators and controls (left) and between recurrent patellar dislocators and one-time dislocators (right). COI, child opportunity index 2.0; SE, socioeconomic; HE, health; ED, education.

Conclusion: The cohorts assessed in this study have predominantly low/very low COI ratings. Certain measures of SDoH were found to be predictive of PD compared to control in this cohort, but not predictive of RPD compared to OTD.

Significance: It is important to understand underlying risk factors for patellar dislocation to improve health outcomes. Conducting similar analyses among more socioeconomically diverse patient populations may yield different results.

References:
[1] diversitydatakids.org: Child Opportunity Index 2.0 database, 2024. Available at: https://data.diversitydatakids.org/dataset/coi20-childopportunity-index-2-0-database?_external=True. Accessed October 14, 2024.
[2] Shanahan KH, Subramanian SV, Burdick KJ, Monuteaux MC, Lee LK, Fleegler EW. Association of Neighborhood Conditions and Resources for Children With Life Expectancy at Birth in the US. JAMA Netw Open. 2022;5(10):e2235912. doi:10.1001/jamanetworkopen.2022.35912
[3] Hoffman A, Alvandi LM, Gjonbalaj E, et al. Child Opportunity Index and Diagnosis of Developmental Dysplasia of the Hip: Insights From a Children's Hospital Serving Disadvantaged Communities. J Am Acad Orthop Surg. 2024;32(17):807-813. doi:10.5435/JAAOS-D-24-00417

ABSTRACT #048

Higher Distressed Community Index and Initial Fracture Treatment Outside of the United States Associated with Failure to Achieve Bone Union Within 12 Months of Nonunion or Malunion Corrective Surgery

Morgan Roche, BS[1]; Mihir Sharma, BS[1]; Mohammed Bashier, BA[1]; Sirjanhar Singh, MD[2]; Yungtai Lo, PhD[3]; Mani Kahn, MD[2]

[1]Albert Einstein College of Medicine, Bronx, New York
[2]Montefiore Einstein Department of Orthopaedic Surgery, Bronx, New York
[3]Montefiore Einstein Department of Epidemiology and Population Health, Bronx, New York

Background:

Failed fracture healing – manifesting as nonunion or malunion – can result from inadequate reduction or fixation, infection, or underlying systemic disease. Treatment is costly, time-consuming, and requires significant patient engagement; in severe cases, the goal of nonunion treatment is limb salvage. While studies have reported comorbidities and fracture-related factors associated with failed healing, the impact of key social determinants of health (SDOH) on treatment outcomes for nonunions and malunions has not been established.

Objective:

To determine if SDOHs are associated with complications or delayed bone union following nonunion or malunion corrective surgery.

Methods:

We conducted a retrospective cohort study of patients with fracture nonunion or malunion who underwent surgical correction at a single center between November 2015 and June 2024. Patients were included if they were treated surgically for fracture nonunion or malunion of any bone following traumatic or iatrogenic injury and were ≥ 18 years old at the time of original injury. SDOHs considered include race, ethnicity, spoken language, insurance status (none, public, private), Distressed Community Index (DCI), and the geographic location of initial fracture treatment (domestic, abroad). The DCI is a zip-code-based index that uses poverty rate, median income ratio, changes in employment and establishments, housing vacancy rate, and high school diploma rates to represent a community's economic well-being; higher scores indicate more distress. Outcomes assessed included radiographic bone union within 12 months of surgery, the success of the original surgical plan in achieving union, and the incidence of any complication within 3, 6, and 12 months postoperatively. Complications included infection, hardware failure, pulmonary embolism, deep vein thrombosis, myocardial infarction, and unexpected reoperation. Patients who were lost to follow-up before union was achieved were considered not united. Associations of the selected SDOHs with radiographic bone union within 12 months of surgery, union achieved with the original surgical plan, and any complication within 3, 6, and 12 months postoperatively were examined using chi-square or Fisher's exact tests for race, ethnicity, spoken language, and insurance status, and Wilcoxon rank-sum tests for DCI.

Results:

Of 246 patients analyzed, high DCI (p=0.014) and initial fracture treatment outside of the United States (p=0.047) were both significantly associated with failure to achieve radiographic union within 12 months of surgical nonunion or malunion correction. In 135 patients achieving union, median (IQR) time to union after the planned corrective operation was 254 (121, 474) days, ranging from 37 to 2398 days. Initial treatment location abroad was significantly associated with longer time to union (238 vs. 357 days, p=0.022). Public insurance status was associated with radiographic union achieved with the original surgical plan (p=0.027). Race, ethnicity, spoken language, insurance, DCI, and initial treatment location were not significantly associated with having one or more complications within 3, 6, or 12 months of surgery.

Conclusions:

Individuals who were initially treated for their fractures abroad and individuals living in more distressed communities were less likely to achieve radiographic union within 12 months of nonunion or malunion surgical correction.

Significance:

Patients from economically distressed communities face higher rates of delayed or failed healing following treatment for fracture nonunion and malunion. Patients initially treated abroad may require more dramatic revision; understanding this association empowers physicians to inform patients of treatment expectations and design treatment plans accordingly. To improve outcomes, targeted interventions should focus on making fracture care more accessible for distressed populations.

Disparities in Education and Socioeconomic Status Are Associated with Increased Severity of Presentation of Early-Onset Blount Disease

Eduardo Valero-Moreno[1], Zachariah Samuel[1], Leila M. Alvandi[1], Edina Gjonbalaj[1], Melinda Sharkey [1]
Affiliations : [1]Montefiore Medical Center, Bronx, NY

Objective: Children's Opportunity Index (COI) measures the quality of resources and conditions at the zip code level and stratifies data into quintiles (very low, low, moderate, high, very high). Prior research at our institution, which primarily serves patients from very low/low COI neighborhoods, showed no differences in accessing timely orthopaedic care for infant hip dysplasia or adolescent ACL tears. Because of this, we hypothesized that patients from lower COI neighborhoods do not present later or with more severe disease in early-onset Blount Disease.
Methods: In this IRB-approved, retrospective study, demographic, clinical, and radiographic data were obtained through chart review for all patients presenting to a single academic institution with early-onset Blount Disease over 17 years. Overall COI 3.0 scores, as well as three subdomains: education, socioeconomic status (SES), and health were collected. Patients were separated into two groups based on COI quintiles: very low/low and moderate/high/very high. Chi-square and Fisher's exact tests were used to compare groups.
Results: Out of 98 patients, 88 came from low/very low COI neighborhoods, while 10 resided in moderate/high/very high COI neighborhoods. The average age at presentation was 3.39±2.32 years for the low/very low COI group and 2.92±1.90 years for the moderate/high/very high COI group (p=0.53) trending toward older presentation in the very low/low COI group. Significant differences in Langenskiöld stage and varus deformity (measured by mechanical axis deviation (MAD)) were found, with patients in the low/very low COI group presenting with more advanced disease than those in the moderate/high/very high COI group (p=0.034 and p=0.043, respectively). Sub-analysis revealed that the differences in Langenskiöld stage and MAD were primarily associated with the education and SES COI subdomains. The health COI subdomain could not be analyzed as all patients fell into the moderate/high/very high group, suggesting equitable access to medical care in our area.
Conclusion: Patients from very low/low COI neighborhoods presented with more advanced disease compared to those from higher COI neighborhoods. This difference in severity at presentation was associated with education and SES COI subdomains. The average age at presentation did not differ significantly between groups, however there is a trend toward older age at presentation in the very low/low COI group.
Significance: Despite similar access to care, patients from very low/low COI neighborhoods presented with more severe disease. This highlights the need for increased awareness among the public as well as primary care providers in our area for diseases like Blount Disease that primarily affect children of color.

Table 1: Demographics and Presenting Characteristics Stratified by Total COI

	Low/Very Low Total COI	Moderate/High/Very High Total COI	P Value
n	88	10	
Age at Diagnosis (mean (SD))	3.39 (2.32)	2.92 (1.90)	0.533
Female (%)	42 (48.8)	4 (44.4)	1
Race/Ethnicity (%)			0.139
Black or African-American	28 (31.8)	5 (50.0)	
Spanish/Hispanic/Latino	25 (28.4)	0 (0.0)	
Unknown	35 (39.8)	5 (50.0)	
BMI percentile (mean (SD))	91.69 (15.38)	95.29 (6.34)	0.543
Bilateral (%)	65 (77.4)	8 (88.9)	0.71
Initial Treatment (%)			0.493
Guided growth	27 (31.0)	5 (50.0)	
Osteotomy	8 (9.2)	0 (0.0)	
External Fixator	4 (4.6)	0 (0.0)	
Nonoperative	48 (55.2)	5 (50.0)	
Langenskiöld at Presentation (%)			**0.034**
1	43 (53.1)	5 (62.5)	
2	20 (24.7)	1 (12.5)	
3	2 (2.5)	2 (25.0)	
4	8 (9.9)	0 (0.0)	
5	8 (9.9)	0 (0.0)	
Drennan Angle at Presentation (mean (SD))	17.60 (9.71)	14.06 (5.94)	0.316
mLDFA At Presentation (mean (SD))	99.24 (9.87)	96.37 (8.42)	0.432
MAD At Presentation (%)			**0.043**
1	6 (8.1)	1 (14.3)	
2	14 (18.9)	4 (57.1)	
3	54 (73.0)	2 (28.6)	

ABSTRACT #050

Predictors of Quality of Life After Pediatric Anterior Cruciate Ligament Reconstruction: A Longitudinal Analysis of Knee Injury and Osteoarthritis Outcome Score Subscale Recovery and Patient Acceptable Symptomatic State Achievement

Zachariah Samuel[1], Eduardo Valero-Moreno[1], Anisha Duvvi[1], Leila M. Alvandi[1], Edina Gjonbalaj[1], Jacob F. Schulz[1], Mauricio Drummond[1], Eric D. Fornari[1]
Montefiore Medical Center, Bronx, NY

Objective: The long-term recovery of knee function and patient-reported outcomes following anterior cruciate ligament reconstruction (ACLR) remains a critical area of interest, particularly concerning the achievement of Patient Acceptable Symptom State (PASS) across different Knee Injury and Osteoarthritis Outcome Score (KOOS) subscales. The aim of this study was to evaluate progression of KOOS subscale scores over time identify predictors of achieving PASS for the KOOS Quality of Life (QOL) subscale in pediatric patients after ACLR.

Methods: An IRB-approved retrospective review of pediatric patients at a tertiary care center, ages 10-21, who underwent primary ACLR from 2013-2021 was performed. Demographics and clinical data were recorded, including KOOS scores assessed preoperatively and at 6 months, 1 year, and 2 years postoperatively. Analysis of variance and post-hoc analyses were used to examine how QOL compared to the other subscales. PASS achievement rates were calculated at each time point using threshold values established in prior literature (88.9 for pain, 75.0 for symptoms, 98.5 for activities of daily living (ADLs), 75.0 for sport, and 68.8 for QOL).[1] Multivariate logistic regression was performed to identify predictors of KOOS QOL PASS.

Results: A total of 246 patients (mean age 16.51±1.72, 66.7% male, 63.1% with public insurance) were included in this study. Each KOOS subscale improved over time, but the trends differed, with QOL remaining significantly lower than all other subscales at each time point ($p < 0.001$). The mean preoperative QOL score was 43.51, increasing to 77.15 at 2-year follow-up. The subscales with the highest proportion of patients achieving PASS were symptoms (95.1%) and sport (94.9%), followed by 79.5% in pain and ADLs, and 66.7% in QOL. Multivariate regression revealed that higher preoperative KOOS QOL (OR=1.10 [1.03, 1.20]), male sex (OR=10.78 [1.92, 103.59]), and older age (OR=2.70 [1.41, 6.66]) were associated with higher odds of achieving PASS in QOL.

Conclusion: KOOS scores demonstrate substantial recovery following pediatric ACLR, particularly in symptoms and sport subscales. However, the lower PASS rates for KOOS QOL highlight persistent challenges in achieving optimal quality of life post-surgery, particularly in younger females with low baseline KOOS QOL.

Significance: Although ACLR leads to substantial recovery in most KOOS subscales, quality of life remains a critical area of concern, especially for younger females with low preoperative scores. Interventions should focus on improving the mental health and quality of life in younger females with low preoperative KOOS QOL to mitigate long-term deficits.

Figure 1: Average KOOS Scores Over Time

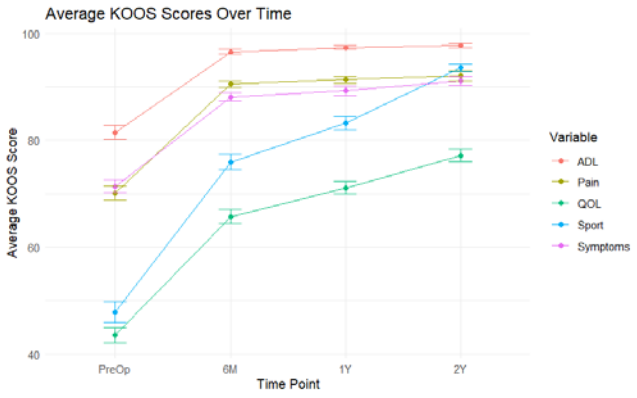

Table 1: PASS Achievement Rates of the ACLR Cohort

PRO	Preop (%)	6 Months (%)	1 Year (%)	2 Years (%)
KOOS Pain	18.3	66.7	74.6	79.5
KOOS Symptoms	51.2	85.7	86.6	95.1
KOOS ADL	21.0	57.6	67.5	79.5
KOOS Sport	21.6	67.5	75.7	94.9
KOOS QOL	11.2	49.2	60.7	66.7

Table 2: Multivariate Logistic Regression for Predictors of KOOS QOL PASS

Variable	Odds Ratio ($n = 139$)	*P* value
Preop KOOS QOL	1.10 [1.03, 1.20]	**0.009**
Male Sex	10.78 [1.92, 103.59]	**0.016**
Age at Surgery	2.70 [1.41, 6.66]	**0.010**

References: 1. Maheshwer B, Polce EM, Parvaresh KC, Paul K, Yanke AB, Forsythe B, Bush-Joseph CA, Bach BR, Cole BJ, Verma NN, Kogan M, Chahla J. Establishing Clinically Significant Outcomes After Anterior Cruciate Ligament Reconstruction in Pediatric Patients. J Pediatr Orthop. 2022 Jul 1;42(6):e641-e648. doi: 10.1097/BPO.0000000000002143. Epub 2022 Mar 17. PMID: 35297390.

Unicompartmental Knee Arthroplasty or Total Knee Arthroplasty? An Analysis of Randomized Controlled Trials Utilizing Dichotomous and Continuous Fragility Metrics

Adriano Cuadros BS[1], Francesca Docters BA[1], Andrew Chow[2], Avanish Yendluri BS[1], Auston Locke BS[1], Suraj Dhanjani MD[1], Robert L. Parisien MD[1]

[1]*Department of Orthopedic Surgery, Icahn School of Medicine at Mount Sinai, 1 Gustave L. Levy Pl, New York, NY*

[2]*Department of Orthopedic Surgery, Virginia Commonwealth University School of Medicine, 1016 East Clay Street, Richmond, VA*

INTRODUCTION

Randomized controlled trials (RCTs) comparing unicompartmental arthroplasty (UKA) and total knee arthroplasty (TKA) for osteoarthritis of the knee often report p-values that influence surgical decision-making.

OBJECTIVE

This study utilized the dichotomous and continuous fragility indices (FI) and fragility quotient (FQ) metrics to assess the statistical stability of outcomes reported in RCTs comparing UKA to TKA for osteoarthritis of the knee.

METHODOLOGY

PubMed, Embase, and MEDLINE were queried for RCTs published January 1, 2010 to September 1, 2024 comparing UKA and TKA for osteoarthritis. The FI and reverse fragility index (rFI) were calculated for dichotomous outcomes and were defined as the number of event reversals needed to alter the statistical significance for significant and non-significant outcomes. The continuous fragility index (cFI) was used to evaluate statistically significant continuous variables. The FQ was calculated by dividing the FI, rFI, or cFI by the respective sample size.

RESULTS

Of 545 RCTs screened for inclusion, 10 were included for analysis. A total of 26 continuous outcomes and 104 dichotomous outcomes were extracted. The median cFI across the 26 continuous outcomes was 11.3 (IQR 5.3-19.6). The dichotomous outcomes were found to be more fragile with a median FI of 5 (IQR 3-6) across all 104 outcomes. Statistically significant dichotomous outcomes particularly demonstrated considerable fragility with a median FI of just 2 (IQR 1-4). Furthermore, in 84.6% of statistically significant outcomes, the number of patients lost to follow-up was greater than the median FI. Non-significant outcomes had a median rFI of 5 (IQR 4-6).

CONCLUSION AND SIGNIFICANCE

Continuous outcomes comparing UKA and TKA for osteoarthritis are more robust than dichotomous outcomes. Statistically significant dichotomous outcomes demonstrated considerable fragility and may be reversed by less attrition in the RCTs assessed. cFI is a novel, valuable tool that allows for assessment of fragility for continuous outcomes, and reporting alongside FI, rFI, and FQ with p-values is recommended to assess the reliability of RCTs.

Socioeconomic Disadvantage Predicts Decreased In-Hospital Ambulation After Hip Fracture Surgery

Mohammed Bashier[1], Brandon Wang[1], Jessica Chao[1], Margaret Fagan[1], Megan Darrell[1], Dylan Horan[2], Leila M. Alvandi[2], Wanda Horn[2], Mani D. Kahn[2]

[1]Albert Einstein College of Medicine, Bronx, NY, [2]Montefiore Einstein, Department of Orthopaedic Surgery, Bronx, NY

Objective

The objective of this study was to investigate how established measures of socioeconomic deprivation, the Area Deprivation Index (ADI) and the Distressed Communities Index (DCI), correlate with outcomes in elderly patients who undergo surgical management of hip fractures. We hypothesized that higher ADI and DCI values, which indicate greater degrees of socioeconomic deprivation, are correlated with worse functional and health outcomes.

Methods

This study was a retrospective chart review of hip fracture patients over the age of 65 who underwent surgical management at a single academic tertiary care center between January 1, 2019 and September 30, 2022 and met our inclusion criteria. Fractures were classified as femoral neck or intertrochanteric fractures, and treatment modalities consisted of hemiarthroplasty, total arthroplasty, closed reduction with percutaneous pinning, or cephalomedullary nailing. Patients who sustained pathologic fractures or underwent nonsurgical treatment were excluded from the study. Patients were categorized as having either low (<50th percentile—less deprivation) or high (≥50th percentile—greater deprivation) ADI or DCI. To evaluate the effect of socioeconomic deprivation (using ADI and DCI, determined by patient address) as a predictor of postoperative outcomes, while adjusting for confounding patient characteristics, we employed multivariate logistic regression using Jamovi V.2.3. Variables assessed by multivariate regression include postoperative infection, pneumonia, pulmonary embolism, myocardial infarction, stroke, atrial fibrillation, urinary retention, urinary tract infection, delirium, opioids received during admission, rates of in-hospital ambulation and in-hospital mortality, and postoperative follow-up within three weeks. We utilized a mixed model to identify predictors of time to surgery and length of stay.

Results

We identified 482 patients that met our inclusion criteria. Univariate analysis revealed that high DCI patients had a significantly greater proportion of Spanish-speaking patients compared to low DCI (25.9% vs 7.0%, $p = 0.019$); no differences were observed between low and high ADI. Multivariate logistic regression showed that higher ADI was associated with lower rates of in-hospital ambulation ($Z = -2.091$, $p = 0.037$). We also found that higher DCI was associated with lower rates of in-hospital mortality ($Z = -1.969$, $p = 0.049$), which refutes our initial hypothesis. There were no other statistically significant correlations observed.

Conclusion

The results of our study show that higher levels of socioeconomic disadvantage are associated with lower rates of in-hospital ambulation among elderly postoperative hip fracture patients even when adjusting for patient characteristics. Higher socioeconomic disadvantage is associated with poorer health literacy, which could impact patient understanding of the importance of in-hospital ambulation for better hip fracture outcomes. It is also associated with poorer nutritional, physical, and mental health, which may make it more difficult for disadvantaged patients to regain their ability or motivation to ambulate postoperatively. Interestingly, higher socioeconomic disadvantage is also associated with decreased rates of in-hospital mortality. The nature of this relationship is unclear but may potentially be explained by certain aspects of patients' baseline health or in-hospital management that were not controlled for in our analysis.

Significance

The results of this study suggest that patients who are socioeconomically disadvantaged may be at greater risk of failing to meet key milestones in the immediate postoperative recovery period. Greater focus on in-hospital ambulation for disadvantaged groups may be necessary in order to promote equitable hip fracture outcomes.

ABSTRACT #053

Union rate of pathologic fractures sustained in patients with metastatic bone disease: a retrospective study

Dylan Horan MD, Deena Najjar BS, Ryan Yang, Jenna Le MD, Beverly Thornhill MD, Youngtai Lo PhD, Sung-Suk Chae PhD, Ranxin Zhang MD, Jichuan Wang MD, Fnu Hasibagan PhD, Bang Hoang MD, Rui Yang MD, David Geller MD
Affiliations : Montefiore Medical center; Albert Einstein College of Medicine

Background
Metastatic bone disease (MBD) causes significant morbidity, pain, and inferior quality of life. [i],[ii],[iii],[iv] Treatment focuses on improving skeletal stability, with the aim to provide a durable orthopedic solution for a patient's remaining life. Historically, union rates for pathologic fractures were considered according to histology type, with some cancers reliably healing while others exhibited dismal healing rates. These historical rates, which have not been updated in over 40 years, have continued to inform surgeons, influencing the type of surgery recommended and the inherent risks incurred.[v] Given advances in tumor profiling and classification, as well as in adjuvant therapies, a more contemporary review of bone healing is warranted and may improve expectations, decision making, and management recommendations.

Methods:
An IRB approved retrospective review spanning from 2014 to 2024 was conducted at an NCI-designated comprehensive cancer center. Inclusion criteria included patients ≥18 years of age with MBD that either underwent prophylactic fixation (PF) or internal fixation (IF) for MBD. Patients with primary bone malignancies, spinal metastases, and/or treated with endoprosthesis were excluded. The primary outcome was histology specific-bone healing rate, determined by radiographs reviewed by a fellowship-trained musculoskeletal radiologist. Additional data such as overall survival, treatment, and fixation type were assessed as well.

Results:
A review from 2014-2024 has revealed a total of 205 patients who underwent fixation for either an impending or pathologic fracture. Of these patients, 76 were impending fractures and 129 were pathologic fractures. Preliminary results demonstrate a marked improvement in healing rates from historical controls in which the healing rates for multiple myeloma, breast cancer, and lung cancer were 67%, 37%, and 0% respectively. Additionally, our study demonstrates an improved survival of patients with lung cancer after sustaining a pathologic fracture compared to previous studies, in which patients did not live beyond 6 months.

Conclusion:
While data capture and analysis is ongoing, initial review suggests bony union rates have substantially improved from historic values. Additionally, it appears there is near universal healing in multiple myeloma and meaningful potential for bony healing in the setting of other histologies that historically demonstrated poor healing rates. More accurate prognostication, in the setting of molecular profiling, targeted treatments, and immunotherapy, will allow surgeons to make more informed and accurate recommendations. Having accurate and contemporary expectations is of immense importance in guiding patients, making surgical recommendations, and managing complex patients living with metastatic cancer.

[i] Jiang W, Rixiati Y, Zhao B, Li Y, Tang C, Liu J. Incidence, prevalence, and outcomes of systemic malignancy with bone metastases. *Journal of Orthopaedic Surgery*. 2020;28(2).
[ii][ii] Cosphiadi I, Atmakusumah TD, Siregar NC, Muthalib A, Harahap A, Mansyur M. Bone Metastasis in Advanced Breast Cancer: Analysis of Gene Expression Microarray. Clin Breast Cancer. 2018 Oct;18(5):e1117-e1122. doi: 10.1016/j.clbc.2018.03.001. Epub 2018 Mar 8. PMID: 29609951.
[iii] Logothetis C, Morris MJ, Den R, Coleman RE. Current perspectives on bone metastases in castrate-resistant prostate cancer. Cancer Metastasis Rev. 2018 Mar;37(1):189-196. doi: 10.1007/s10555-017-9719-4. PMID: 29380085; PMCID: PMC5801387.
[iv] Bienz M, Saad F. Management of bone metastases in prostate cancer: a review. Curr Opin Support Palliat Care. 2015 Sep;9(3):261-7. doi: 10.1097/SPC.0000000000000157. PMID: 26262831.
[v] GAINOR, BARRY J. M.D.; BUCHERT, PETER M.D.. Fracture Healing in Metastatic Bone Disease. Clinical Orthopaedics and Related Research 178():p 297-302, September 1983.

Impact of Patient Matched Constitutional Alignment on the Early Clinical Outcomes of Robotic-Assisted Total Knee Arthroplasty

Carlos Salazar[1], Zeynep Seref-Ferlengez PhD[2], Brenden Cutter MD[2], Carlos Alvarado MD[2]
[1]*Albert Einstein College of Medicine, Bronx, NY 10461*
[2]*Department of Orthopedic Surgery, Montefiore Medical Center/Albert Einstein College of Medicine, Bronx, New York 10461*

Background: The optimal alignment target for patients undergoing total knee arthroplasty (TKA) remains a controversial topic. The mechanical alignment method, which aims for a neutral mechanical axis, has been the gold standard for over 40 years. Despite achieving good long-term survivorship, authors report dissatisfaction rates of up to 20% with mechanically aligned total knees. The pursuit of improved patient satisfaction has led some to target a personalized alignment strategy that aims to recreate a patient's pre-arthritic or constitutional alignment, stating that this may better restore soft tissue balancing and kinematics of the knee. Opponents to this strategy state concerns over increased loosening and complications using these methods, as they require limbs to be aligned outside of the traditional safe zone of 3 degrees in certain individuals. The aim of this paper is to determine if robotic-assisted total knee arthroplasty performed to match a patient's constitutional alignment results in safe and acceptable outcomes, even when the limb alignment is outside the safe zone of 3 degrees from neutral.

Methods: A retrospective review of patients undergoing TKA between 2021 and 2023 using robotic-assisted surgery was conducted. Patients were placed into two cohorts based on their postoperative Hip Knee Ankle angle (HKA), with those falling within 3 degrees of neutral as the "neutral" cohort and patients aligned outside of 3 degrees as the "non-neutral" cohort. Alignment was determined intra-operatively, aiming to restore pre-arthritic alignment while maintaining a balanced knee. All surgical procedures were performed by a single academic surgeon. Patients without a preoperative varus or valgus angle of 3° or greater were excluded. Outcome variables included range of motion (ROM), infection, stiffness, manipulation under anesthesia (MUA), postoperative drainage, revisions, ED visits, and readmission. Operative time and robotic use time were also recorded. Outcomes were compared between the two cohorts using Chi-square and Student's t-tests.

Results: 290 patients were included, 69 (24%) exhibited a post-operative hip-knee-ankle (HKA) angle greater than 3°, indicating non-neutral alignment, while 221 (76%) displayed a post-operative HKA angle of 3° or less, signifying neutral alignment. Patients with non-neutral alignment required a longer robot usage time, averaging an additional 5 minutes and 40 seconds (total robot time of 24 minutes and 8 seconds), compared to the neutral alignment group (total robot time of 19 minutes and 41 seconds) (P value < .001). However, total operating room (OR) time did not exhibit a statistically significant difference, with an average of 164.12 minutes for the neutral alignment cohort compared to 168.38 minutes for the non-neutral cohort (P value .187).There was no significant difference between the two cohorts in any post-operative outcomes, including aseptic loosening, emergency department (ED) visits, readmission rates, infection rates, stiffness, return to OR, manipulation under anesthesia (MUA), and revisions.(Table 1)

Conclusion: In using a constitutional alignment strategy, almost one quarter (24%) of robotically assisted TKAs displayed an end limb alignment of >3 degrees from neutral. These patients displayed no difference in loosening, infection, ROM, or functional outcomes versus those placed in neutral alignment. Although future studies should focus on long-term outcomes of constitutionally aligned TKAs, our paper supports that placement of total knee arthroplasties outside of the traditional safe zone of 3 degrees is safe and effective.

Analysis of Comorbidities and Short-Term Complication Risk in Diabetic Patients Undergoing Peripheral Nerve Neuroplasty

Lekha R. Yaramada B.S.[1], Edward D. Wang M.D.[2]
Lekha.yaramada@stonybrookmedicine.edu

[1]Stony Brook University Renaissance School of Medicine, Stony Brook, NY
[2]Department of Orthopaedics, Stony Brook University, Stony Brook, NY

Introduction:
In diabetic patients, peripheral nerve neuroplasty can alleviate pain and numbness caused by diabetic neuropathy. Diabetic patients are also more prone to complications due to impaired wound healing, susceptibility to infection, and vascular problems. We aim to compare comorbidities and 30-day complications in diabetic patients with and without insulin dependence after peripheral nerve neuroplasty.

Methods:
A retrospective analysis was performed using the ACS National Surgical Quality Improvement Program database from the years 2015-2022. We filtered patients using Current Procedure Terminology codes 64702, 64704, 64708, 64712, 64713, 64722, 64726, and 64727. Patients were sorted by diabetic status, and bivariate analysis was performed to compare comorbidities and complications. Multivariable logistic regression analyses were performed to identify independent associations in 30-day postoperative complication rates.

Results:
A total of 4,144 patients were included: 3,572 in the non-diabetic cohort, 359 in the non-insulin-requiring diabetic cohort, and 213 in the insulin-requiring diabetic cohort. The non-insulin-requiring diabetic cohort was significantly associated with age > 40 years ($P < 0.001$), BMI [body mass index] >30.0 ($P < 0.001$), ASA [American Society of Anesthesiologists] Class ≥3, ($P < 0.001$), COPD [chronic obstructive pulmonary disease] ($P = 0.007$), hypertension ($P < 0.001$), and outpatient status ($P = 0.012$). The insulin-requiring diabetic cohort was significantly associated with age > 40 years ($P < 0.001$), BMI >30.0 ($P < 0.001$), ASA Class ≥3, ($P < 0.001$), COPD ($P = 0.013$), CHF [congestive heart failure] ($P = 0.014$), hypertension ($P < 0.001$), dialysis ($P < 0.001$), and outpatient status ($P = 0.005$). The overall complication rate was 4.9% for non-diabetics, 6.4% for non-insulting-requiring diabetics, and 8.0% for insulin-requiring diabetics. Neither diabetic group was independently associated with any specific complication.

Discussion:
Patients with diabetes had greater rates of comorbidity, including advanced age, greater BMI, greater ASA class, COPD, CHF, hypertension, and dialysis. Although complication rates were higher in both diabetic groups, once confounding factors were controlled for, neither group was independently associated with any specific complication. We found that diabetic status was linked to higher comorbidities but did not correlate with an increased risk of 30-day complications following peripheral nerve neuroplasty.

ABSTRACT #056

Orthopedic Injuries Among Adults Associated with Electric Skateboard Use

Rachel Katz[1], Morgan Roche[1], Alexa Karkenny MD[2]
[1]Albert Einstein College of Medicine, Bronx, NY, United States, [2]Montefiore-Einstein, Bronx, NY, United States

Objective: Electric skateboards have surged in popularity since their invention in the 1970s, providing an accessible mode of transportation. Electric skateboards are equipped with motors inside the wheels and speed control by a handheld remote, reaching 20-50 miles per hour in seconds. While previous studies have explored injuries related to use of hoverboards, electric scooters, and electric bicycles, research on electric skateboard orthopedic injuries among adults remains limited, despite their association with numerous hospital visits. This study aims to deepen the understanding of orthopedic injuries in adults related to electric skateboards, guiding advocacy and injury prevention strategies.

Methods: The National Electronic Injury Surveillance System (NEISS) database was queried between 2014 and 2023 for patients aged 18+ presenting to the U.S. Emergency Departments (EDs) who were injured after usage of electric skateboards, one-wheels, or longboard vehicles. Patient demographics, diagnosis, injury location, narrative description of incident, and disposition data were collected from ED encounters. Primary outcomes included fracture and dislocation diagnoses. Secondary outcomes included diagnoses of amputations, concussions, contusions/abrasions, hematomas, strains/sprains, lacerations, punctures, crushing, nerve damage, and foreign bodies.

Results Obtained: 331 total patients sustained electric skateboard injuries in 2014-2023, with 466 total diagnoses. The incidence of electric skateboard injuries rose over the past ten years with 83.38% of cases (n=276) occurring in the last five years. The most common injuries included fractures (32.19%, n=150), contusion/abrasions (17.38%, n=81), and internal organ injury (15.45%, n=72), while dislocations accounted for 2.79% (n=13). The most frequently fractured sites were the clavicle (18%, n=27), ankle (13%, n=19), and wrist (9%, n=14). Out of all diagnoses treated and admitted or transferred, 72.73% were fractures (n=40) and 1.82% were dislocations (n=1). There was 1 documented fatality associated with a fracture. Out of all diagnoses treated and released, 37.41% were fractures (n=101) and 2.22% were dislocations (n=6).

Conclusions: Electric skateboards present a significant risk for orthopedic injuries, demonstrated by a notable increase in ED visits among adults over the past decade.

Significance: The findings underscore the need for enhanced safety measures. Increased awareness of these injury mechanisms among orthopaedists could improve advocacy and discussions with patients about injury prevention. The high incidence of ankle and wrist fractures suggests that protective gear, such as guards, could mitigate injuries, though effective prevention strategies for clavicle fractures remain inconclusive.

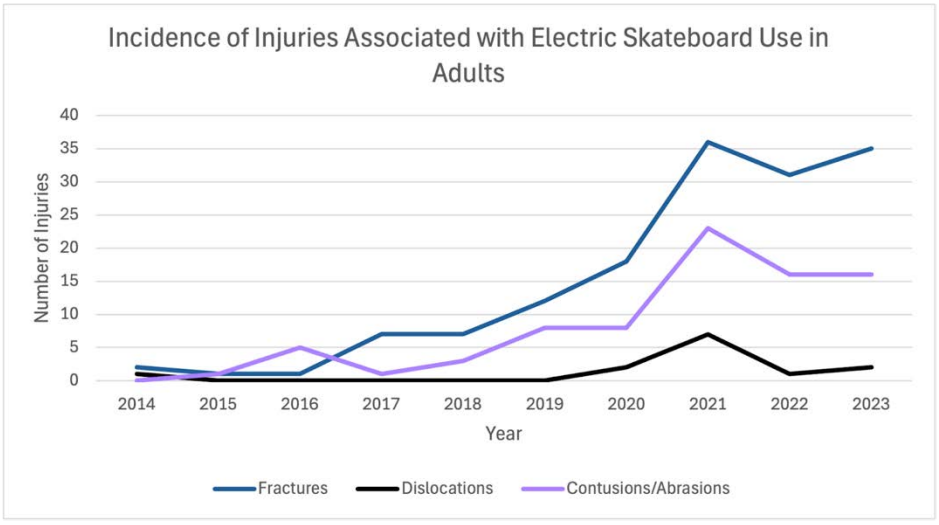

Figure 1. Incidence of Fractures, Dislocations, and Contusions/Abrasions Associated with Electric Skateboard Use Among Adults

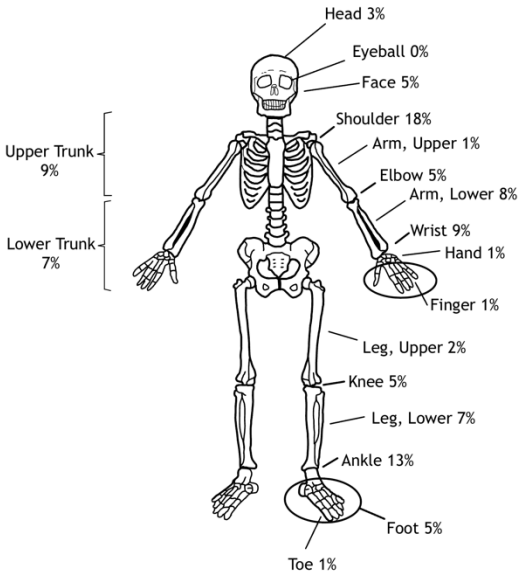

Figure 2. Anatomical Locations of fractures Associated with Electric Skateboard Use Among Adults

Impact of Surgical Timing on Complications in Pediatric Ankle ORIF: A Retrospective Analysis of Socioeconomic Factors and Outcomes

Andrea Muñoz BS, Emily Ferreri BS, Mohammed Bashier BA, Jessica Chao BS, Leila Alvandi PhD, Edina Gjonbalaj BS, Prisco Demercurio MD, Alexa Karkenny MD, Jaime Gomez MD, Mani Kahn MD
Montefiore Einstein Department of Orthopaedic Surgery, Division of Pediatric Orthopaedic Surgery, Bronx, NY

Objective: To assess how socioeconomic factors affect the timing of ankle ORIF and complications from delayed surgery in pediatric patients.

Methods: A retrospective review identified 114 pediatric patients (≤18 years) who underwent ankle ORIF between 2015 and 2023 at a single academic tertiary care center, of which 93 met inclusion criteria. Patients were grouped based on surgery timing: early (≤14 days) and delayed (>14 days). Data collected included insurance type (public or private), Child Opportunity Index 2.0 (COI), post-operative infection, hardware failure, hardware removal, revision surgery, post-operative range of motion, and Visual Analogue Scale (VAS) pain scores. Statistical comparisons between cohorts were performed using t-tests and chi-square analyses.

Results: The mean time to surgery for the early (n=75) and delayed (n=18) cohorts was 8.23 and 22.00 days, respectively ($p<0.001$). There were no significant differences in demographic characteristics, insurance type, COI, complications, range of motion, or VAS pain scores at 3 and 6 months post-operation between the cohorts.

Conclusion: Neither insurance type nor COI significantly affected surgery timing (>14 days) or short-term outcomes, including infection rates, hardware complications, or range of motion. While no short-term complications were linked to delayed surgery, further research is needed to assess potential long-term risks.

Significance: The findings suggest that neither insurance type nor COI significantly impact the timing of surgery or subsequent short-term outcomes for pediatric ankle fractures.

Table 1. Demographic comparison of patients based on injury to surgery days.

Parameter		Injury to surgery (≤ 2 weeks) n = 75	Injury to surgery (> 2 weeks) n = 18	P-value
Age at Injury, *years (Mean±SD)*		14.79±2.08	14.11± 2.67	0.151
Time from Injury to Surgery, *days (Mean±SD)*		8.23±3.89	22.00±6.89	**<0.001**
Sex, *n (%)*				
	Female	28 (37.3%)	10 (55.6%)	0.188
	Male	47 (62.7%)	8 (44.4%)	
Race, *n (%)*				
	White	10 (13.3%)	3 (16.7%)	0.938
	Black or African American	19 (25.3%)	5 (27.8%)	
	Asian	2 (2.7%)	1 (5.6%)	
	Other	32 (42.7%)	7 (38.9%)	
	Unknown	12 (16.0%)	2 (11.1%)	
Ethnicity, *n (%)*				
	Spanish/Hispanic/Latino	38 (50.7%)	8 (44.4%)	0.704
	Not Spanish/Hispanic/Latino	30 (40.0%)	9 (50.0%)	
	Unknown	7 (9.3%)	1 (5.6%)	
Insurance, *n (%)*				
	Public	51 (68.0%)	13 (72.2%)	0.484
	Private	24 (32.0%)	5 (27.8%)	
Statewide Total-COI, *n (%)**				
	Moderate, high, or very high	11 (14.9%)	3 (16.7%)	1.000
	Low or very low	63 (85.1%)	15 (83.3%	
Statewide Education-COI, *n (%)**				
	Moderate, high, or very high	13 (17.3%)	4 (22.2%)	0.797
	Low or very low	61 (81.3%)	14 (77.8%)	
Statewide Socioeconomic-COI, *n (%)**				
	Moderate, high, or very high	11 (14.7%)	5 (27.8%)	0.380
	Low or very low	63 (84.0%)	13 (72.2%)	
Statewide Health-COI, *n (%)**				
	Moderate, high, or very high	40 (53.3%)	7 (38.9%)	0.452
	Low or very low	34 (45.3%)	11 (61.1%)	

*COI data was unavailable for one zipcode

Table 2. Post-op complications and functional outcomes between patients based on injury to surgery days.

Parameter		Injury to surgery (≤ 2 weeks) n = 75	Injury to surgery (> 2 weeks) n = 18	P-value
Post-op Infection, *n (%)*				
	No	71 (94.7%)	17 (94.4%)	0.668
	Yes	4 (5.3%)	1 (5.6%)	
Revision Surgery, *n (%)*				
	No	73 (97.3%)	18 (100%)	0.649
	Yes	2 (2.7%)	0 (0.0%)	
Post-op Hardware failure, *n (%)*				
	No	75 (100%)	18 (100%)	-
	Yes	0 (0.0%)	0 (0.0%)	
Hardware Removal, *n (%)*				
	No	61 (81.3%)	15 (83.3%)	0.574
	Yes	14 (18.7%)	3 (16.7%)	
Ankle Motion Dorsiflexion Score at 3 Months, *n (%)*				
	Not Normal	7 (9.3%)	3 (16.7%)	0.660
	Normal (10-20)	17 (5.3%)	4 (5.6%)	
	Unknown	51 (68.0%)	11 (61.1%)	
Ankle Motion Plantarflexion Score at 3 Months, *n (%)*				
	Not Normal	7 (9.3%)	5 (27.8%)	0.140
	Normal (40-55)	8 (10.7%)	1 (5.6%)	
	Unknown	60 (80.0%)	12 (66.7%)	
VAS Pain Score at 3 Months, *n (%)*				
	>5	2 (2.7%)	1 (5.6%)	0.797
	≤5	44 (58.7%)	11 (61.1%)	
	Unknown	29 (38.7%)	6 (33.3%)	
Ankle Motion Dorsiflexion Score at 6 Months, *n (%)*				
	Not Normal	2 (2.7%)	0 (0.0%)	0.406
	Normal (10-20)	15 (20.0%)	2 (11.1%)	
	Unknown	58 (77.3%)	16 (88.9%)	
Ankle Motion Plantarflexion Score at 6 Months, *n (%)*				
	Not Normal	4 (5.3%)	1 (5.6%)	0.518
	Normal (40-55)	3 (10.7%)	0 (0.0%)	
	Unknown	68 (90.7%)	17 (94.4%)	
VAS Pain Score at 6 Months, *n (%)*				
	>5	1 (1.3%)	0 (0.0%)	0.074
	≤5	32 (42.7%)	3 (16.7%)	
	Unknown	42 (56.0%)	15 (83.3%)	

A Classification System of Trochlear Dysplasia Severity Utilizing the Sulcus Angle

Authors: Jason Brenner, BS[1], Leila Mehraban Alvandi, PhD[1,2], Steven M. Henick, MD[2], Edina Gjonbalaj[2], Benjamin J Levy, MD[1,2], Jacob Schulz, MD[1,2], Eric Fornari, MD[1,2], Mauricio Drummond, MD[1,2]
Affiliations: [1]Albert Einstein College of Medicine, Bronx, NY,[2]Montefiore Einstein Department of Orthopaedic Surgery, Division of Pediatric Orthopaedic Surgery, Bronx, NY

Introduction: The cartilaginous sulcus angle (cSA) effectively and reliably quantifies trochlear dysplasia (TD) in patients with patellar dislocation (PD)[1]. TD in the proximal trochlear groove (TG) is more anatomically relevant than TD more distally. However, to best understand this complex structural anomaly, TD must be evaluated throughout the entire TG.

Objective: To classify the severity of TD using the cSA and to apply this method to determine whether TD severity is associated with PD recurrence.

Methods: Following institutional review board approval, we retrospectively reviewed (Level III) pediatric patients at a single institution treated for PD into two cohorts: recurrent patellar dislocators (RPDs) and one-time dislocators (OTDs). The OTDs were called to confirm their history of just one PD. Patients with prior surgery in the affected knee and those with substandard MRI studies were excluded. cSA is the angle formed by the lateral and medial trochlear facets; measurements were recorded on MRI at four consecutive axial images (cSA1 – most proximal, cSA2, cSA3, cSA4 – most distal). The proximal TG was defined as the most proximal axial image in which the cartilage of the medial and lateral trochleae is visible. Optimal cutoff values for the cSA were identified using the 25th percentile of the RPD group as the cutoff. Patients were then classified by TD severity based on how many of their four cSA measurements were above the established cutoff value. All four cSA values were dysplastic – high grade dysplasia; two or three dysplastic cSA values - moderate grade dysplasia; one dysplastic cSA value – low grade dysplasia; no dysplastic cSA values – no dysplsia. Frequencies were calculated; chi-squared tests and odds ratios were utilized to compare the frequency of high-grade dysplasia between RPDs and OTDs.

Results: After applying inclusionary and exclusionary criteria, 173 patient-knees were analyzed; 106 were RPDs and 67 were OTDs (overall recurrence rate = 61.3%). The cutoff values were: cSA1>162°, cSA2>155°, cSA3>151°, cSA4>146°. View Table 1. More severe dysplasia was associated with RPD (p=.019); high-grade dysplasia is associated with an odds ratio of 1.5 (95% CI 1.1, 2.0) for being a RPD versus an OTD.

Table 1: Frequency of trochlear dysplasia (TD) severity type by patellar dislocation cohort. High-grade TD is associated with RPD. Low-grade TD is associated with OTD. is Recurrent patellar dislocation, RPD; one-time dislocation, OTD.

	RPD	OTD	P-value
High-grade TD	**63/106 (59%)**	**29/67 (43%)**	**.019**
Moderate TD	23/106 (22%)	15/67 (22%)	.457
Low-grade TD	**8/106 (8%)**	**13/67 (19%)**	**.015**
No TD	12/106 (11%)	10/67 (15%)	.148

Conclusion: The proposed classification system establishes four severity types of TD utilizing the cSA. The majority of RPDs have high-grade TD; high-grade TD is more prevalent in RPDs than in OTDs.

Significance: Patients with high-grade TD, defined as an elevated cSA throughout the entire TG, are 1.5 times more likely to be RPDs than OTDs.

Reference:

1. Davies AP, Costa ML, Shepstone L, Glasgow MM, Donell S. The sulcus angle and malalignment of the extensor mechanism of the knee. *J Bone Joint Surg Br*. Nov 2000;82(8):1162-6. doi:10.1302/0301-620x.82b8.10833

Molecular heterogeneity within an untreated osteosarcoma following upfront surgery

Sung-Suk Chae[1], Hasibagan Borjihan[1], Mia Thi[1], Deyou Zheng[2], Ranxin Zhang[1], Abhijith Annasamudram[1], Rui Yang[1], Bang Hoang[1], David Geller
1 Department of Orthopedic Surgery, Montefiore Medical Center, Albert Einstein College of Medicine, Bronx, New York.
2 Department of Genetics, Albert Einstein College of Medicine, Bronx, New York.

Background: Osteosarcoma has been reported to exhibit tremendous alterations in gene expression, which are partly attributed to chromosomal abnormality owing to chromothripsis (1, 2, 3). While heterogeneity between tumors is widely studied, similar heterogeneity within a single tumor remains less clear. Biopsy samples are, small and only represent a single location within the tumor, while chemotherapy treated samples undergo treatment stress that may mask important transcriptomic data. Defining and studying the heterogeneity of untreated tumor from upfront surgery might provide valuable insights into a cancer's behavior, and might in turn, aid in the development of targeted therapies and personalized treatment plans.

Method: Wide excision of a distal femoral osteosarcoma was performed via an IRB approved upfront surgery protocol. Tissue samples from various regions were collected for nucleic acid extraction. For total RNA extraction, frozen tissue samples were pulverized using a Cryomill 400, transferred to Trizol solution, and mechanically homogenized. RNAs were extracted from the homogenized samples following the Trizol protocol and further purified using the Qiagen RNeasy Plus Mini Kit. Bulk RNA-Seq was then performed using the purified total RNAs.

Results: Principal Component Analysis (PCA) of RNA-seq data reveals distinct differences in gene expression profiles among tumors and normal bone. Additionally, intramedullary tumor differs significantly from near extraosseous (nEO) and far extraosseous (fEO) tumors, whereas nEO and fEO tumors exhibit similarities. Notably, Gene ontology analysis of tumor regions revealed that nEO and fEO tumors showed increased activity in biological processes related to cell proliferation, while processes related to immune responses were decreased.

Conclusions: Cancer cells diversify through the accumulation of genetic and epigenetic alterations, which can change their fitness and consequently lead to clonal selection under selective pressure. Bulk RNA-seq analysis has uncovered regional heterogeneity within the same tumor tissue, with different gene sets being dysregulated in a region-dependent manner. Our early results support ongoing clonal evolution, showing substantial differences between the "earlier" intramedullary tumor and the "later" extraosseous tumor. This suggests that studying whole tumors resected during upfront surgery can effectively capture tumor progression and associated microenvironmental changes. Further studies using additional untreated tumors from osteosarcoma patients are warranted.

Reference.

1. Laplane, L., Maley, C.C. The evolutionary theory of cancer: challenges and potential solutions. *Nat Rev Cancer* **24**, 718–733 (2024)
2. Song YJ, Xu Y, Deng C, Zhu X, Fu J, Chen H, Lu J, Xu H, Song G, Tang Q, Wang J. Gene Expression Classifier Reveals Prognostic Osteosarcoma Microenvironment Molecular Subtypes. Front Immunol. 2021 Apr 20;12:623762.
3. Zheng X, Liu X, Zhang X, Zhao Z, Wu W, Yu S. A single-cell and spatially resolved atlas of human osteosarcomas. J Hematol Oncol. 2024 Aug 20;17(1):71.

Using percutaneous microfracture induced bone healing in the treatment of unicameral bone cyst in pediatric patients

Rui Yang, MD, Sara Orr, MD, Jichuan Wang, MD, Bang Hoang, MD, and David S. Geller, MD

Background: Unicameral Bone Cyst (UBC) is one of the most common benign bone lesions in pediatric patients with a high rate of pathological fracture. The treatment for UBC remains controversial, varying from open surgery to steroid or bone marrow injection, and resulting in about 30-50% healing rates. Here we describe a pilot study using percutaneous microfracture induced bone healing in the treatment of UBCs.

Methods: From 2017-2021, we treated 12 patients with UBCs with percutaneous microfracture. The average age is 9.8 yo (3-16). Six were in the humerus and 4 in the proximal femur. Seven of them were presented initially with pathological fractures.

Results: On average, 1.6 procedures of microfracture were performed in these patients. Two additional open surgeries with implantation were performed in a 3 yo patient after recurrence. Patients younger than 10 yo needed on average 2.4 procedures as compared to 1.3 procedures in patients older than 10 yo. The minimal follow up time was 2 years unless lesions healed earlier. At the time of the last follow up, seven and 5 patients had Neer's grade 1 and 2 healing, respectively. One patient had a pathological fracture during postoperative healing. There is no deformity or other complications in this group of patients.

Conclusions: Percutaneous microfracture induced bone healing is minimally invasive and well tolerated in pediatric patients with UBCs. Our pilot study showed a high rate of healing after less than 2 sessions of treatments. Additional study is needed to further explore this novel procedure in the treatment of UBCs.

Post-Pandemic Disparities in Access to Care Among Ankle Fracture Patients

Mohammed Bashier[1], Emily Ferreri, Andrea Muñoz[1], Jessica Chao[1], Prisco DeMercurio[2], Edina Gjonbalaj[2], Leila Mehraban Alvandi[2], Huai Ming Phen[2], Mani Kahn[2]

[1]Albert Einstein College of Medicine, Bronx, NY [2]Montefiore Einstein, Department of Orthopaedic Surgery, Bronx, NY

Objective

The relationships of race and socioeconomic deprivation with respect to access to care and patient outcomes have been widely researched. However, the residual effects of the COVID-19 pandemic on these disadvantaged populations have not been adequately assessed by earlier studies, particularly within orthopedic surgery. Given that the inability to access care can significantly affect health and functional outcomes, particularly in the case of unstable fractures, this study sought to investigate changes in access to care among ankle fracture patients within our underserved urban population that may have manifested in the wake of the pandemic.

Methods

This retrospective chart review involved adult patients within an underserved urban population in the United States who underwent open reduction and internal fixation (ORIF) for ankle fractures at a single academic tertiary care center between September 2016 and June 2023. We excluded patients whose date of surgery occurred from September 2019 to March 2021 to minimize variations in patterns surrounding patient care while permitting the assessment of six-month follow-up. Patients whose surgery occurred later than six months from the date of injury were also excluded. Demographic data and outcome variables of interest were compared across the pre- and post-pandemic groups. Categorical variables were analyzed using Chi-square analysis (or Fisher's exact test, when applicable) and continuous variables were compared using two-sample t-test or Wilcoxon rank-sum test. Multivariate logistic regression was employed to assess differences between both groups after adjusting for potential confounding variables.

Results

We identified 330 pre-pandemic patients and 310 post-pandemic patients that met our study criteria, for a total of 640 patients. Compared to pre-pandemic baseline levels, our post-pandemic ankle ORIF patients had a younger mean age (47.9 vs 44.8, $p = 0.017$), higher and lower proportions of Black and White patients, respectively ($p = 0.003$), fewer privately insured patients compared to those with public or no insurance ($p = 0.003$), and fewer patients with diabetes ($p = 0.007$). We also found that post-pandemic patients had a modest yet statistically significant increase in the median number of days between injury and initial presentation (1 vs 2 days, $p < 0.001$), but no difference in time from initial presentation to surgery. After adjusting for potential confounding patient characteristics, post-pandemic patients were less likely to initially present to the emergency department (OR = 0.65, 95% CI: 0.45–0.93) compared to the outpatient clinic setting. Additionally, patients in the post-pandemic group were overall more likely to have been seen at an urgent care center or a primary care provider prior to presentation compared to the pre-pandemic group (OR = 2.21, 95% CI: 1.11–4.56), but there was no difference with respect to external ED visits prior to presentation. Furthermore, post-pandemic patients exhibited a lower ED admission rate (OR = 0.65, 95% CI: 0.45–0.93), were more likely to undergo outpatient surgery (OR = 1.80, 95% CI: 1.27–2.57), and were less likely to have a postoperative ED visit for their ankle fracture (OR = 0.50, 95% CI: 0.28–0.88). There were no changes in six-month loss to follow-up or physical therapy participation rates.

Conclusion

The results of this study ultimately show that our post-pandemic population of ankle ORIF patients differ from the pre-pandemic era in inherent patient characteristics as well as in their utilization of and presentation to care. Specifically, post-pandemic patients present to care slightly later than before, which may be a result of seeing more outside providers (such as urgent care centers) prior to presenting to care at our institution. Additionally, there was an overall significant decrease in ED utilization, but there was no notable change in the frequency of outside ED visits prior to initial presentation for treatment.

Significance

Delayed presentation to care has the potential to prolong a patient's uncontrolled pain, inability to ambulate, and could negatively impact their clinical course and functional outcomes. A post-pandemic increase in the number of different providers seen by a patient on their route to definitive care reflects a potentially new barrier in the prompt treatment of orthopedic conditions. Additionally, the observed decrease in ED utilization may place unprecedented stress on other avenues of care such as urgent care centers. Further research may help shed light on how access to care among specific disadvantaged groups was disproportionately affected by the pandemic.

ABSTRACT #062

Proinflammatory Cytokines Are Expressed In Bone After Rotator Cuff Tears

Dylan Horan MD[1], Jayson Lian MD[1,3], Lisa Franks PA-C[1], Giulia DiRaimo BS[1], Yungtai Lo PhD[1], Luke Cooper MRes, CPSS [4], Eloy Tabeayo MD[1], Mia M Thi PhD[1,2], David Gonzalez MD[1]

Departments of [1]Orthopedic Surgery and [2]Molecular Pharmacology, Montefiore Medical Center and Albert Einstein College of Medicine, Bronx, NY. [3]Cedars-Sinai Kerlan Jobe Institue, [4]Sports Science at New York City Football Club

Introduction: Rotator cuff tears often lead to significant pain, limiting daily activities and reducing quality of life. Approximately 2 million people in the United States visit their doctors each year because of rotator cuff tears. Pain after rotator cuff tears is not well understood with multiple proposed pathways.[1] Previous studies have demonstrated the role of subacromial bursa, rotator cuff tendon, and synovium in pain generation.[2,3] However, no prior study has investigated the role of the greater tuberosity (GT). Our goal was to compare proinflammatory cytokine expression in the exposed footprint of the GT in painful patients undergoing arthroscopic rotator cuff repair (RCR) for full thickness tears versus the lateral aspect of the GT away from any rotator cuff pathology.

Methods: This was a prospective cohort study of patients undergoing arthroscopic RCR for full thickness rotator cuff tears from 2021-2024 at a single institution (IRB 2022-14603). Patients were excluded if there were partial rotator cuff tears, revision rotator cuff repair, frozen shoulder, rheumatoid arthritis, or prior shoulder surgery. Demographic variables included: age, sex, pain, duration of symptoms, preoperative NSAID or corticosteroid injection use. An arthroscopic curette of ~2 mm depth or Lee-Lok bone biopsy kit was used to collect GT subchondral bone at the region of the full thickness cuff tear. A second sample was collected from the lateral GT away from the rotator cuff pathology. Samples were stored in 500 ul of RNAlater solution (Thermofisher) at -80 C. RNA was extracted using RNeasy Mini kit (Qiagen), and quantitative PCR (qPCR) was used to compare mRNA expression levels of cytokines: NGF, MCP1, TNF-a, IL-6, IL-1b and MMP-1. Data were compared using student t-test and chi-square test (GraphPad Prism 10, CA).

Results: Twenty one total patients (16 females, 5 males) who had confirmed full thickness rotator cuff tears were enrolled after inclusion/exclusion criteria. RNA quality was deemed pure for nearly all samples. When compared to the lateral GT bone located away from the diseased rotator cuff, the GT bone at the location of the tear demonstrated statistically increased levels of NGF, MCP-1, TNFa, IL-6 and of IL-1B.

Conclusion: Pain after rotator cuff tears is multifactorial and poorly understood. Previous studies have demonstrated a significant increase in pain mediators in the subacromial bursa, rotator cuff tendon, and synovium. Our study demonstrates that the exposed GT at the region of the rotator cuff tear is a significant source of proinflammatory cytokines in rotator cuff-deficient patients and therefore a source of pain. Understanding the source of pain in these patients helps physicians tailor treatment and guide management. Given that the exposed GT is a source of pain mediators, rotator cuff repair that aims to reestablish the rotator cuff footprint and cover exposed bone argues in favor of surgical repair in patients that are refractory to conservative measures.

Significance: The characterization of proinflammatory cytokine expression from exposed greater tuberosity in painful patients with rotator cuff tears is a significant step towards understanding the underlying mechanisms of shoulder pain. By advancing our understanding of the inflammatory processes involved in shoulder pain, we can develop more effective and targeted treatments to alleviate suffering and improve the quality of life for patients.

Funding: Funding for this project was supported by the Montefiore Orthopaedic Research Seed Grant.

References:

1. Dean BJF, Gwilym SE, Carr AJ. Why does my shoulder hurt? A review of the neuroanatomical and biochemical basis of shoulder pain. *Br J Sports Med*. 2013;47(17):1095-1104. doi:10.1136/BJSPORTS-2012-091492
2. Gotoh M, Hamada K, Yamakawa H, et al. Interleukin-1-induced subacromial synovitis and shoulder pain in rotator cuff diseases. *Rheumatology (Oxford)*. 2001;40(9):995-1001. doi:10.1093/RHEUMATOLOGY/40.9.995
3. Voloshin I, Gelinas J, Maloney MD, O'Keefe RJ, Bigliani LU, Blaine TA. Proinflammatory cytokines and metalloproteases are expressed in the subacromial bursa in patients with rotator cuff disease. *Arthroscopy*. 2005;21(9):1076.e1-1076.e9. doi:10.1016/J.ARTHRO.2005.05.017